microRNA FUNCTION IN ZEBRAFISH DEVELOPMENT AND REGENERATION

By

Nergis Kara

Dissertation

Submitted to the Faculty of the

Graduate School of Vanderbilt University

in partial fulfillment of the requirements

for the degree of

DOCTOR OF PHILOSOPHY

in

Biological Sciences

December 15, 2018

Nashville, Tennessee

Approved:

John A. Capra, Ph.D.

Wenbiao Chen, Ph.D.

Douglas G. McMahon, Ph.D.

James G. Patton, Ph.D.

DEDICATION

To my grandmother Fatma Aliye Pamuk,

and

my beloved family,

ACKNOWLEDGEMENTS

This thesis would not have been possible without the help, support and guidance of many people. First, I want to thank to my mentor Dr. James Patton for his excellent mentorship, motivation and support. He has helped me in numerous ways to develop the skills of an independent scientist and explore projects I enjoy. It was truly a privilege to be his graduate student. I'm thankful to my committee members: Dr. Doug McMahon, Dr. Wenbiao Chen, Dr. Tony Weil, and Dr. Tony Capra, for their expertise, suggestions and contributions during committee meetings. I appreciate the time they spent with me during committee meetings and always providing me a new perspective and insight into my research. I also want to thank Dr. Josh Gamse for providing me feedback and support during my early years of graduate school.

I would like to thank Qiang Guan for all his help in maintaining the fish facility. Thank you to fellow zebrafish labs and the Program in Developmental Biology for sharing reagents, feedbacks and providing a collaborative research environment. Thank you to the Department of Biological Sciences, especially to the PhD program coordinators, Leslie Maxwell, Angela Titus, LaDonna Smith, and Alicia Goostree. Thank you also to all my funding sources, including the Stevenson and Gisela Mosig endowments that made my attendance to excellent meetings and courses possible.

Thank you all the members of the Patton lab for their friendship as well as their scientific support and encouragement. Past members of the lab, Kamya Rajaram, Chunyao Wei, Mahesh Rao and Diana Cha were incredibly supportive in all means since I joined lab. I am very thankful to Dominic Didiano and Matthew Kent for their

TABLE OF CONTENTS

LIST OF TABLES

LIST OF FIGURES

LIST OF ABBREVIATIONS

AAA   alpha-aminoadipate

Ago   Argonaute

Ascl1   achaete-scute complex-like 1a

bHLH   basic helix-loop-helix

BrDU   bromodeoxyuridine

cDNA   complementary DNA

ChIP   chromatin immunoprecipitation

CMZ   ciliary marginal zone

CNS   central nervous system

dkk   Dickkopf

Dot1l   disrupter of telomeric silencing 1 like

dpf   days post fertilization

ECM   extracellular matrix

EGF   epidermal growth factor

EGFP   enhanced green fluorescent protein

ESC   embryonic stem cells

FGF   fibroblast growth factor

GABA   ϒ-aminobutyric acid

GCL   ganglion cell layer

GFAP   glial fibrillary acidic protein

Hb-EGF   heparin binding EGF

hpf	hours post fertilization
Igf-1	insulin-like growth factor-1
IKM	interkinetic nuclear migration
IL11	interleukin 11
INL	inner nuclear layer
IPL	inner plexiform layer
iPSC	induced pluripotent stem cells
MG	Müller glia
miRNA	micro RNA
MNU	N-methyl-N-nitrosourea
MO	morpholino
mRNA	messenger RNA
nGFP	nuclear green fluorescent protein
NMDA	N-methyl-D- aspartic acid
NPC	neural progenitor cells
ONL	outer nuclear layer
OPL	outer plexiform layer
Pax	paired homeobox
PcG	Polycomb group
PCNA	proliferating cell nuclear antigen
PIC	pre-initiation complex
pri-miRNA	primary miRNA
qRT-PCR	quantitative reverse transcription polymerase chain reaction

RGC   retinal ganglion cells

RISC   RNA-induced silencing complex

RPE   retinal pigmented epithelium

Std-ctl   standard control

TNF-α   tumor necrosis factor-alpha

TUNEL   terminal deoxynucleotidyl transferase dUTP nick end labeling

UTR   untranslated region

UV   ultraviolet

CHAPTER I

INTRODUCTION

microRNAs (miRNAs)

microRNA (miRNAs) are evolutionarily conserved, small non-coding RNAs that post-transcriptionally regulate gene expression. They were initially identified in forward genetic screens in *C.elegans* as regulators of developmental timing (Lee et al., 1993; Wightman et al., 1993). Later, they were also discovered in plants, flies and vertebrates, involved in nearly all developmental and pathological processes (Ambros, 2003; Chen et al., 2005; Lagos-Quintana et al., 2003; Pasquinelli et al., 2000). As of March 2018, the miRNA registry (http://www.mirbase.org/) contained 38,589 miRNAs in vertebrates and invertebrates, with 2588 annotated miRNAs in the human genome; although biological functions of most of these miRNAs remain to be discovered (Griffiths-Jones et al., 2006).

miRNA-mediated gene silencing involves two main components, miRNAs base-paring with their target mRNAs in complex with Argonaute (AGO) proteins thereby recruiting factors that initiate translational repression as well as mRNA deadenylation and decay (Huntzinger and Izaurralde, 2011). miRNA binding sites are generally located in the 3' untranslated region (UTR) of mRNAs and referred as miRNA recognition elements (MREs) (Bartel, 2009). For target recognition, the crucial region on the miRNA is located from nucleotides 2 to 7 and termed as the 'miRNA seed'. Meanwhile, the

nucleotides downstream of the seed sequence are involved in additional imperfect base-pairing of the miRNA with the target mRNA. In the human genome, more than 60% of protein-coding genes carry at least one conserved MRE. When non-conserved MREs are also taken into consideration, most protein-coding genes are thought to be regulated by miRNAs (Friedman et al., 2009). While miRNAs can bind to many target mRNAs, multiple miRNA can also target the same mRNAs. This characteristic makes miRNAs unique potent regulators of gene expression. Thus, the biogenesis and function of miRNAs themselves are tightly regulated as well.

Due to gene duplication in the genomes of many species, there are multiple related miRNA loci with related sequences. miRNAs with identical seed sequences are generally referred as 'miRNA families' (Bartel, 2009). One example is the *let-7* family which consists of 14 paralogous loci in the human genome. miRNA family members generally have redundant functions, although some distinct roles have been reported as well (Ha and Kim, 2014). Some miRNAs may share common evolutionarily origins, but nevertheless diverge in their seed sequences. One such example is *miR-141* and *miR-200c* miRNAs that derived from *miR-200* superfamily but their seed sequences vary by 1 nucleotide. It has been shown that targets of *miR-141* and *miR-200c* do not overlap; therefore each miRNA has distinct functions (Kim et al., 2013).

miRNA biogenesis and function

Generation of active ~22 nt long mature miRNAs is facilitated by series of biogenesis events as illustrated in Figure 1. Genomic localization of miRNAs is diverse. They can either be located intragenically, in introns or exons of annotated genes or

intergenically. While the majority of the miRNAs are encoded by the introns of coding

and non-coding transcripts in the human genome, less than 15% of zebrafish miRNAs

have intragenic localizations (Ha and Kim, 2014; Rodriguez et al., 2004). miRNAs that

are located in close proximity to each other in the genome are transcribed as a single

polycistronic transcriptional unit. Interestingly, miRNAs in such clusters often display

individual regulatory targets (Roush and Slack, 2008).

Transcription of miRNAs is mediated by RNA Polymerase II (RNA Pol II) (Cai

et al., 2004; Lee et al., 2004). The long primary miRNA transcripts (pri-miRNA)s can

take on a number of forms but most commonly form a long transcript with one or more

characteristic hairpin structures. A typical pri-miRNA is composed of a 33-35bp long

stem, a terminal loop and single-stranded RNA segments at the 5' and 3' sides (Lee et al.,

2002). The maturation process is initiated by the nuclear RNase III-like enzyme Drosha

which crops the stem-loop to release a ~65-70 nt long small hairpin-shaped precursor

miRNA (pre-miRNA) (Lee et al., 2003). This cleavage is catalyzed by the Drosha along

with its essential cofactor Dgcr8 which together make up the Microprocessor complex,

(Denli et al., 2004; Gregory et al., 2004; Han et al., 2004). Drosha and Dgcr8 are

conserved in animals and they are essential for embryonic development (Chong et al.,

2010; Wang et al., 2007).

The pre-miRNA is exported out of the nucleus in an Exportin 5 dependent manner

(Lund et al., 2004; Yi et al., 2003). Upon export to the cytoplasm, the pre-miRNA is

acted upon by a second RNase III-like enzyme, Dicer (Bernstein et al., 2001; Hutvágner

et al., 2001; Ketting et al., 2001). Dicer associates with its binding partner TRBP and

cleaves the loop region of the pre-miRNA, liberating a small RNA duplex approximately
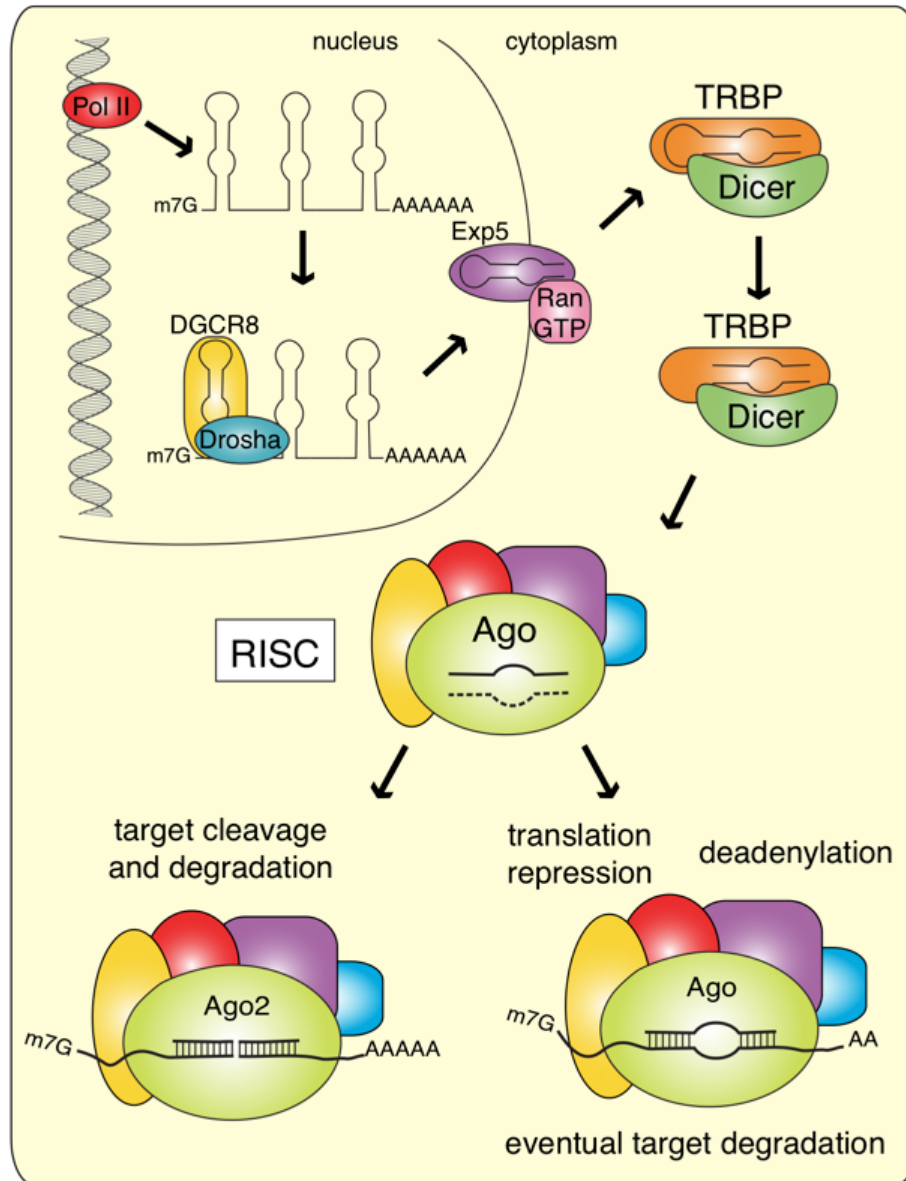
Figure 1 miRNA biogenesis and function

miRNAs are transcribed by RNA polymerase II to generate pri-miRNAs that are generally composed of several stem-loop structures. Pri-miRNAs are further processed by the Drosha-Dgcr8 complex to form pre-miRNAs which are exported from the nucleus by Exportin5 in a Ran-GTP dependent manner. Pre-miRNAs are processed by Dicer to generate small RNA duplexes which are incorporated into RNA Induced Silencing Complexes (RISC). After strand selection, one strand is retained in RISC and this mature miRNA guides RISC to the 3'UTR of target mRNAs. Perfect complementarity between miRNA and target mRNA leads to mRNA cleavage and imperfect base pairing is followed by translation repression and mRNA deadenylation. Figure by Abby Olena.

21 nucleotides long (Grishok et al., 2001; Haase et al., 2005). This small RNA duplex is subsequently loaded onto one or more Ago proteins to form the ribonucleoprotein complex called the RNA induced silencing complex (RISC). Following the loading of the miRNA duplex, the 'passenger' strand, the one with less thermodynamic stability at the 5' end, is quickly removed (Khvorova et al., 2003; Schwarz et al., 2003). The remaining strand of the complex, the 'guide' strand, stays incorporated and a mature RISC is formed. Another determinant for guide strand selection is the composition of the first nucleotide (Czech et al., 2009; Ghildiyal et al., 2010; Okamura et al., 2009).

Animal miRNAs function by binding to specific mRNA targets, typically in the 3' untranslated region (UTR), with imperfect base pairing. The seed region plays an important role in miRNA-target association (Lewis et al., 2003). For most efficient miRNA-mediated RNA silencing, there is perfect base pairing between the seed sequence and complementary sites in the 3'UTR of the target mRNA, called the miRNA recognition element (MRE) (Doench and Sharp, 2004; Lewis et al., 2005). The 3' end of the miRNA can also contribute to target recognition but most pairing arrangements result in a bulge in the center of the miRNA:mRNA which blocks cleavage by Ago2 s (Kiriakidou et al., 2004). Besides these common requirements for miRNA-target interaction, noncanonical miRNA target recognition types are fairly common, especially with imperfect seed pairing (Li 2008, Shin 2010, Loeb 2012). Imperfect pairing in this manner complicates in silico target prediction. Nevertheless, target repression is mediated by RISC in two modes; through promoting mRNA destabilization and repression of translation, both leading to target mRNA degradation (Ameres and Zamore,

2013). These two modes of miRNA-mediated target repression are not necessarily

mutually exclusive (Bazzini et al., 2012; Djuranovic et al., 2012).

miRNAs in vertebrate embryogenesis

Since the first discovery of miRNAs in regulating developmental timing in

C.elegans, biological roles of miRNAs have been tested during various developmental

processes in multiple model organisms (Alvarez-Garcia and Miska, 2005). One strategy

to determine the general requirement for miRNAs in development is to interfere with the

miRNA biogenesis pathway. Dicer knockout mutants have been generated in multiple

model organisms, though I summarize the findings only in two vertebrates, mice and

zebrafish here.

In mice, Dicer1 mutants die at 7.5 days of gestation (Bernstein et al., 2003).

Dicer1 mutant embryos have defects in axis formation and gastrulation, while the

embryonic stem cell pool is also affected. Conditional deletion of Dicer1 in embryonic

stem cells leads to proliferation and differentiation defects (Kanellopoulou et al., 2005;

Murchison et al., 2007). Since Dicer is a shared enzyme also required for the RNA

interference (RNAi) pathway, the defects observed in Dicer mutants may not be only

attributed to defects in miRNA biogenesis. Therefore, to specifically interfere with

canonical miRNA production, Dgcr8 mutants were generated (Suh et al., 2010). DGCR8

is the essential cofactor of Drosha and specifically required in miRNA biogenesis (Chong

et al., 2010; Han et al., 2004). Zygotic Dgcr8 knockout embryos undergo embryonic

arrest prior to E6.5 (Wang et al., 2007). However, together with the analysis of maternal

zygotic mutants of Dgcr8, it has been shown that Dgcr8 null embryos can develop

through the blastocyst stage (Suh et al., 2010). Therefore, canonical miRNAs are not required for preimplantation development.

In zebrafish, zygotic mutants of Dicer undergo developmental arrest 7 to 10 days post fertilization (Wienholds 2003). To assess the maternal contribution of Dicer in these embryos, maternal zygotic Dicer (MZ*dicer*) mutants were generated (Giraldez et al., 2005). MZ*dicer* mutants display earlier morphogenesis defects affecting gastrulation, somitogenesis, brain and heart development, while early embryonic patterning and cell specifications appear normal. Interestingly, expression of *miR-430* in MZ*dicer* mutants can rescue many of the defects described above (Giraldez et al., 2005). Injection of *miR-430* leads to normal brain ventricle formation as well as rescue of the midbrain-hindbrain boundary. Additionally, there is partial rescue of gastrulation, somitogenesis, and retinal development. This shows that defects observed in MZ*dicer* mutants in zebrafish can be attributed to loss of miRNA function. Further analysis of *miR-430* and MZ*dicer* mutants showed that *miR-430* is responsible for targeting and depleting the pool of maternal mRNAs during the maternal-zygotic transition (MZT) (Giraldez et al., 2006). This demonstrates how a single miRNA can solely regulate one of the major developmental steps by targeting hundreds of mRNAs.

As the requirement of canonical miRNAs in vertebrate development is well-understood by generation of knockout alleles of proteins involved in miRNA biogenesis, the roles of single miRNAs are less well known. miRNA expression analyses through extensive in-situ hybridization analyses, as well as high-throughput sequencing has clearly shown that miRNAs have highly specific temporal and spatial expression patterns (Ason et al., 2006; Kloosterman et al., 2006; Kloosterman and Plasterk, 2006; Wei et al.,

2012; Wienholds, 2005). Due to embryonic lethality in zygotic Dicer1 mutants in mice, several groups generated conditional alleles of Dicer in mice and reported various tissue-specific roles of miRNAs (Amiel et al., 2012). In zebrafish, there are numerous reports of miRNAs regulating various developmental processes (Alvarez-Garcia and Miska, 2005; Wienholds and Plasterk, 2005; Zhao and Srivastava, 2007).

Our laboratory has focused on novel functions of miRNAs during zebrafish development, such as *miR-214* modulating Hedgehog signaling in muscle cell specification (Flynt et al., 2007), *miR-8* regulating osmotic stress response (Flynt et al., 2009), *miR-92* regulating the endoderm formation and left-right asymmetry (Li et al., 2011a), *miR-153* regulating synaptic transmission during neuronal development (Wei et al., 2013) and *miR-216a* regulating Notch signaling during retinal development (Olena et al., 2015).

Zebrafish Retina Regeneration

Neural degeneration in the retina is the main cause of blindness and other retinal diseases with vision impairment in humans. A potential strategy for the treatment of these types of retina diseases is to induce the regenerative potential of the retina itself. However, mammals are not capable of endogenous repair for retinal damage. Zebrafish is an ideal system to study retina regeneration because they have a full regenerative capacity upon retinal damage, which is especially intriguing because the structure, function, and cell types of the zebrafish retina are largely conserved (Fadool and Dowling, 2008; Gallina et al., 2013; Lamba et al., 2008; Stenkamp, 2007). Therefore,

understanding the molecular mechanisms controlling the robust regenerative capacity in the zebrafish retina may reveal new information to develop therapeutics for human retinal diseases.
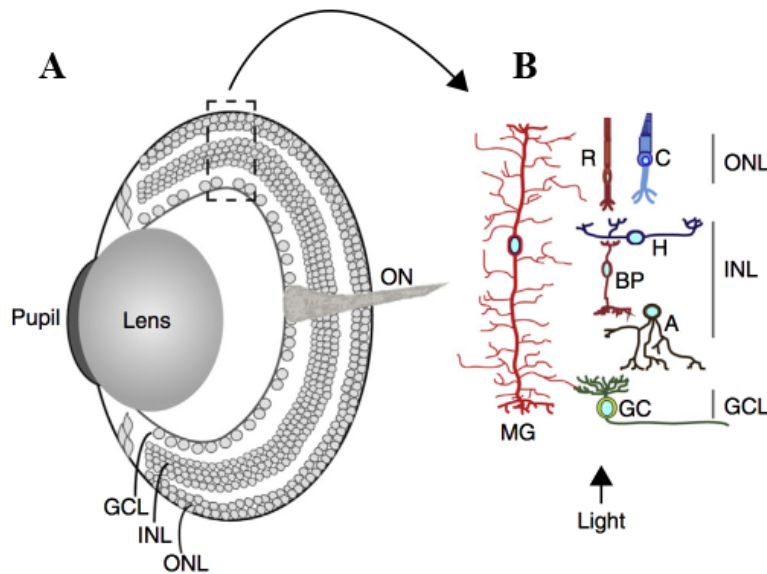
Figure 2   **Vertebrate retinal anatomy.**

(A) The diagram of the eye with the retina lining the back of the eye. Axons of the ganglion cells make up the optic nerve (ON). The retina has three nuclear layers separated by two synaptic layers; outer nuclear layer (ONL), inner nuclear layer (INL) and ganglion cell layer (GCL). (B) Illustration of the cell types located in each nuclear layer of the retina. Rod (R) and cone (C) photoreceptors are located in the ONL. Bipolar (BP), horizontal (H), amacrine (A) cells and Müller glia are located in the INL. MG's processes extend into the ONL and GCL. Ganglion cells (GC) are located in the GCL. Adapted from (Wan and Goldman, 2016)

Retina Structure

The vertebrate retina is a light-sensitive tissue lining the posterior eye and functions to convert signals from the photons into neural stimuli, followed by transmission of this information to processing centers in the brain (Bassett and Wallace, 2012). It develops as a part of the central nervous system (CNS) and forms a three-

layered structure (Fig 1) (Chuang and Raymond, 2002; Otteson et al., 2001; Stenkamp, 2007).

The outer nuclear layer (ONL) or the photoreceptor layer of the retina consists of cone and rod photoreceptors. The interneurons, including horizontal, bipolar, amacrine cells and one type of glia, Müller glia, reside in the inner nuclear layer (INL) of the retina, and retinal ganglion cells (RGCs) are in the innermost layer. There are two synaptic layers in the retina: the outer plexiform layer (OPL) that separates the ONL and the INL; and the inner plexiform layer (IPL) that separates the INL and the ganglion cell layer.

Retina Cell Types

The major classes of interneurons, ganglion cells and cone photoreceptors are further subdivided into subpopulations based on their morphology and function. It is estimated that there are more than 60 cellular subpopulations which contribute to the complex circuitry of the vertebrate retina (Masland, 2012, 2001). Recent advances in single cell RNA sequencing have confirmed that at least 39 transcriptionally distinct populations can be detected in the retinas and potentially more cell types can be identified with improved techniques (Macosko et al., 2015).

Photoreceptors are the sensory or input neurons that mediate phototransduction in the retina. Rod cells mediate dim light vision, while cone cells mediate vision in high intensity light enabling responses to different wavelengths of light (Kolb et al., 2001). In zebrafish, there are four classes of cone cells based on spectral sensitivity and morphology (Allison et al., 2010; Fadool and Dowling, 2008; Raymond et al., 1993).

Red and green-sensitive cones are paired as long double cones. The long single cones are blue-sensitive and the short single cones are ultraviolet (UV)-sensitive cones. The cones in the zebrafish retina are arranged in a "row mosaic" in which rows of blue and UV-sensitive cones alternate with rows of red and green-sensitive double cones. This geometric mosaic organization of cones is thought to be crucial for spatial resolution of color vision (Solomon and Lennie, 2007).

Bipolar cells are involved in transmitting signals from the photoreceptors to the ganglion cells. Early studies suggested that there are four main types of bipolar cells: ON, OFF, sustained and transient, based on their response to stimuli from the photoreceptors and signal types postsynaptic to bipolar cells (Kaneko, 1970; Masland, 2012; Werblin and Dowling, 1969). However, recent studies have shown that the true number of bipolar cells is 12, connected either to one cone or a few rod cells (Masland, 2012).

Horizontal cells are the inhibitory interneurons that modulate the signaling between photoreceptors and bipolar cells (Poché and Reese, 2009; Thoreson and Mangel, 2012). They are located in the upper INL and have lateral processes within the OPL. There are two or three types of horizontal cells in most vertebrates, although mice have only one type of horizontal cell. They provide inhibitory feedback to rods and cones and possibly to dendrites of bipolar cells (Masland, 2012).

Amacrine cells constitute another class of inhibitory neurons with nearly 30 different subtypes (Masland, 2012; Zhang and McCall, 2012). They have multiple connectivity and provide the majority of the synaptic input to the ganglion cells, exert inhibitory

signals at the axon terminals of the bipolar cells, and also synapse with each other (de

Vries et al., 2011; Eggers and Lukasiewicz, 2011).

Müller glia (MG) are the predominant glial cell and comprise approximately 4-5% of

all cells in the retina (Jadhav et al., 2009; Reichenbach and Bringmann, 2010a). They

have processes spanning all three layers and provide physical support to other neurons.

They also provide homeostatic and metabolic support to other neurons by regulating K+

concentration, buffering neurotransmitters, providing neurons for nutrients, and removing

metabolic waste of the neurons (Bringmann et al., 2006; Newman and Reichenbach,

1996; Reichenbach and Bringmann, 2013, 2010b). MG are also important players in

retina regeneration, as discussed below.

Ganglion cells are the output neurons of the retina, connecting visual input signals to

visual centers in the brain (Lamba et al., 2008). Since various combinations of inputs

from bipolar and amacrine cells combine, there are multiple number of functional types

of ganglion cells (Masland, 2012).

Response to retinal damage

Retinal damage response in mammals

In mammals, retina regeneration does not occur spontaneously. Endogenous

response to injury in mammalian retina typically involves reactive gliosis, which may

have neuroprotective roles early after injury but leads to detrimental effects on nearby

neurons at later stages (Bringmann et al., 2006; Bringmann and Reichenbach, 2009;

Reichenbach and Bringmann, 2010b). Some of the characteristics of reactive gliosis are

upregulation of glial fibrillary acidic protein (GFAP), hypertrophy, loss of supportive functions of MG, and formation of glial scars by some of the MG that reentered the cell cycle (Bringmann et al., 2006; Fawcett and Asher, 1999; Honjo et al., 2000). These responses of MG to injury inhibit proper retina regeneration in mammals.

Due to the lack of spontaneous neuron replacement after retinal injury, it was thought that MG only undergo reactive gliosis without any neurogenesis. However, later reports showed that MG have a neurogenesis potential but with a very limited proliferative response to injury. Neurotoxin N-methyl-D- aspartic acid (NMDA)-induced excitotoxic retinal damage was shown to promote MG dedifferentiation, cell cycle re-entry and the generation of limited numbers of new bipolar cells and rod photoreceptors (Ooto et al., 2004). The proliferative response of MG in adult mice can be stimulated even more by intraocular injections of alpha-aminoadipate (AAA), glutamate, NMDA, or N-methyl-N-nitrosourea (MNU) (Karl et al., 2008; Ooto et al., 2004; Osakada et al., 2007). Transgenic lineage tracing following NMDA induced damage and treatment with either EGF or FGF and insulin showed that MG were the source of bromodeoxyuridine (BrdU)-labeled cells, some of which later differentiated into amacrine cells (Karl et al., 2008).

Another strategy to induce reprogramming of mouse MG to a neurogenic state is to express proneural transcription factors. This strategy originated somatic cell reprogramming experiments in which fibroblasts or astrocytes in culture were directly reprogrammed to neurons using proneural transcription factors (Ang and Wernig, 2014; Guo et al., 2014; Vierbuchen et al., 2010). One such factor is achaete-scute complex-like 1 (Ascl1) which is a member of basic helix-loop-helix (BHLH) family of transcription

factors. Ascl1 is normally expressed during retinal development and regulates neural progenitor cell (NPC) proliferation (Castro et al., 2011); however it is not expressed in adult mouse retina after retinal damage or growth factor treatment (Karl et al., 2008). Interestingly, Ascl1is also capable of direct reprogramming of fibroblasts (Vierbuchen et al., 2010) and astrocytes (Berninger et al., 2007) into neurons in culture. In dissociated cultures of MG and it was shown that overexpressing Ascl1 could convert mouse MG to a neural progenitor state, confirmed by upregulation of neural progenitor genes and downregulation of glial genes, along with in vitro differentiation assays (Pollak et al., 2013). This finding led to subsequent efforts to test whether forced expression of Ascl1 was sufficient for MG reprogramming *in vivo*. By expressing Ascl1 specifically in MG using a transgenic line Glast-CreER/tetO-Ascl1, it was shown that MG are able to generate progenitors after NMDA induced damage in mice up to two weeks old (Ueki et al., 2015). MG-derived progenitors were able to give rise to neurons with detectable markers for amacrine , bipolar cells and photoreceptors. However, by postnatal day 16, MG lose their neurogenic capacity regardless of forced expression of Ascl1. Recently, the same group showed that it is possible to stimulate MG to generate neural progenitors in adult mice by using forced expression of Ascl1 approach along with treatment with a histone deacetylase inhibitor after NMDA damage in 3-5 months old adult mice (Jorstad et al., 2017). These findings, collectively, show that MG have neurogenic potential in mice although with limited proliferative response. The implications are that neurogenic capacity can be stimulated when the molecular mechanisms that normally limit the MG reprogramming are resolved and therapeutic strategies are developed accordingly.

Retina regeneration in zebrafish

Zebrafish has become a popular model organism for regeneration studies with a robust regeneration capacity of multiple tissue types including fins (Knopf et al., 2011; Nakatani et al., 2007; Thatcher et al., 2008), heart muscle (Poss et al., 2002; Zhang et al., 2013), pancreas (Curado et al., 2007; Moss et al., 2009), nervous tissue of the central nervous system (CNS), including the spinal cord (Becker et al., 1997; Goldshmit et al., 2012) and the retina (Stenkamp, 2007). Retina regeneration in teleost fish has been well

post-mitotic MG	dedifferentiated MG	NPCs	Rod cell	Cone cell
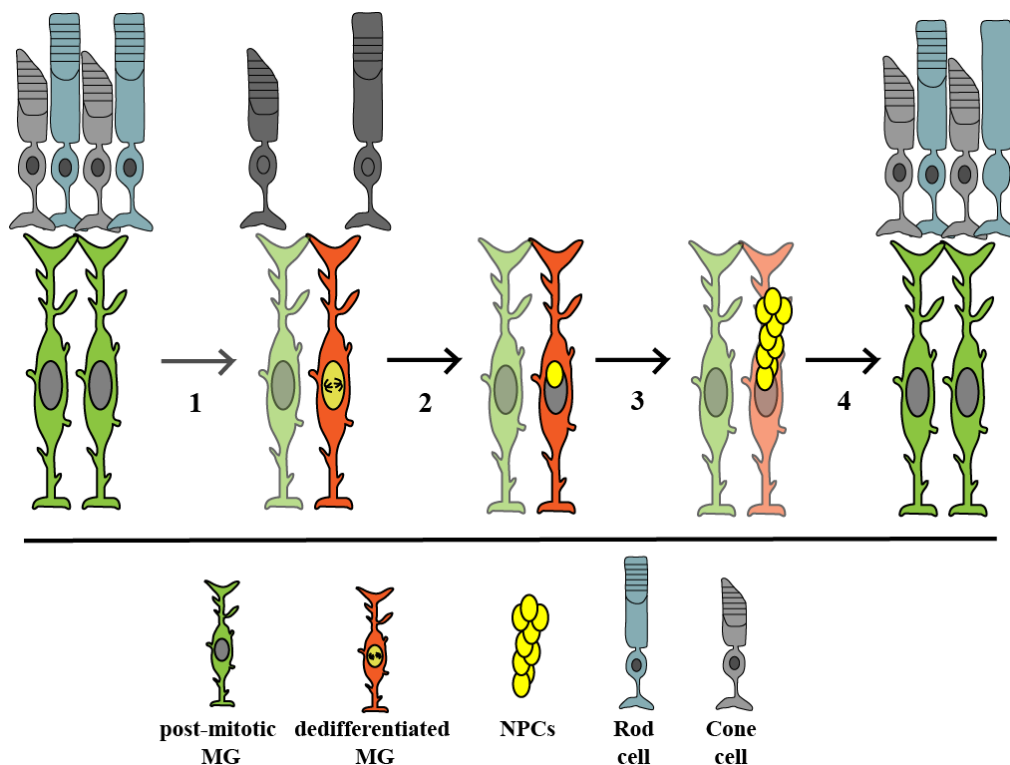
Figure 3   Zebrafish retina regeneration model upon constant intense light lesion.

(1) Constant intense light lesion leads to apoptosis of photoreceptors, rod and cones. Upon retinal damage, MG dedifferentiate into a multipotent state and re-enter the cell cycle. (2) MG undergo asymmetric cell division to give rise to a neural progenitor cells (NPCs). (3) NPCs undergo multiple rounds of cell division to produce NPC clusters which migrate to the outer nuclear layer (ONL) and differentiate into photoreceptor cells (or any missing cell type). (4) Photoreceptor cells completely regenerate 28 days after constant intense light exposure.

15

documented since initial experiments in goldfish (Lombardo, 1972, 1968). Goldfish are

capable of regenerating their retina upon partial surgical ablation. This was later

confirmed using the Na+/K+-ATPase inhibitor oubain to destroy retinal neurons (Maier

and Wolburg, 1979; Raymond et al., 1988). Interestingly, most of the cells that

proliferate upon damage did not seem to originate from the circumferential marginal zone

(CMZ), which is the site of stem cells at the periphery of the retina that normally

contribute to persistent neurogenesis throughout the life of teleost fish. Proliferating

radially elongated cell clusters were instead mostly detected in the central retina, in the

INL and ONL; their cellular origin was originally thought to be rod precursor cells

(Braisted et al., 1994; Hitchcock et al., 1992; Negishi et al., 1991; Otteson and Hitchcock,

2003).

Rod precursor cells are found in the ONL and are a persistent source of rod

photoreceptors (Stenkamp, 2011). As fish grow throughout life, the retina extends and

cones, ganglion cells and INL neurons are spaced further apart. On the other hand, rod

photoreceptors increase in density during larval development and maintain a constant

density as the retina expands (Johns and Easter, 1977; Stenkamp, 2011). Rod precursor

cells were first identified by ^{3}H-thymidine-labeling experiments (Johns and Fernald,

1981; Johns, 1982). These studies showed ^{3}H-thymidine incorporation into the ONL and,

on longer post-treatment retinal sections, incorporation into rod photoreceptor nuclei.

Interestingly, radiolabel was also associated with spindle-shaped cells associated with

Müller glial (MG) processes in the INL, although in lesser numbers (Raymond and

Rivlin, 1987). Later studies showed that the source of rod progenitors is the population

of slowly dividing cells with spherical nuclei at the base of INL, and these cells give rise

to the spindle-shaped proliferating cell clusters migrating from the INL into the ONL (Julian et al., 1998; Otteson et al., 2001).

Identification of the rod-lineage in the INL strengthened hypotheses that the source of rod precursors in the normal retina and regenerated neurons in the damaged retina could be the same. Following different types of retina damage in zebrafish including laser lesion (Wu et al., 2001), surgical lesion (Yurco and Cameron, 2005), heat lesion (Raymond et al., 2006), and constant intense light damage (Vihtelic and Hyde, 2000), the INL showed robust proliferative activity and spindle-shaped nuclei migrated from the INL to ONL along MG processes. The cells that re-enter the cell-cycle in the INL near the site of local ablation are characteristic of MG (Raymond et al., 2006; Wu et al., 2001; Yurco and Cameron, 2005). Further studies comfirmed that MG are the source of progenitor cells during retina regeneration ((R. L. Bernardos et al., 2007; Fausett and Goldman, 2006). Fausett and Goldman generated a transgenic zebrafish expressing GFP driven by a fragment of the α1 tubulin promoter (*tuba1a-GFP*) which showed GFP expression was specific to MG in injured retinas (Fausett and Goldman, 2006). By bromodeoxyuridine (BrDU) labeling and stem cell marker expression analyses, MG were shown to dedifferentiate, become multipotent, and give rise to proliferating progenitors. These findings are supported using a different transgenic fish expressing nuclear-targeted GFP in glial cells driven by the zebrafish glial fibrillary acidic protein (GFAP) regulatory elements (*gfap-nGFP*) (Rebecca L Bernardos et al., 2007). Again, GFP expression was specific to MG after retinal damage and the levels were sufficient to lineage trace the MG-derived progenitors as they proliferated and differentiated. The results support that MG are the source of rod progenitor cells in undamaged retina and also the source of

NPCs upon constant intense light damage. MG-derived NPCs replace lost photoreceptors after intense light damage (Rebecca L Bernardos et al., 2007) and also any other lost retina cell type after mechanical injury (Fausett and Goldman, 2006).

Molecular mechanisms underlying MG Reprogramming

The current model for retina regeneration in adult zebrafish is shown in Figure 3. The very first step of regeneration is that MG sense damage in the retina and consequently dedifferentiate. Extrinsic factors that are sensed by MG upon retinal damage have not been completely identified or characterized. TNF-α, produced by dying neurons, can stimulate MG to dedifferentiate (Nelson et al., 2013). However, it is still not clear whether TNF-α is sufficient to induce MG to proliferate and dedifferentiate in the undamaged retina. Ɣ-aminobutyric acid (GABA) levels decrease after photoreceptor death and a decrease in GABA levels has also been proposed to stimulate MG to dedifferentiate and proliferate (Rao et al., 2017). Other factors proposed to regulate the initiation of retina regeneration are genes encoding growth factors and cytokines including Hb-EGF, insulin, Igf-1, IL11 and leptin (Wan et al., 2014, 2012a; Zhao et al., 2014). These genes are induced in the retina after injury and are involved in stimulation of MG proliferation. However, as opposed to TNF-α and GABA-mediated MG activation, these factors are expressed by MG-derived progenitors; therefore they are likely to be acting downstream in either autocrine and paracrine fashion.

As MG sense damage, one of the first physical events observed in MG is interkinetic nuclear migration (IKM) by which injury induced MG nuclei migrate apically along radial glia processes towards the outer limiting membrane (R. L.

Bernardos et al., 2007; Lahne et al., 2015). IKM is a distinctive property of neuroepithelial cells and radial glia; and is thought to be required for mitotic division (Del Bene et al., 2008; Murciano et al., 2002).

Upon retinal damage, MG dedifferentiate to a stem cell-like state and re-enter the cell cycle. During this step, gene programs characteristic of both dedifferentiation and proliferation are induced in MG by increased expression of cell cycle genes, such as PCNA and Cyclin B1 (Kassen et al., 2007); cytoskeletal components Tuba1a (Fausett and Goldman, 2006); the proneural bHLH transcription factor gene Ascl1a (Fausett et al., 2008); and the pluripotency factor genes Lin28, Oct4, Nanog, Klf4, Myca, Mycb, and Sox2 (Ramachandran et al., 2010b). One important signaling pathway that regulates the dedifferentiation of MG is the canonical Wnt pathway (Ramachandran et al., 2011). Activation of the Wnt pathway through β-catenin stabilization is necessary and sufficient for MG to re-enter the cell cycle and produce multipotent neural progenitors. Initial reentry into the cell cycle is by asymmetric division to replace the parent cell and produce multipotent NPCs that then undergo additional rounds of replication (Rebecca L Bernardos et al., 2007; Gorsuch and Hyde, 2013; Nagashima et al., 2013; Thummel et al., 2010a, 2008). Neural progenitors continue proliferating and produce clusters of cells that migrate in close association with the radial processes of dedifferentiated MG. The adherence of neural progenitor cells to MG processes is thought to be mediated by N-cadherin (Nagashima et al., 2013). Loss of N-cadherin function leads to mislocalization of proliferating NPCs preventing them from migrating back to the INL. Only a few factors have been identified that regulate NPC proliferation. Pax6b regulates the

proliferation during early NPC cluster formation while Pax6a is responsible for NPC proliferation after the early NPC clusters have already formed (Thummel et al., 2010a).

Once the NPCs arrive at the site of damage, they exit the cell cycle and differentiate into lost neural cell types. The timing of cell cycle exit of NPCs and how they are specified to regenerate the correct cell types remains poorly understood (Gorsuch and Hyde, 2013). Apical-basal gradients of signaling environments may play a role in cell fate specification as in retinal patterning during development (Del Bene et al., 2008; Hochmann et al., 2012; Qin et al., 2011). In any case, the regenerated retina of teleost fish is fully functional and visually mediated behaviors are recovered (Fimbel et al., 2007; Mensinger and Powers, 1999; Sherpa et al., 2008).

miRNAs in Retina Regeneration

Despite the various factors and signaling pathways identified as regulators of retina regeneration, the role of non-coding RNAs is less well-understood, especially miRNAs. The first discovery for the role of miRNAs in retina regeneration was made using the zebrafish model where *lin-28* expression is induced within 6 hours of puncture-induced retinal damage leading to depletion of *let-7* in MG-derived progenitors (Ramachandran et al., 2010a). *let-7* normally represses regeneration-associated mRNAs that are required for MG dedifferentiation. Therefore, *lin-28* mediated depletion of *let-7* relieves the block for MG dedifferentiation.

Rajaram et. al. demonstrated a global requirement for the miRNAs during retina regeneration in zebrafish by showing that Dicer is required for the proliferation of the MG-derived neural progenitors (Kamya Rajaram et al., 2014a). Dynamic expression

patterns of miRNAs using RNAseq from RNA purified from whole retinas identified 36 differentially expressed miRNAs (Kamya Rajaram et al., 2014a). Using morpholino-mediated knock-down, *miR-142b, 146a, 71, 27c* and *31* were found to be required for the proliferation of MG-derived progenitors during regeneration. Among 23 miRNAs with reduced expression, *miR-203* was found to regulate NPC proliferation through targeting of *pax6b* (Kamya Rajaram et al., 2014b). Elevated levels of *miR-203* inhibit the expansion of progenitor cells but do not affect MG dedifferentiation or the initial generation of of NPCs. Interestingly, Pax6b was previously found to play a role during early neural progenitor cell divisions during retina regeneration (Thummel et al., 2010b).

Recent reports support for a conserved role for miRNAs during retina regeneration between zebrafish and mammals. Lin28-mediated inhibition of *let-7* is required for MG-derived NPC formation and proliferation after NMDA-induced retina damage in young adult mice (Yao et al., 2016). In addition, overexpression of Lin-28 through intravitreal viral-mediated gene transfer in mice is sufficient to induce MG proliferation through suppressing *let-7*.

In mice, a cell-autonomous role for miRNAs in controlling MG cell fate has recently started to be explored. miRNA expression profiles of cultured MG and freshly isolated MG from adult mouse retinas were generated using a variation of DNA microarrays, NanoString nCounter (Stefanie G. Wohl and Reh, 2016). Seven miRNAs were found to be enriched in MG, including *miR-204*, *miR-9*, and *miR-125–5p*. Conditional knockout of Dicer in mouse MG also demonstrated a global requirement for miRNAs in the maintenance of glial homeostasis and retinal architecture (Wohl et al., 2017). Also, overexpression of *miR-9* was able to partially rescue the Dicer knockout

defects in MG phenotype. Cell-autonomous role of miRNA in neurogenic potential of

MG has only been addressed in vitro by using postnatal day 12 cultured MG (Quintero et

al., 2016; Stefanie Gabriele Wohl and Reh, 2016). These studies showed evidence for the

role of miR-124-9-9 in potentiating the reprogramming of cultured MG into neurons.

Recent reports also support for a conserved role for miRNAs during retina regeneration

between zebrafish and mammals. Lin28-mediated inhibition of *let-7* is required for MG-

derived NPC formation and proliferation after NMDA-induced retina damage in young

adult mice (Yao et al., 2016). In addition, overexpression of Lin-28 through intravitreal

viral-mediated gene transfer in mice is sufficient to induce MG proliferation through

suppressing *let-7*.

Epigenetic Regulation of MG Reprogramming

Epigenetics play an essential role in the regulatory mechanisms of gene

expression (Barrero et al., 2010; Telese et al., 2013). Two main components of

epigenetic modification are DNA methylation and histone posttranslational

modifications. The main focus in this thesis will be on histone modifications.

In eukaryotic cells, DNA is organized into chromatin through highly-ordered

packaging with histone proteins. The fundamental unit is the nucleosome, in which four

histone proteins, H2A, H2B, H3 and H4, are organized into an octomeric structure

encompassing 146 bp of DNA (Kornberg, 1974; Kornberg and Thomas, 1974; Luger et

al., 1997). This core nucleosome and the unwrapped connector DNA can be visualized

as a "beads on a string" structure (Olins and Olins, 1974). One of the striking features of

histones that contributes to chromatin complexity are a group of post translational

modifications that alter the N-terminal "tails" that protrude out of the core nucleosome (Barrero et al., 2010; Kouzarides, 2007). Some of these modifications introduce changes in chromatin structure, chromatin compaction or relaxation, while others act as docking sites for recruiting and stabilizing additional protein complexes. Among the most common post translational modifications are phosphorylation of serine and lysine residues, acetylation or methylation of arginine and lysine residues, and sumoylation and ubiquitylation of specific lysine residues. Methylation in mono-, di-, or trimethyl forms adds extra complexity. The collection of enzymes that add and remove these histone modifications, as well as the proteins that interact with them are known as chromatin-modifying factors.

Genome-wide analyses of histone modifications have shown that these modifications are not uniformly distributed. Each type of modification has certain common features based on the genomic loci where they are enriched (Bernstein et al., 2012; Ernst et al., 2011; Liu et al., 2005; Pokholok et al., 2005). While acetylation of histones is almost always associated with transcriptional activation, methylation of lysine residues on histones is correlated with different transcriptional states depending on which residue is modified (Bernstein et al., 2007, 2005; Campos and Reinberg, 2009; Kouzarides, 2007). Methylation of H3 lysine 4 (H3K4), H3 lysine 36 (H3K36) and H3 lysine 79 (H3K79) mostly correlates with active transcription. On the other hand, methylation of H3 lysine 9 (H3K9), H3 lysine 27 (H3K27) and H4 lysine 20 (H4K20) are associated with the transcriptional repression. Histone acetylation leads to neutralization of positive charges and thereby a reduction in histone-DNA interactions. This mechanism is thought to drive open chromatin formation and increase the accessibility of

DNA for the transcriptional machinery (Dion et al., 2005; Hongs et al., 1993; Megee et al., 1995; Shogren-knaak et al., 2006; Zentner and Henikoff, 2013). On the other hand, methylation of lysine resides does not interfere with ionic interactions between histones and the DNA and instead alters docking sites for recruiting proteins with different methyl binding domains. For example, H3K4 tri-methylation (H3K4me3) at actively transcribed genes facilitates transcription by recruiting the chromatin remodeler CHD1 through its chromo domain (Gaspar-Maia et al., 2009). It has been also shown that H3K4me3 interacts with the TAF3 subunit of the general initiation factor TFIID, which then promotes the assembly/stabilization of the pre-initiation complex (PIC) (Lauberth et al., 2013; Vermeulen et al., 2007).

The significance of epigenetic mechanisms is well defined through chromatin modification mapping studies in embryonic stem cells (ESCs) and differentiated cell types. In pluripotent ESC, genes controlling developmental pathways, especially lineage specific transcription factors, are repressed by Polycomb group (PcG) proteins and are preferentially de-repressed during differentiation (Boyer et al., 2006; Bracken, 2006; Lee et al., 2006).

Given that reprogramming events during early development (Gifford et al., 2013; Mikkelsen et al., 2007; Vastenhouw et al., 2010), induced pluripotent stem cell (iPSC) generation (Maherali et al., 2008; Mansour et al., 2012), and nuclear transfer (Wilmut et al., 2002) involve changes in histone methylation patterns, characterizing the epigenetic regulators of MG reprogramming is more or less expected. Epigenetic regulation of zebrafish retina regeneration has been studied in the context of DNA methylation (Powell et al., 2013, 2012). Genome-wide DNA methylation analysis in purified MG showed that

transcriptional regulatory regions of regeneration and pluripotency-associated genes such as Ascl1a, Hb-egfa, lin28, Oct4 and Sox2 have low methylation levels and there is no change in the methylation levels in these regions compared to dedifferentiated MG after retinal damage (Powell et al., 2013). This suggests that regeneration-associated genes are already poised for activation in post-mitotic MG. To determine whether low DNA methylation patterns underlie the high regenerative potential of zebrafish MG, the same DNA methylation analysis was performed on mouse retinas and found to be very similar (Powell et al., 2013). Therefore, the restricted regenerative potential of mouse MG cannot be attributed to DNA methylation on regeneration-associated genes. This suggests that other epigenetic mechanisms such as posttranslational histone modifications and chromatin modifiers might be key to understanding the restricted regenerative potential of MG in mammals. Indeed, comparing young postnatal and adult mouse retinas showed that accessible chromatin in mouse mature MG decreases rapidly with age, concomitant with decreased regenerative potential (Jorstad et al., 2017; Ueki et al., 2015). However, to date, no precise histone modification signatures on regeneration-associated genes, as well as role of chromatin modifying enzymes have been identified.

Summary

The work presented in this thesis focuses on characterizing functions of miRNAs in craniofacial development and retina regeneration in zebrafish. Chapter II describes the role of *miR-27* in regulating the chondrogenesis during pharyngeal morphogenesis. Chapter III focuses on retina regeneration in adult zebrafish and describes how *miR-216*

regulates the initiation of retina regeneration through targeting a histone

methyltransferase. In Chapter IV, I present the genome-wide transcriptome analysis of

MG dedifferentiation during retina regeneration serving as a resource for further

functional analysis to discover novel miRNA-target interactions. Collectively, this thesis

demonstrates the key instructive roles of miRNAs in development and regeneration.

CHAPTER II

miR-27 REGULATES CHONDROGENESIS BY SUPPRESSING FOCAL ADHESION KINASE DURING PHARYNGEAL ARCH DEVELOPMENT

Nergis Kara, Chunyao Wei[b], Alexander C. Commanday, and James G. Patton[c]

Abstract

Cranial neural crest cells are a multipotent cell population that generate all the elements of the pharyngeal cartilage with differentiation into chondrocytes tightly regulated by temporal intracellular and extracellular cues. Here, we demonstrate a novel role for *miR-27*, a highly enriched microRNA in the pharyngeal arches, as a positive regulator of chondrogenesis. Knock down of *miR-27* led to nearly complete loss of pharyngeal cartilage by attenuating proliferation and blocking differentiation of pre-chondrogenic cells. Focal adhesion kinase (FAK) is a key regulator in integrin-mediated extracellular matrix (ECM) adhesion and has been proposed to function as a negative regulator of chondrogenesis. We show that FAK is downregulated in the pharyngeal arches during chondrogenesis and is a direct target of *miR-27*. Suppressing the accumulation of FAK in *miR-27* morphants partially rescued the severe pharyngeal cartilage defects observed upon knock down of *miR-27*. These data support a crucial role for *miR-27* in promoting chondrogenic differentiation in the pharyngeal arches through regulation of FAK.

Keywords

Introduction

Craniofacial abnormalities are among the most common human birth defects, cleft lip and palate being among the five most common congenital malformations (Gorlin et al., 1990). Although an increasing number of genetic mutations have been implicated with these malformations, there is limited information about the etiology of congenital craniofacial disorders. In zebrafish, many features that control craniofacial development and pharyngeal skeletal elements are conserved with that of higher vertebrates (Yelick and Schilling, 2002). Most skeletal structures in the skull and the entire pharyngeal skeleton are derived from a unique population of cells, cranial neural crest (CNC) cells (Couly et al., 1993; Lumsden et al., 1991; Schilling and Kimmel, 1994). CNC cells migrate from the dorsal neural tube in three streams to populate the pharyngeal arches. Post-migratory CNC cells go through mesenchymal condensation during which pre-chondrogenic cells (PCCs) aggregate and increase their cell-cell contacts. Coincident with dynamic changes in the extracellular matrix (ECM), PCCs differentiate into chondrocytes surrounded by a type-II collagen and aggrecan rich matrix (Hall and Miyake, 2000; Kozhemyakina et al., 2015).

Vertebrate CNCs are a migratory, multipotent cell population, able to differentiate into cartilage, bone, teeth forming cells, and non-ectomesenchyme derivatives, such as neurons, pigment cells and glia (Baroffio et al., 1991). Chondrogenic differentiation of CNC cells is regulated by various signaling pathways including Tgf-β, Bmp, and Fgf pathways, as well as changes in cell shape (Kozhemyakina et al., 2015). As cell-cell interactions increase during mesenchymal condensation, PCCs become more rounded. Recent studies have shown that restricting cell spreading on synthetic substrates, or by

maintaining high-cell density to prevent cell spreading, promotes chondrogenic differentiation of mesenchymal stem cells (Gao et al., 2010; McBride and Knothe Tate, 2008). Interestingly, mechanical forces or changes in the ECM that perturb cell shape lead to the formation of integrin-mediated focal adhesions, which in turn prevents chondrogenesis (Eyckmans et al., 2011; Tang et al., 2013a; Yim and Sheetz, 2012). Focal adhesion kinase (FAK) is a non-receptor tyrosine kinase and an essential component of focal adhesions (Parsons, 2003). Apart from its well-established roles in cell adhesion and migration, FAK is also involved in regulating mesenchymal stem cell fates in response to cell shape changes and integrin-$\beta 1$ activation (Mitra et al., 2005; Pala et al., 2008; Takahashi et al., 2003; Tang et al., 2013a). Exactly how FAK is regulated in the pharyngeal arches during chondrogenesis is not known.

miRNAs are small noncoding RNAs that regulate the expression of target mRNAs at the post-transcriptional level. miRNAs bind to the 3'UTR of their targets with imperfect base pairing and induce deadenylation, translational repression, and degradation of the target mRNA (Huntzinger and Izaurralde, 2011; Krol et al., 2010). Tissue-specific expression of miRNAs allows them to regulate multiple developmental processes in diverse organisms (Flynt et al., 2007; Giraldez et al., 2005; Li et al., 2011b; Wei et al., 2013; Wienholds, 2005). Previous studies reported that miRNAs are required for skeletal development using mice with conditional deletion of Dicer, an RNaseIII-like enzyme required for miRNA biogenesis, in either NC cells or early chondrocytes in the craniofacial cartilage or growth plate (Kobayashi et al., 2008; Zehir et al., 2010). Global deficiency of all miRNAs in NC cells resulted in the loss of the majority of NC-derived craniofacial cartilage and bone (Zehir et al., 2010). These studies show that miRNA

expression is crucial for skeletal development but only a small subset of miRNAs have been characterized as to their targets and control of whole organism cartilage and bone development (*miR-92a*, *miR-140* and *miR-452*) (Eberhart et al., 2008; Nakamura et al., 2011; Ning et al., 2013; Sheehy et al., 2010).

In this study, we demonstrate a novel role for *miR-27*, a highly conserved miRNA family, during craniofacial cartilage development. Knock down of *miR-27* inhibited pharyngeal arch morphogenesis and caused severe defects in the neurocranium. We show that these craniofacial defects are caused by impaired proliferation and differentiation of chondrogenic progenitors. Knock down of *ptk2aa (FAK),* a direct target of *miR-27*, can partially rescue the cartilage defects in *miR-27* morphants indicating a novel mechanism whereby *miR-27* regulates chondrogenic differentiation in the pharyngeal arches through modulation of FAK levels.

Results

Zebrafish miR-27 is expressed in pharyngeal arches

In zebrafish, there are five members of the *miR-27* family with nearly identical mature miRNA sequences, but encoded on separate chromosomes (**Fig. 4A**). *miR-27* is a highly conserved miRNA family, the sequences of mature *miR-27a* among different vertebrate species are identical except for a single nucleotide at the 3' end (**Fig. 4B**). The seed sequences are identical among family members suggesting that identical target mRNAs are commonly regulated. Microarray and high-throughput sequencing analyses during early zebrafish development have shown that *miR-27* family members are

expressed as early as 24 hours post fertilization (hpf), but upregulated at later stages (Wei et al., 2012; Wienholds, 2005).
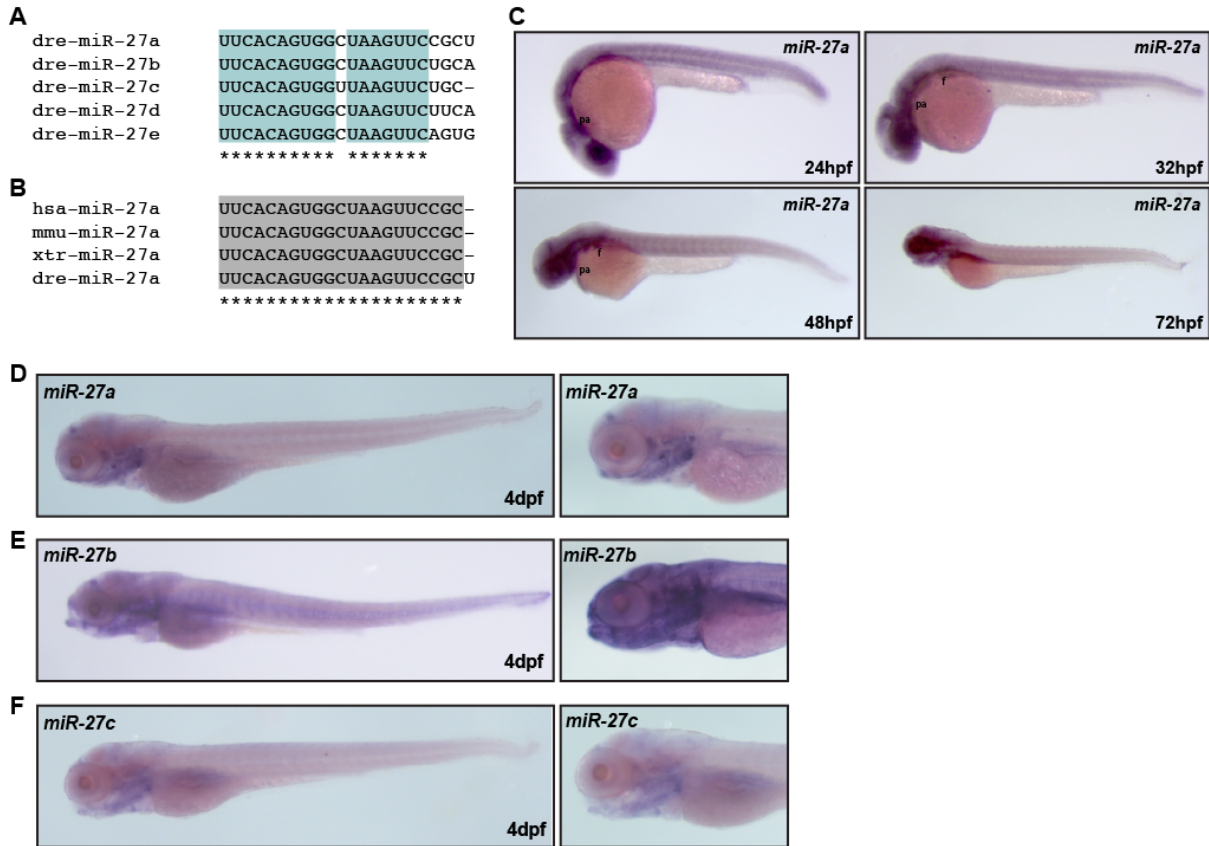
Figure 4 *miR-27* is a highly conserved miRNA with enriched expression in the pharyngeal arches.

(A) Alignment of the zebrafish *miR-27a-e* sequences by ClustalW2, with conserved regions highlighted in blue and indicated with stars. (B) Alignment of *miR-27a* sequences from human (hsa), mouse (mmu), xtr (Xenopus), and dre (zebrafish). (C) *miR-27a* expression in embryos between 24 hpf to 72 hpf, detected by whole-mount *in situ* hybridization. Expression of *miR-27a* (D), *miR-27b* (E), *miR-27c* (F), in 4dpf embryos detected by whole-mount *in situ* hybridization. Lateral views with images on the right are closed up views of the head.

To determine the onset of expression of each *miR-27* member, we performed qRT-PCR at several key developmental stages starting from the 1-cell stage **(Fig.5A,B)**. Overall, all *miR-27* members have low expression levels between the 2 somite-stage (2ss) and 24hpf,

while their expression is upregulated starting at 48hpf, reaching a peak at 72hpf. *miR-27c* is expressed at significantly higher levels compared to other members, while *miR-27d* and *miR-27e* have very low expression levels throughout the stages we analyzed. For this reason, we focused on spatial expression of *miR-27a*, *miR-27b* and *miR-27c* by performing whole-mount *in situ* hybridization by locked nucleic acid (LNA) probes on zebrafish embryos (**Fig. 5C-E, Fig. 4C-F).** At 4dpf, *miR-27a, b and c* are expressed strongly in the pharyngeal arches **(Fig. 5C-E, Fig. 4D-F)**. Earlier during development, *miR-27a* is detected in the pharyngeal arch primordia that are composed of post-migratory chondrocyte progenitors, as well as in the eye, vasculature, the midbrain-hindbrain boundary (MHB), and the pectoral fins at 24 and 32 hpf **(Fig. 4C)**. At 48 and 72hpf, *miR-27a* expression is more confined to the pharyngeal cartilage, cartilage joints and pectoral fins along with less expression in the ethmoid plate (EP) and brain. Strong expression of *miR-27* in the pharyngeal arches, as well as earlier prechondrogenic mesenchyme, suggest that *miR-27* may regulate cartilage development in zebrafish.

Knockdown of miR-27 leads to craniofacial and pectoral fin cartilage defects

To determine the function of *miR-27*, we performed loss-of-function experiments by injecting antisense morpholinos against *miR-27*. The first morpholino we tested was designed complementary to the mature *miR-27* sequence (MO-27) and targets all members of the *miR-27* family **(Table 1)**. Injection with MO-27 resulted in approximately 70% loss of *miR-27* (**Fig. 5J**). Knockdown of *miR-27* did not lead to any gross morphological changes during early development, but by 3 dpf and even more so
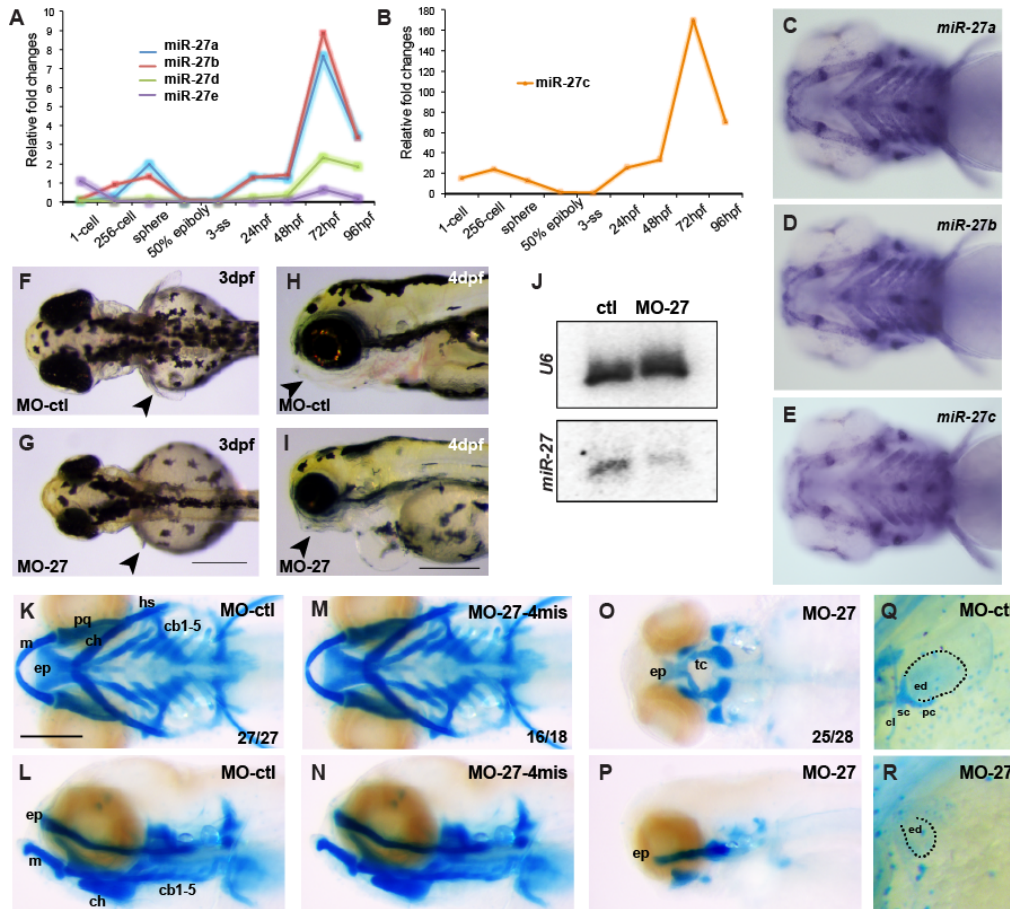
Figure 5 Knock down of *miR-27* leads to craniofacial and pectoral fin defects.

(A,B) qRT-PCR for *miR-27a-e* at the indicated developmental stages normalized to U6 snRNA. Fold changes were calculated using $\Delta\Delta C(t)$ method comparing all *miR-27* levels to *miR-27c* levels at the 3 somite stage (ss). Due to comparably higher levels, *miR-27c* expression profile is shown separately. (C-E) Expression of *miR-27a, miR-27b* and *miR-27c* in 4dpf embryos detected by whole-mount *in situ* hybridization by locked nucleic acid (LNA) probes. All are ventral views of the head. (F,G) Dorsal view of 3 dpf live embryos injected with either 5ng standard control morpholino (MO-ctl) or MO-27 at the single-cell stage. Pectoral fins are indicated with arrowheads. (H,I) Morphology of the head in 4 dpf embryos injected with either MO-ctl or MO-27. Lateral views, jaws are indicated with arrowheads. Scale bar, 300µm. (J) *miR-27* and *U6* levels in uninjected control and *miR-27* morpholino (MO-27) injected embryos at 48hpf detected by Northern blot. (K-P) Head cartilages stained with Alcian blue in 4dpf embryos injected with (K,L) standard control morpholino (MO-ctl), (M,N) 4-mismatch *miR-27* morpholino (MO27-4mis) and (O,P) MO-27. Top panels, ventral views; bottom panels, lateral views. The indicated ratio represents the number of embryos with the represented phenotype/total number of observed embryos. Cartilage labels: ep, ethmoid plate; tc, trabeculae cranii; m, Meckel's cartilage; pq, palatoquadrate; ch, ceratohyal; hs, hyosymplectic; cb, ceratobranchial. Anterior side of the embryos is to the left. (Q,R) Staining of pectoral fin skeleton in 4dpf embryos by Alcian blue. The right side pectoral fin is shown with anterior to the top. The cleithrum (cl) and scapulocoracoid (sc) cartilages and postcoracoid process (pc) of pectoral fins are missing and the endoskeletal disc cartilage (ed) is smaller in *miR-27* morphants compared to the controls. Scale bar, 200 µm.

34

by 4 dpf, *miR-27* morphants displayed pectoral fin outgrowth defects and severely

reduced pharyngeal cartilage, concomitant with smaller heads and eyes (**Fig. 5F-I**). To

analyze the cartilage defects more specifically, we performed Alcian blue staining. In

miR-27 morphants, nearly all of the cartilage in the pharyngeal arches, as well as in the

pectoral fins, was missing (**Fig. 5O-R**). In addition, *miR-27* knockdown led to an

abridged palate in the neurocranium, where the bilateral trabeculae were joined in the

midline but the ethmoid plate did not extend properly. Closer examination of the pectoral

fins revealed that the cleithrum (cl) and scapulocoracoid (sc) cartilages and postcoracoid

process (pc) of pectoral fins were missing and the endoskeletal disc cartilage (ed) was

smaller in *miR-27* morphants compared to the controls **(Fig. 5Q,R)**.

To ensure specificity with the morpholino knockdowns, we performed a series of

control experiments. First, apart from the use of a standard control morpholino (MO-ctl;

Gene Tools), we designed a morpholino containing four-base mismatches (MO27-4mis)

compared to MO-27 **(Fig. 5M,N)**. MO27-4mis injection did not cause any defects in

pharyngeal arch morphogenesis. Second, we designed a third set of morpholinos

complementary to the loop sequences of each precursor *mir-27* member **(Fig. 7A-C,**

Table 1). Compared to MO-27 which targets all *miR-27* family members, loop

morpholinos target individual family members by inhibiting the processing of the

corresponding precursor miRNA (Kloosterman et al., 2007). Knock down of *miR-27a* by

MO27a loop led to exactly the same phenotype as the MO-27 injections with loss of

nearly all the pharyngeal cartilage and a severely reduced neurocranium. **(Fig.7A)**.

Knock down of *miR-27b* using the MO27b loop morpholino led to loss of branchial
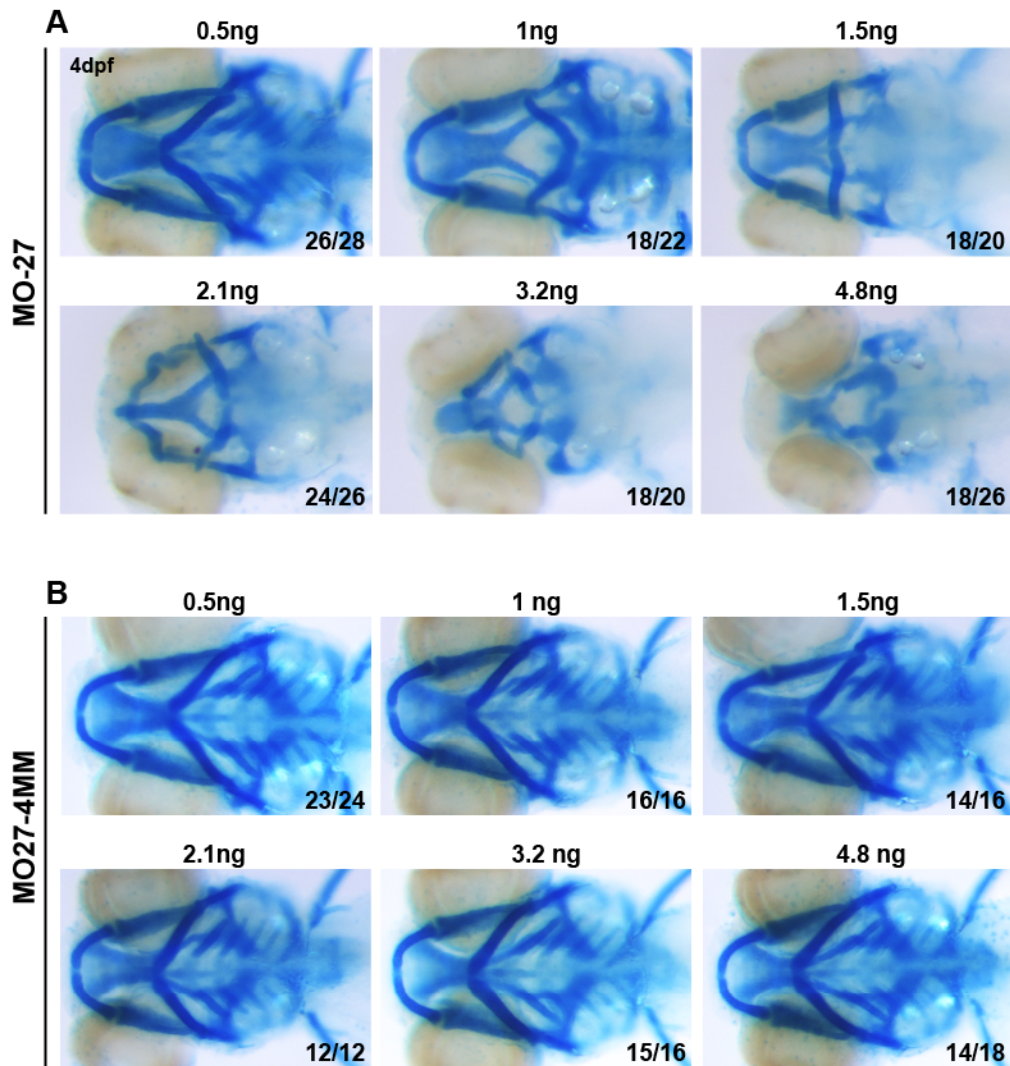
Figure 6 Dose-dependent changes in cartilage defects by mature *miR-27* knock-down.

(A) Head cartilage staining by alcian blue of 4 dpf old embryos injected with different doses of the MO-27 morpholino. (B) Head cartilage staining by alcian blue of 4 dpf old embryos injected with different doses of the MO-27-4MM morpholino that is complementary to the mature *miR-27* with 4 base-pair mismatches. All are ventral views and the ratio of the observed phenotype to the total number of embryos is shown for each image.

arches along with severely reduced Meckel's and ceratohyal cartilage, as well as an

abridged neurocranium **(Fig. 7B)**. In contrast, knockdown of *miR-27c* did not affect the

pharyngeal arches **(Fig. 7C)**. These experiments enabled us to determine which *miR-27*

members are involved in pharyngeal cartilage formation, as well as provide evidence that the defects observed upon loss of all *miR-27* family members using the MO-27 morpholino are unlikely to be due to nonspecific effects or toxicity. In addition, the effects of the MO-27 and *miR-27* loop morpholinos were dose dependent across an order of magnitude concentration as determined by alcian blue staining on embryos injected with different doses **(Fig. 6A-B, Fig.7A-C)**. Injection of the mismatch morpholino did not generate any observable phenotypes at any concentration tested **(Fig. 6A,B)**. Knockdown *miR-27a* and *miR-27b* separately also showed dose-dependent defects in pharyngeal cartilage formation **(Fig. 7A,B)**. Finally, we tested the knockdown efficiency of each morpholino. By Northern blots, we confirmed approximately 70% loss of *miR-27* upon MO-27 injection at the single cell stage **(Fig. 5J)**. To determine the efficacy of the miRNA loop morpholinos, we performed qRT-PCR for *miR-27a*, *miR-27b* and *miR-27c* in 48hpf embryos injected with two different concentrations of MO-27a loop, MO-27b loop and MO27c loop **(Fig. 7E-G)**. All loop morpholinos led to knockdowns in the range of 50-90% of the targeted mature *miR-27*.

As *miR-27* is required for pharyngeal arch development, we next tested whether conditional *miR-27* overexpression would induce any craniofacial cartilage defects as well. To conditionally overexpress *miR-27*, we established two separate transgenic lines, *Tg(hsp70l:miR27^{eGFP})* in which pri-*miR-27b* is expressed under the heat shock promoter (hsp70l), and *Tg(sox10:miR-27^{eGFP})* in which pri-*miR-27* is expressed under the neural-crest specific sox10 promoter **(Fig. 8)**. We induced the expression of *miR-27* in *Tg(hsp70l:miR27^{eGFP})* at 24 hpf and confirmed upregulation at 48hpf by qRT-PCR **(Fig. 8B)**. After overexpression, we performed alcian blue staining at 4 dpf and detected no
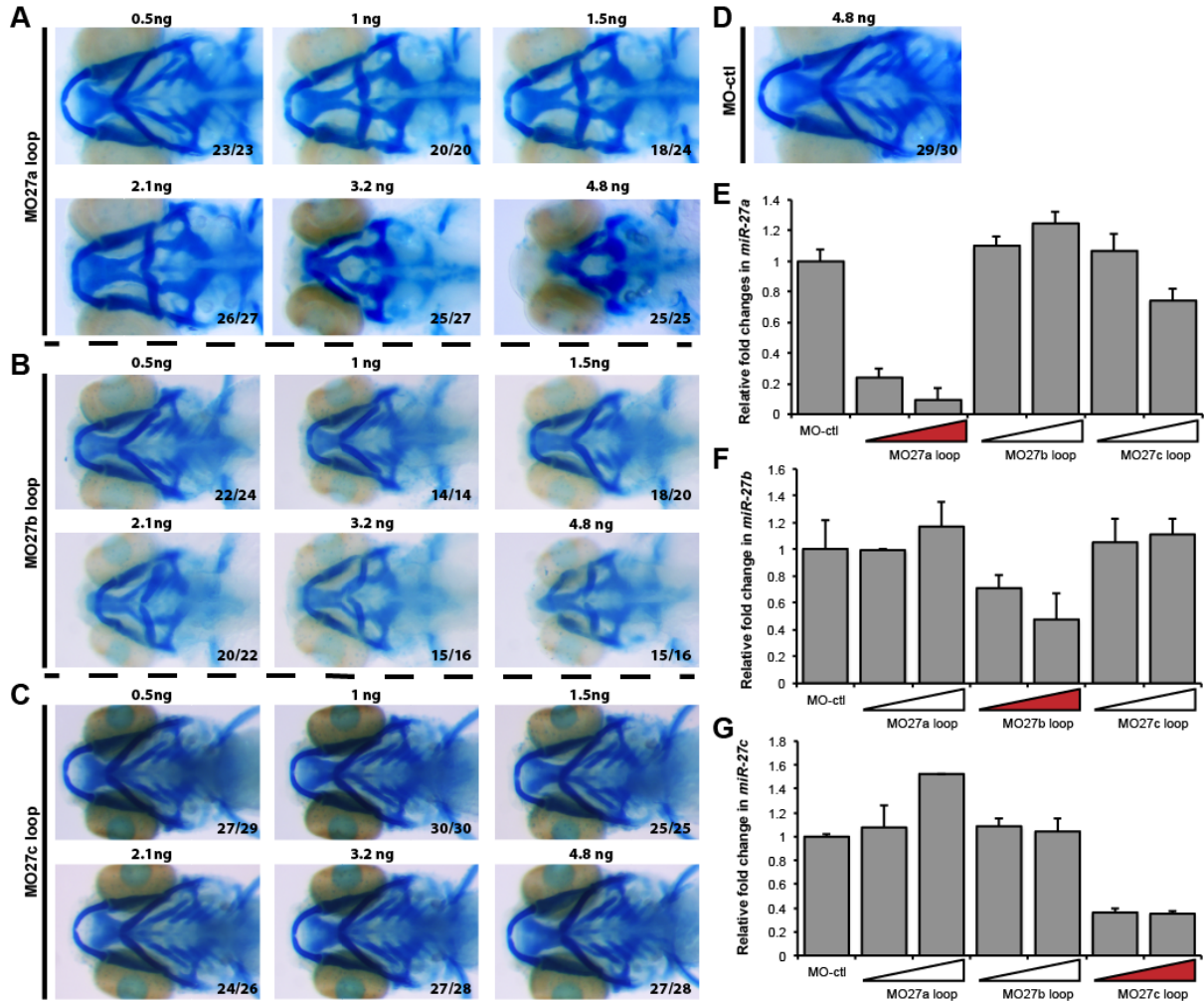
Figure 7 Dose-dependent changes in cartilage defects by mature *miR-27 a, b and c* knock-down.

Head cartilage staining of 4 dpf old embryos injected with different doses of the MO-27a loop (A) MO-27b loop (B) MO-27c loop (C) morpholinos complementary to the loop and Dicer cleavage site of the corresponding precursor *miR-27*. All are ventral views and the ratio of the observed phenotype to the total number of embryos is shown for each image. (D) Alcian blue staining of the 4dpf embryos injected with 4.8 ng MO-ctl. qRT-PCR of *miR-27a* (E), *miR-27b* (F), and *miR-27c* (G) in 30hpf old embryos injected with 4.8ng MO-ctl, MO27a loop, MO27b loop, and MO27c loop at either 2.4ng or 4.8ng.

significant differences in the pharyngeal cartilage as well as in the neurocranium in $hsp70:miR27^{eGFP}$ transgenic embryos relative to their non-transgenic siblings **(Fig. 8A)**. When *miR-27* was overexpressed in the sox10+ NC cells in *Tg(sox10:miR-27b^{eGFP})* embryos, we again did not detect any defects in craniofacial cartilage morphogenesis in the transgenic embryos compared to their non-transgenic siblings **(Fig.8C)**.
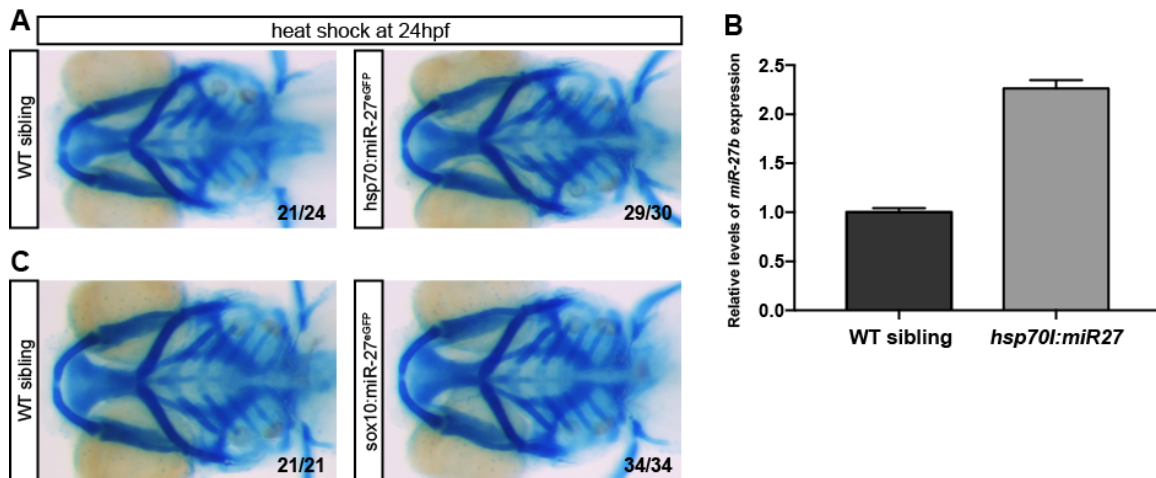
Figure 8   Conditional and neural crest-specific *miR27* overexpression does not lead to any defects in pharyngeal arch morphogenesis.

(A) Alcian blue staining of heat shocked Tg*(hsp70:miR-27b-eGFP)* and wild-type siblings. Heat shock was performed at 24 hpf and embryos were fixed and stained at 4dpf. Images are ventral views of the head cartilage and the ratio of the observed phenotype to the total number of embryos is shown for each image. (B) qRT-PCR of *miR-27b* in 72hpf old Tg*(hsp70:miR-27b-eGFP)* and wild-type siblings. Relative *miR-27b* levels were normalized to control U6 snRNA.

miR-27 is required in post-migratory CNC cells for proper pharyngeal arch morphogenesis

Because craniofacial cartilage elements are derived from ectomesenchymal CNC cells, we tested whether *miR-27* knockdown perturbs early neural crest migration. To determine whether the migration of CNC cells was affected, we analyzed CNC cells

during migration into the pharyngeal arches using a transgenic line that expresses another marker of CNC cells, *sox10* (*Tg(sox10(7.2):mRFP)vu234)*(Dutton et al., 2001). The *sox10*[+] arches did not differ in size between embryos at 18 and 24 hpf (**Fig. 9A**). Complementary *in situ* hybridization experiments for *sox10* and another CNC cell marker, *dlx2a*, showed the same expression patterns at 16 hpf and 22 hpf in morphants and controls (**Fig. 9B,C**), suggesting that *mir-27* knockdown does not affect CNC cell specification or migration.
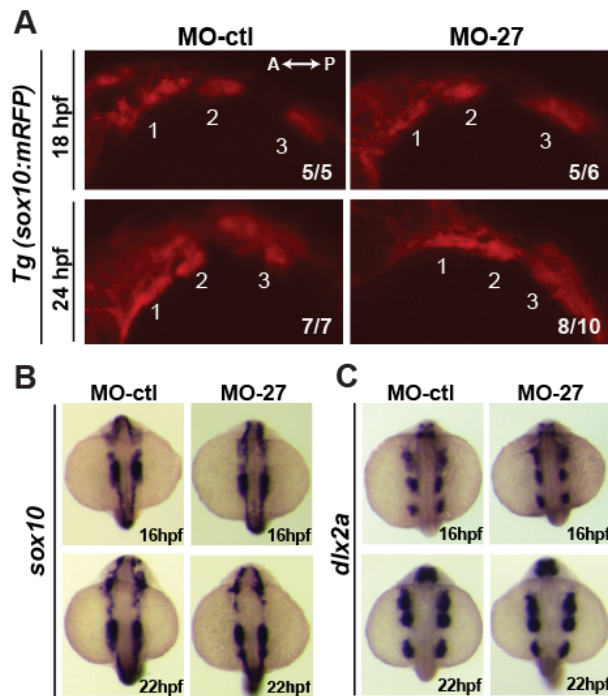
Figure 9   Early cranial neural crest (CNC) cell specification and migration are not affected in *miR-27* morphants.

(A) Lateral view of *Tg(sox10(7.2):mRFP)vu234* embryos injected either with MO-ctl or MO27 showing cranial neural crest cell streams populating the pharyngeal arches at 18hpf and 24hpf. Anterior is to the left and posterior is to the right. Neural crest streams are numbered from 1-3. The indicated ratio represents the number of embryos with the represented phenotype/total number of observed embryos. (B,C) Expression of the neural crest cell marker, *sox10*, and CNC marker *dlx2a* in MO-ctl and MO27 embryos at 16 hpf and 22 hpf detected by whole-mount *in situ* hybridization. Dorsal view of embryos with anterior side to the top.

To determine the earliest time point when the *miR-27* morphants show defects in craniofacial development, we analyzed pre-cartilage condensation within the pharyngeal arches using a transgenic line marking the ectomesenchyme lineage of CNC cells (*Tg(fli1a:eGFP)y1*) (Lawson and Weinstein, 2002) (**Fig. 10A**). In *Tg(fli1a:eGFP)y1* embryos at 26 hpf, we did not detect any differences in the size and patterning of the *fli:EGFP$^+$* arches. However, at 30 and 36 hpf, the size and fluorescence intensity of the *fli1a:eGFP$^+$* arches were significantly perturbed in the *miR-27* morphants (**Fig. 10A,B**). We also detected reduced expression domains for the post-migratory CNC cell marker, *dlx2a*, at 36 hpf in the posterior pharyngeal arches, while at 30 hpf there was not a detectable reduction in *dlx2a* expression yet (**Fig. 10C,D**). It is important to note that by 36 hpf, the patterning of the pharyngeal arches was similar between control embryos and *miR-27* morphants, while elongation of the arches along the dorsal-ventral axis was disrupted upon *miR-27* knockdown. By 48 hpf, defects in the pharyngeal arch sizes were more severe in the morphants and morphogenesis of the first two arches was not complete **(Fig. 10A, B)**. These data suggest that the onset of the pharyngeal arch morphogenesis defects upon loss of *miR-27* is between 30 and 36 hpf.

To gain insight into the requirement of *miR-27* in pharyngeal arch morphogenetic movements, we performed *in vivo* time-lapse imaging of pre-chondrogenic crest cells in *Tg(fli1a:eGFP)y1* embryos. Time-lapse imaging showed that migration of CNC cells into the pharyngeal arches in the anterior-posterior axis was slower in *miR-27* morphants compared to the controls. Convergence of the first two arches by 48hpf was not complete in the morphants as the first pouch in between the two arches was still visible, while in
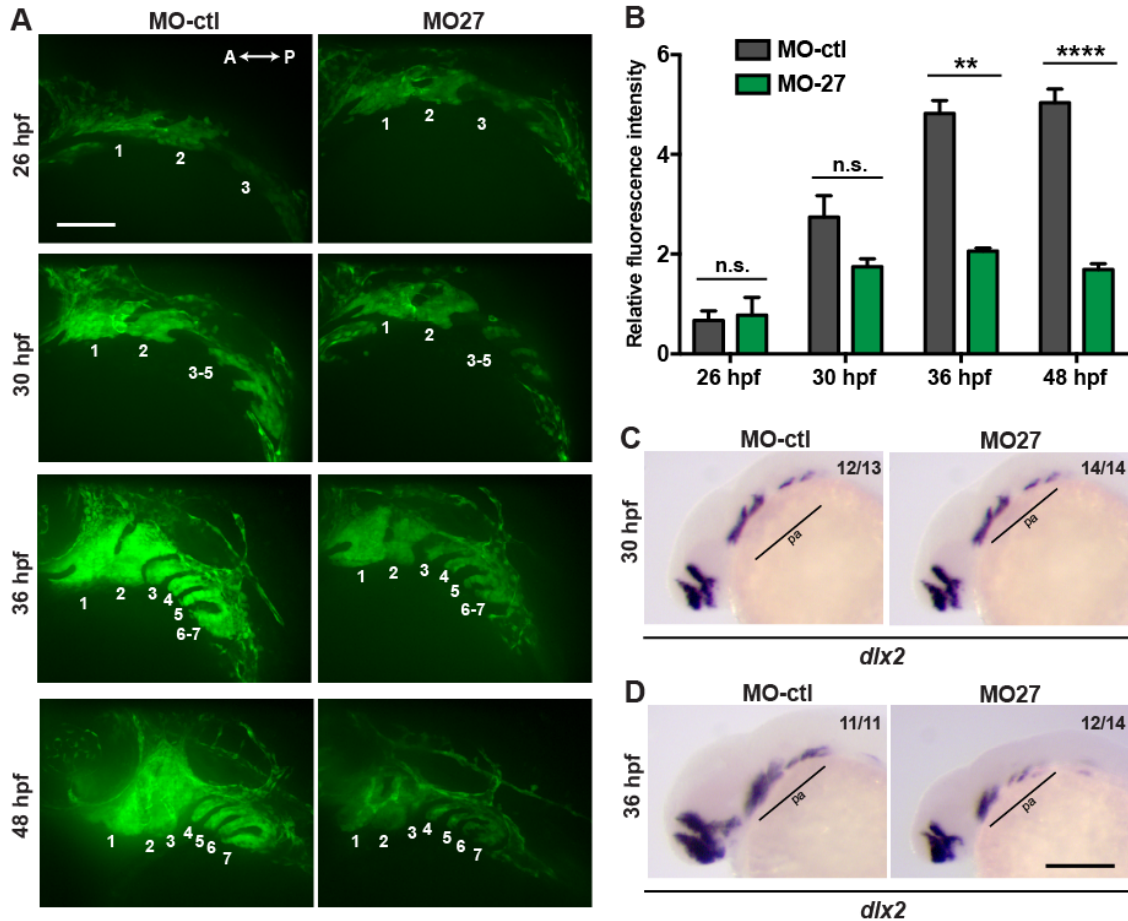
Figure 10   Morphogenesis of the pharyngeal arches is disrupted in *miR-27a* morphants between 30 and 36hpf.

(A) Live images of *Tg(fli1a:eGFP)y1* embryos at 26, 30, 36, 48 hpf; lateral views with anterior to the left. Each pharyngeal arch is numbered. Embryos were injected with either 5ng MO-ctl or MO-27 at the single cell stage and observed with confocal microscopy at the indicated stages. Time-lapse videos captured by spinning-disk confocal microscopy are shown in Supp. Movies 1 and 2. Scale bar, 100 μm. (B) Quantification of normalized and relative *fli1a:eGFP* fluorescence intensity in the pharyngeal arches of MO-ctl and MO-27 embryos at the indicated time points. The relative fluorescence intensities were normalized to the area of the arches selected and the fluorescence background in each image. Error bars indicate SEM and the number of embryos analyzed is indicated above the bars. For 26 hpf, n=3; for 30 hpf, n=5; for 36 hpf, n=4; for 48 hpf, n=4. Data represent three independent experimental trials. The n.s. non-significant, **p<0.01, ****p<0.0001 (Student's t-test). (C-D) Expression of the CNC marker *dlx2a* in embryos at 30 and 36 hpf. Embryos were injected with the corresponding morpholinos as described above. Pharyngeal arch expression domains are labeled. The indicated ratio represents the number of embryos with the represented phenotype/total number of observed embryos. Scale bar, 200 μm.

control embryos the first two arches did not have any clear boundary at this point (**Movies A1 and A2**). These findings suggest that *miR-27* is required for pharyngeal arch morphogenesis, but not in early patterning of the arches by 30hpf.

miR-27 is required for the differentiation of pre-chondrogenic crest cells

To identify what stage of cartilage development *mir-27* regulates, we analyzed pharyngeal mesenchymal condensation and chondrogenic differentiation of post-migratory PCCs. To assess mesenchymal condensation, we stained with peanut agglutinin (PNA), a lectin that preferentially binds to the cell surface during condensation (Hall and Miyake, 1995). PNA staining of the *fli1a:eGFP*[+] PCCs showed that mesenchymal condensations were equally detectable in *miR-27* morphants and control embryos at 48 hpf (data not shown). Next, we analyzed the distribution of the extracellular matrix (ECM) protein fibronectin which is highly expressed during mesenchymal condensation (Hall and Miyake, 2000; Singh and Schwarzbauer, 2014). PCCs in both morphants and control embryos had equal fibronectin matrix distribution at 48 hpf (**Fig. 11**). To analyze the differentiation of PCCs, we performed *in situ* hybridization for the chondrogenic differentiation marker *sox9a* (Bi et al., 1999; Yan et al., 2002) at 55 hpf and for *col2a1a*, the major collagen in chondrocytes, at 72hpf (**Fig. 12A**). Both markers showed reduced expression domains in the ethmoid plate precursor and first two pharyngeal arches, as well as complete loss of expression in the ventral pharyngeal arches of the *miR-27* morphants. We could not detect expression of the osteogenic differentiation marker, *runx2b* (Flores et al., 2004) in the pharyngeal arches of *miR-27* morphants at 60hpf.
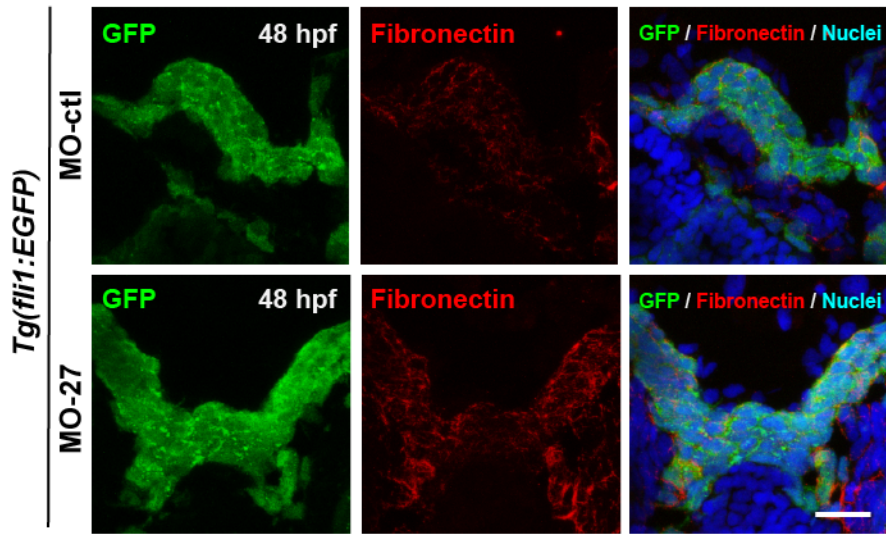
Figure 11 **Fibronectin matrix of pre-chondrogenic crest (PCC) cells during mesenchymal condensation is not affected by *miR-27* knock down.**

Anti-fibronectin and anti-GFP immunostaining in transverse sections of *Tg(fli1a:eGFP)y1* embryo heads at 48hpf. Embryos were injected with either 5ng MO-ctl or MO-27 at the single cell stage. TOPRO-3 was used as a nuclei marker.

To assess the differentiation of PCCs further, we analyzed mature chondrocytes in the pharyngeal arches by immunostaining with anti-Col2 in *fli1a:eGFP* embryos at 61hpf. In control embryos we could easily detect *fli1a:eGFP*^{+} cells in the first two arch condensations that are secreting Col2 into the ECM, while in *miR-27* morphants there were very few to no Col2^{+} *fli1a:eGFP*^{+} cells detected (**Fig. 12B**). To determine whether *miR-27* only perturbs collagen production or completely blocks chondrogenic differentiation, we performed wheat germ agglutinin (WGA) staining to detect mature chondrocytes. WGA staining indicated that in *miR-27* morphants, mature chondrocytes are missing, while the control embryos had WGA labeled chondrocytes in *fli1a:eGFP*[+] condensations at 61hpf. These results together suggest that loss of *miR-27* does not affect mesenchymal condensation of CNC cells, but completely blocks differentiation of pharyngeal PCCs.
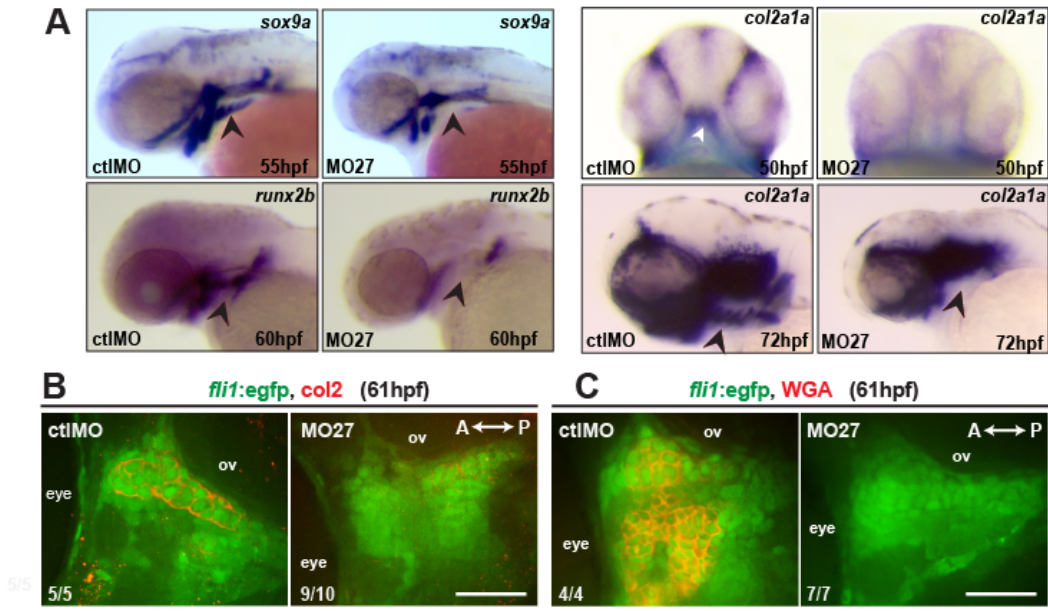
Figure 12   ***miR-27*** **is required for differentiation of pre-chondrogenic crest (PCC) cells in pharyngeal arches.**

(A) Expression of the chondrogenic marker *sox9a*, the osteogenic marker, *runx2b,* and the chondrocyte-specific marker *col2a1a* in MO-ctl or MO-27 (5ng) injected embryos, detected by whole-mount *in situ* hybridization. Arrowheads indicate the expression domain of the ceratobranchial arches. All panels except the top panel for *col2a1a* are lateral views. Top panel for *col2a1a* expression is a ventral view with the first pharyngeal arch indicated by an arrowhead. (B) Anti-Col2 and anti-GFP immunostaining in the pharyngeal arch region between the eye and otic vesicle (ov) in *Tg(fli1a:eGFP)y1* embryos at 61hpf. A single optical section of the confocal stacks is shown in each image, with anterior to the left. Embryos were injected with the corresponding morpholinos as described above. (C) Wheat-germ agglutinin staining and anti-GFP immunostaining in the pharyngeal arch region between the eye and otic vesicle (ov) in *Tg(fli1a:eGFP)y1* embryos at 61hpf. The indicated ratio represents the number of embryos with the represented phenotype/total number of observed embryos. Scale bar, 50 μm.

miR-27 knock down impairs the PCC proliferation and survival

Defects in the extension of the pharyngeal arches in *miR-27* morphants suggest that inactivation of *miR-27* causes PCC proliferation defects. We analyzed the proliferation of pre-chondrogenic cells at 30 and 36 hpf, the earliest time points where defects can be detected in the pharyngeal arches (**Fig. 10A**). Immunostaining for phosphorylated histone 3 (pH3) in *fli1a:eGFP* embryos showed that there was a
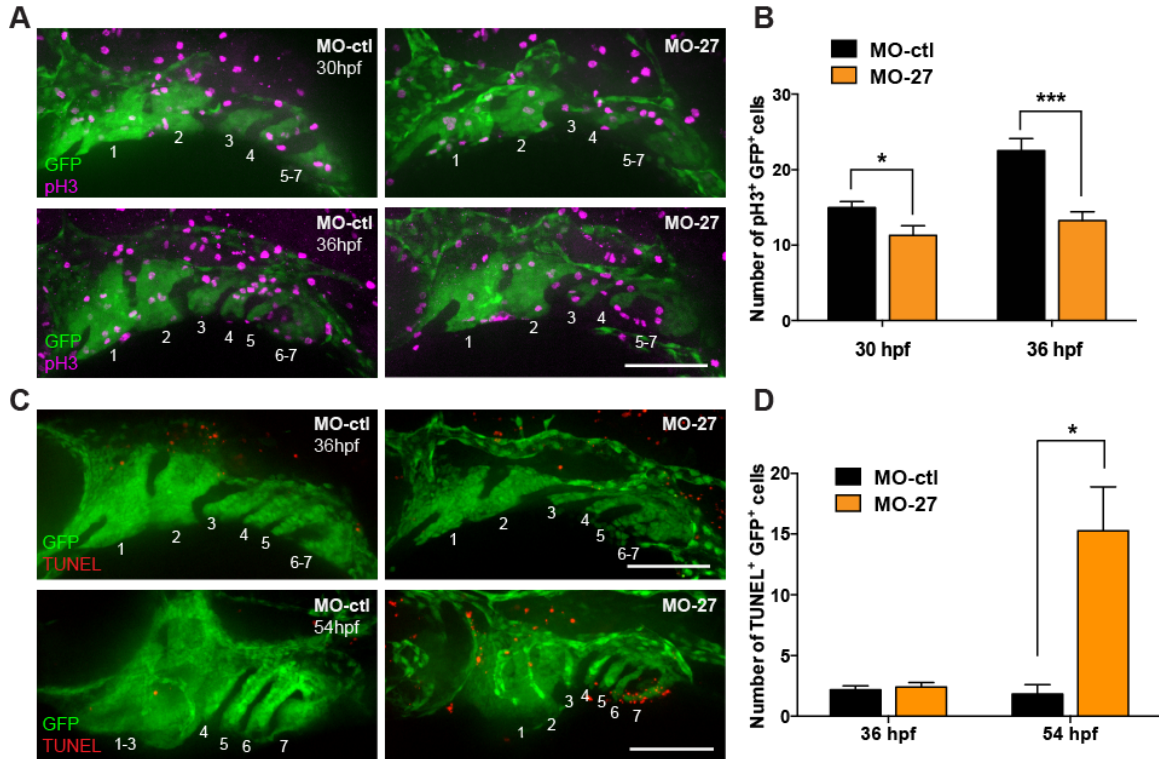
Figure 13   *miR-27* **knock-down impairs proliferation and survival of PCC cells.**

(A) Anti-phospho histone 3 (pH3) and anti-GFP immunostaining in *Tg(fli1a:eGFP)y1* embryos at 32 and 36 hpf. Embryos were injected with either 5ng MO-ctl or MO-27 at the single cell stage. Lateral view with anterior to the left. (B) Quantification of pH3$^+$GFP$^+$ cells normalized to the GFP$^+$ area in each embryo. For 30 hpf, n=7; for 36 hpf, n=8. (C) TUNEL staining and anti-GFP immunostaining in *Tg(fli1a:eGFP)y1* embryos at 36 and 54 hpf. Embryos were injected with the corresponding morpholinos and image layouts are as described above. (D) Quantification of TUNEL$^+$GFP$^+$ cells normalized to the GFP$^+$ area in each embryo. Error bars indicate SEM. For 36 hpf, n=9; for 54 hpf, n=5. *p<0.05, ***p<0.001 (Student's t-test). Data are from four independent experiments. Scale bars, 100 μm.

significant reduction in the number of mitotic PCCs in *miR-27* morphants compared to

controls at both 30 and 36hpf (**Fig. 13A,B**). Upon *mir-27* knockdown, the impairment in

PCC proliferation was more severe at 36hpf compared to 30hpf (**Fig. 13A,B**).

Next, we investigated whether apoptosis in prechondrogenic cells might

contribute to the pharyngeal arch extension defects in *miR-27* morphants. TUNEL assays

in *fli:EGFP* embryos showed that at 36hpf there was not a significant difference in the

number of apoptotic PCCs in *miR-27* morphants compared to control embryos. However, at 54hpf, when PCCs are differentiating into mature chondrocytes, there was a significant increase in the number of apoptotic PCCs in the morphants compared to the controls (**Fig. 13C,D**). These findings suggest that the initial pharyngeal arch growth defects in *miR-27* morphants are due to a decrease in PCC proliferation. At later stages, PCCs that were not able to differentiate into chondrocytes undergo apoptosis.

Ptk2aa (FAK) is a direct target of miR-27 in vivo

To investigate the molecular mechanism through which *miR-27* regulates pharyngeal cartilage development, we tested candidate mRNA targets of *miR-27* using the online target prediction algorithm TargetScanFish (Lewis et al., 2005). We focused on a subset of potential target mRNAs based on their spatiotemporal expression patterns at different developmental stages. After initial testing of multiple candidate mRNAs, *ptk2aa* was selected for further functional analyses. Ptk2aa is a zebrafish focal adhesion kinase (FAK) gene whose expression is ubiquitous at the shield stage and accumulates in the head, axial region and tail at the 10-somite stage (Crawford et al., 2003). At 24hpf, there is strong expression detected in the head and dorsal axis (**Fig. 14A, B**). Since we detected *miR-27* expression in the pharyngeal arch region starting at 24hpf (**Fig. 4C**), and because pharyngeal arch defects in *miR-27* morphants are first observed around 30-36 hpf (**Fig. 10A**), we decided to determine the expression pattern of *ptk2aa* at these crucial time points. Early *ptk2aa* expression was detected strongly in the head, as previously reported, and between 30 and 48 hpf, was detected in the midbrain, MHB, and paraxial mesoderm axis, with low expression in the pharyngeal region (**Fig. 14C-F**) (Crawford et

al., 2003). At 58 hpf, *ptk2aa* expression in the jaw cartilage was not detectable **(Fig.**

14G). Consistent with the *in situ* data, active FAK protein (FAK-pY397) showed little to
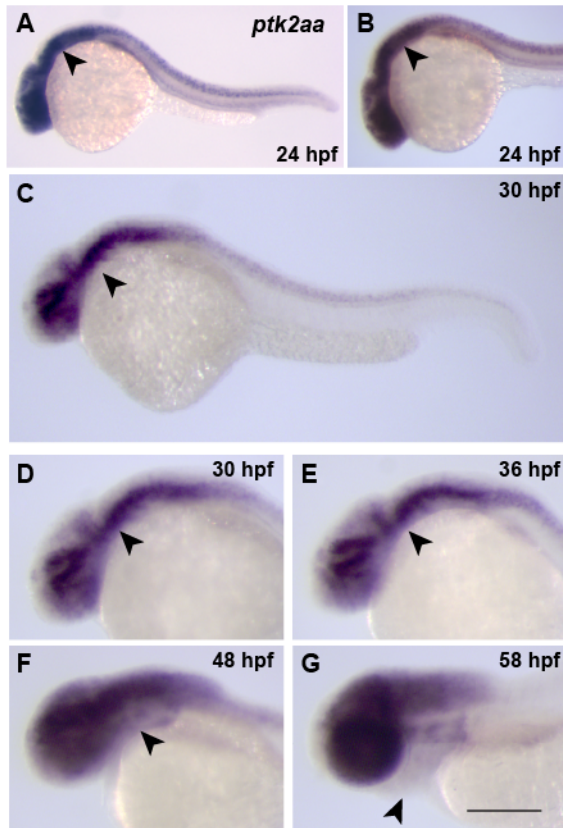
Figure 14   **Expression pattern of *ptk2aa* during development.**

(A-G) *ptk2aa* expression in embryos between 24 hpf and 58 hpf, detected by whole-mount *in situ* hybridization. Lateral views with the pharyngeal arch primordia indicated by an arrowhead.

no co-localization with the arches as marked by *fli1a:eGFP* at 36 and 48hpf **(Fig.15A,B)**.

The reduction of *ptk2aa* expression in the pharyngeal arch region compared to the higher

expression in the head at 24hpf is consistent with the prediction that *ptk2aa* might be

targeted by *miR-27*.
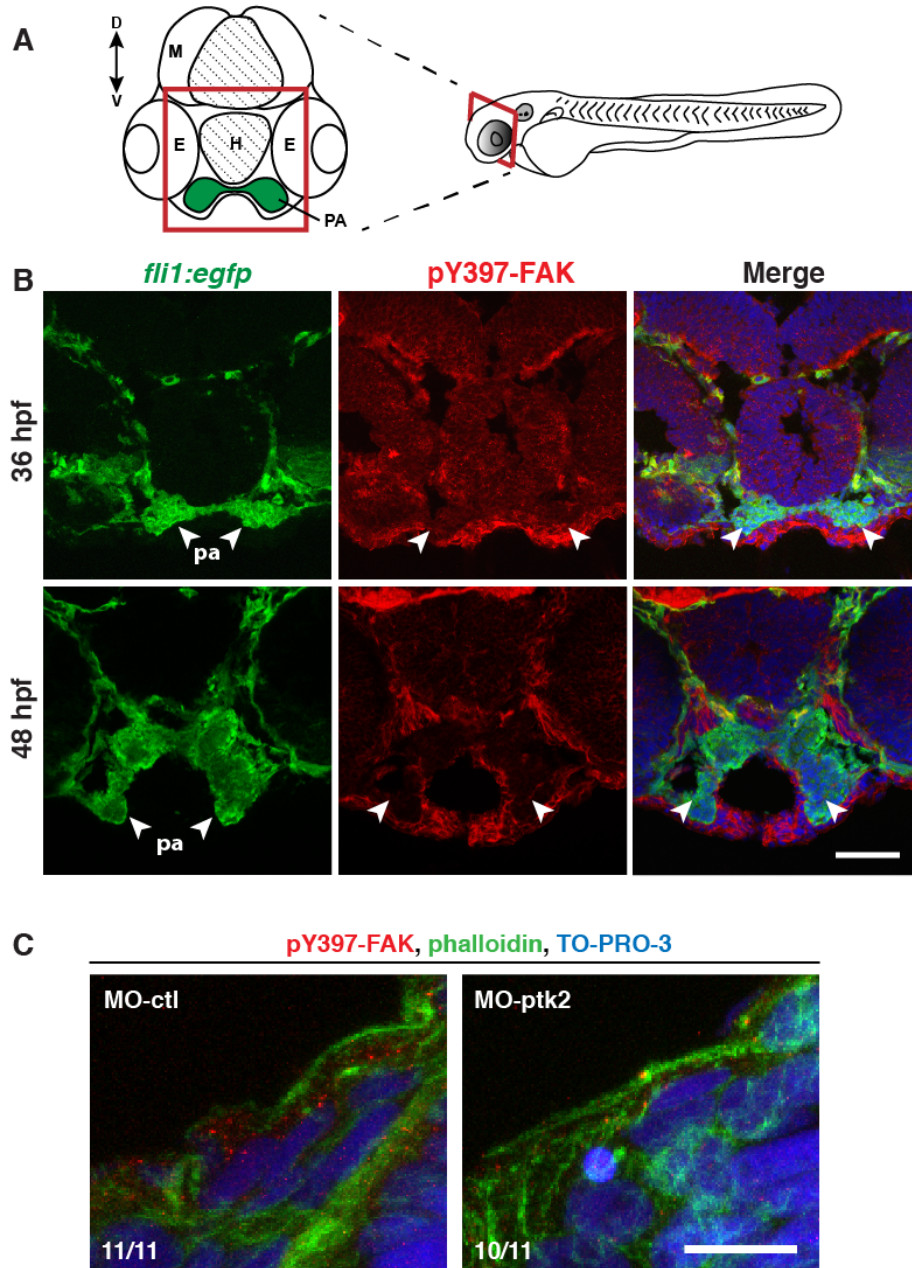
Figure 15   PCC cells in the pharyngeal arches have low levels of active FAK (pY397-FAK) at 36 and 48 hpf.

(A) Schematic of a transverse cross-section of the zebrafish head at 36 hpf. M, mesencephalon; H, hypophysis; E, eye; PA, pharyngeal arch. Dorsal (D) is to the top, ventral (V) is to the bottom. (B) Anti-phospho FAK (pY397-FAK) and anti-GFP immunostaining on transverse sections of *Tg(fli1a:eGFP)y1* embryos at 36 and 48 hpf. PCC cells in the pharyngeal arch (PA) region are indicated by arrowheads. Scale bar, 50 µm. (C) Anti-phospho FAK (pY397-FAK), anti-phalloidin (to label cell borders) and nuclear TO-PRO-3 immunostaining on transverse sections of telencephalon in wild-type embryos at 29 hpf. Embryos were injected with either 3ng MO-ctl or MO-ptk2 at the single cell stage. The indicated ratio represents the number of embryos with the represented phenotype/total number of observed embryos. Scale bar, 10 µm.

Ptk2aa has two miRNA binding elements (MREs) for *miR-27* in the 3'UTR (**Fig. 16A**). To test whether *miR-27* can target *ptk2aa*, we performed GFP reporter assays. As shown in **Fig. 16B**, injection of *GFP-ptk2aa 3'UTR* mRNA into one-cell stage embryos caused strong GFP expression at 24hpf, while co-injection of the mRNA and mature *miR-27* mimic RNAs decreased GFP fluorescence levels. Western blots of pooled protein lysates from these embryos confirmed that co-injection of *miR-27* significantly decreased GFP protein levels (**Fig. 16D,E**). To demonstrate specificity of targeting, we created mutations that disrupted the *miR-27* seed regions within both MREs in the *ptk2aa* 3'UTR. Co-injection of the mutated transcripts with *miR-27* did not decrease the GFP fluorescence compared to injection of the reporters alone **(Fig. 16C)**. These results support the hypothesis that *miR-27* can regulate *ptk2aa* through the two MREs in its 3'UTR.

Next, we tested whether *miR-27* regulates endogenous *ptk2aa*. We injected mature *miR-27* mimic RNAs in two different concentrations into single cell embryos and then prepared protein lysates from injected embryos at 24 hpf followed by western blots with antibodies against FAK. Increasing doses of *miR-27* led to a 50-70% decrease in endogenous FAK protein levels (**Fig. 16F**). As a complementary experiment, we analyzed FAK protein levels when *miR-27* was knocked down. We injected either *miR-27* morpholinos or control morpholinos into single cell embryos at the same concentration as we used in the functional analyses described above. Western blot analyses showed that FAK levels were more than 2-fold upregulated in the *miR-27*

morphants compared to control embryos at 2dpf (**Fig. 16G,H**). Collectively, these results indicate that *miR-27* regulates FAK *in vivo*.
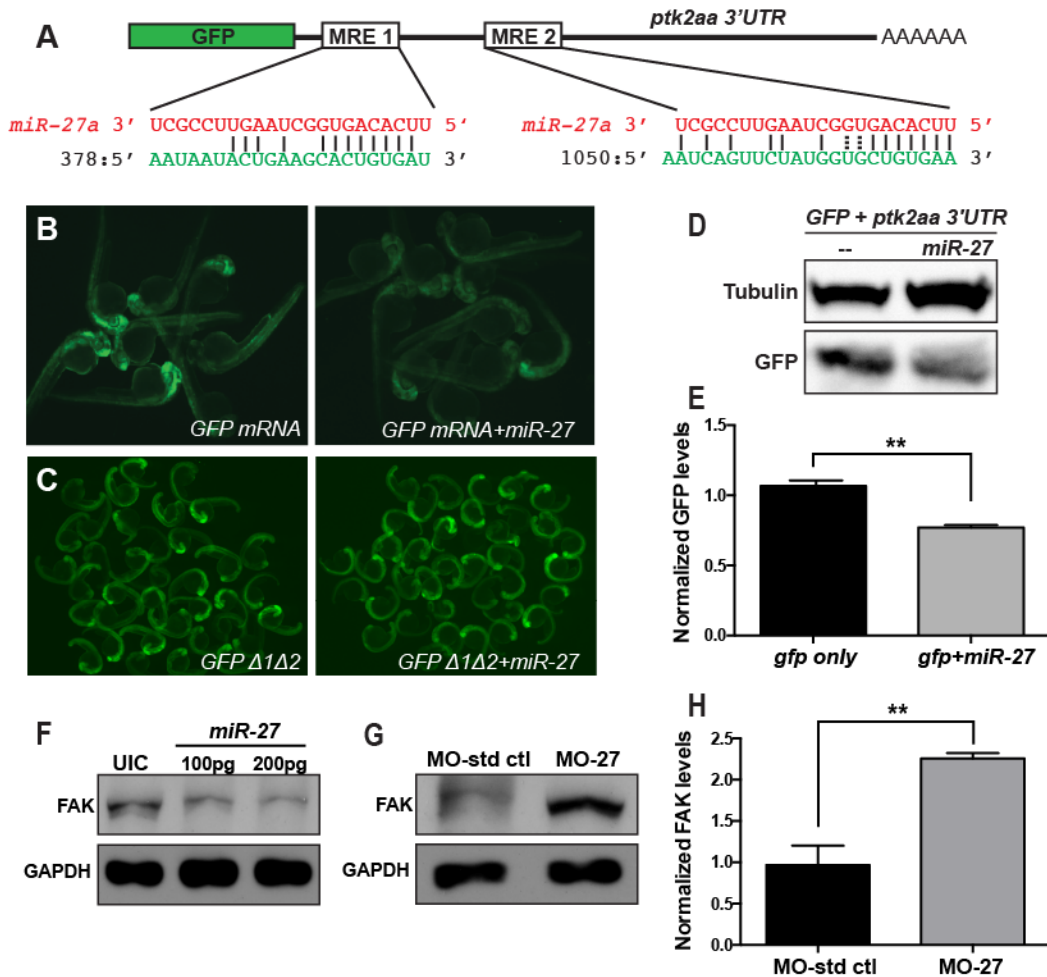
Figure 16   *miR-27* **targets FAK and regulates FAK levels** *in vivo***.**

(A) Schematic of the reporter mRNA consisting of the coding sequence of GFP fused to the *ptk2aa* 3'UTR. Two predicted miRNA recognition elements (MREs) are indicated. Predicted base-pairing between MREs (shown in green) and the *miR-27a* sequence (shown in red). (B) Embryos injected with either *GFP-ptk2aa 3'UTR* reporter mRNA alone or co-injected with *miR-27a* imaged at 24hpf. (C) Reporter assays with *GFP-ptk2aa 3'UTR* mRNA containing mutations in the *miR-27* seed sites. (D) Western blots with anti-GFP and anti-tubulin antibodies using the lysates from embryos injected with the *GFP-ptk2aa 3'UTR* reporter mRNA alone or co-injected with *miR-27a*. (E) Quantification of GFP levels by Western blots normalized to the levels of tubulin. (F) Western blots with anti-FAK and anti-GAPDH antibodies using lysates from 24hpf embryos either uninjected or injected with 100 or 200pg *miR-27a*. (G) Western blots with anti-FAK and anti-GAPDH antibodies using lysates from 48hpf embryos injected either with MO-ctl or MO-27. (H) Quantification of FAK levels from Western blots shown in (G) normalized to the levels of tubulin. At least 20 embryos were pooled for protein lysates. Error bars indicate SEM. **p<0.01 (Student's t-test).

__Knock down of ptk2aa (FAK) partially rescues pharyngeal cartilage defects in miR-27__

__morphants__

Next, we investigated whether the pharyngeal cartilage defects in *miR-27*

morphants are caused by misregulation of *ptk2aa* (FAK). Given that FAK is upregulated

in *miR-27* morphants, we hypothesized that knocking down FAK in the morphants would

rescue the pharyngeal cartilage defects. To knock down FAK, we designed antisense

morpholinos that block the translation start site of both *ptk2aa* and *ptk2ab*. We titrated

the *ptk2* morpholinos and determined the highest concentration (3ng) that did not disrupt

normal morphological development at 1 dpf (data not shown). At this concentration,

Ptk2 morpholinos (MO-ptk2) efficiently blocked translation of a *ptk2aa* reporter

construct (**Fig. 17**). We then injected morpholinos against *miR-27* in two different

concentrations, co-injected with either control or *ptk2* morpholinos, and examined

whether the craniofacial defects were suppressed upon knockdown of *miR-27*. We

categorized the pharyngeal cartilage phenotypes observed at 4 dpf into three groups

(CH1, CH2 and CH3) based on the ceratohyal position and size (**Fig. 18A**). CH1 had the

least severe cartilage phenotype with Meckel's cartilage not as anteriorly extended as

compared to wild type embryos, along with three missing posterior branchial arches. In

CH2, the sizes of all visible pharyngeal cartilage elements were shorter in comparison to

CH1, the ceratohyal cartilage was not able to extend anteriorly, and all branchial arches

were missing. CH3 had the most severe cartilage phenotype with Meckel's cartilage and

the branchial arch phenotypes similar to CH2, but the ceratohyal cartilage had a more

severe phenotype by shifting posteriorly. Co-injection of *ptk2* morpholinos and *miR-27*

morpholinos both at low (2ng) and high (4ng) concentrations increased the frequency of
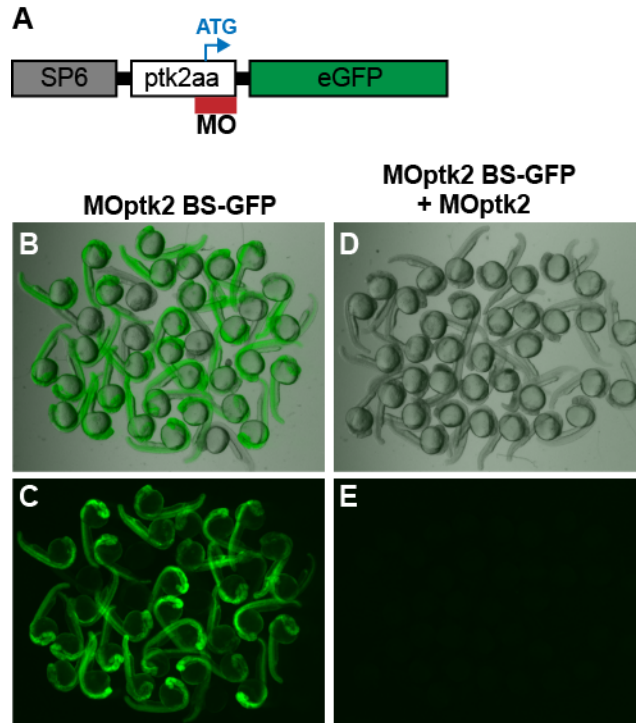
Figure 17   Ptk2 morpholino targets the translation start site of the *ptk2aa*.

(A) Design of the reporter construct (MOptk2 BS-GFP) that carries the *ptk2aa 5'UTR* carrying the translation start site fused to the open reading frame of GFP without the translation start site. This construct carries the SP6 promoter that enables *in vitro* transcription. (B-C) Live images of 1 dpf embryos injected with *MOptk2 BS-GFP* mRNA. (D-E) Live images of 1 dpf embryos injected with *MOptk2 BS-GFP* mRNA and *ptk2a* morpholino (MO-ptk2).

the CH1 phenotype, while significantly decreasing the frequency of the more severe

phenotypes (CH2, CH3) (**Fig. 18B**). The ability to suppress the cartilage defects in *miR-*

27 morphants by coincident knockdown of *ptk2aa* is consistent with regulation of FAK

by *miR-27*.

Next, we quantitatively evaluated the level of rescue in extension of the

ceratohyal cartilage in the anterior-posterior axis. We measured the distance between

Meckel's cartilage and the ceratohyal cartilage to a reference point where the

palatoquadrate cartilage and hyosymplectic cartilage joint (**Fig. 18C**). To normalize

these lengths to the width of the pharyngeal skeleton, we measured the distance between

the palatoquadrate cartilage and the hyosymplectic cartilage joins, as previously

described (Wu et al., 2015). The ratio (C/A), which represents the normalized length of

Meckel's cartilage, did not show any significant difference in MO-ptk2 and MO-27 (2ng)

co-injected embryos compared to injection of only MO-27 (2ng) (data not shown). The

ratio (C-B)/A represents the positional relationship between Meckel's cartilage and the

ceratohyal cartilage. As the phenotypes get more severe, the ceratohyal cartilage shifts

more posteriorly and the (C-B)/A ratio increased in *miR-27* morphants compared to

controls (**Fig. 18D**). However, when we knocked down *ptk2* along with *miR-27*, the ratio

was significantly smaller than in *miR-27* morphants, consistent with defects observed

when we used higher *miR-27* morpholino concentrations (data not shown). This indicates

that *ptk2* knockdown partially suppresses the severe ceratohyal positioning in the mild

miR-27 morphants. Overall, these results demonstrate that *miR-27* knock down leads to

craniofacial cartilage defects due to misregulation of *ptk2*.

Discussion

miR-27 is essential for chondrogenic differentiation

      We show that *miR-27* is required for cartilage development both in the pharyngeal
arches and the pectoral fins, which are derived from CNC cells and the paraxial
mesoderm, respectively (Le Douarin et al., 2004; Lee et al., 2013). Using loss-of-
function studies, we show that *miR-27* knockdown does not affect neural crest
specification and migration of the CNC cell streams, but is instead required for the
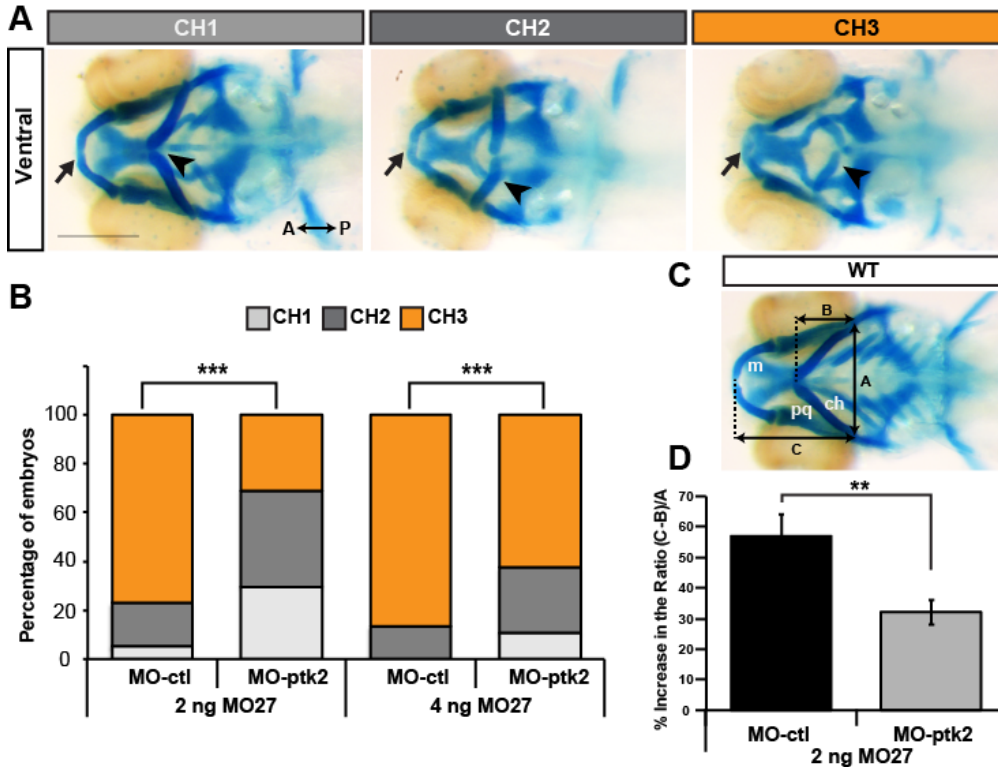
Figure 18   Suppressing FAK in *miR-27* morphants partially rescues cartilage defects.

(A) Three categories of representative head cartilage phenotypes in 4dpf old embryos injected with MO-27, along with either standard control morpholino MO-ctl or translation blocking MO-ptk2 at the single-cell stage. Ventral views of head cartilage stained with alcian blue. Ceratohyal cartilage indicated by an arrowhead and Meckel's cartilage indicated with an arrow. (B) Embryos were injected with 2ng or 4ng MO-27 either co-injected with 3ng MO-ctl or MO-ptk2. Percentage of embryos with the corresponding head cartilage phenotypes (CH1-CH3) at 4dpf. The distribution of phenotypes in MO-ptk2 and MO-27 injected embryos are compared to those injected with MO-ctl and MO-27. ***$p<0.0001$ (Chi-squared goodness of fit test), n=40-60 embryos. Data are from three independent experiments. (C) Analysis of cartilage positions. Ventral view of head cartilages in wild-type embryos stained with alcian blue. A represents the distance between the palataquadrate (pq) and ceratohyal (ch) cartilage joints. B represents the distance from the anterior joint of the two ceratohyals to the baseline shown by a dashed line. C represents the distance from the anterior end of Meckel's cartilage (m) to the baseline. (D) (C-B)/A ratio was calculated for quantitative analysis of anterior-posterior extension of the ceratohyal cartilage. This ratio increases as the ceratohyal position extends posteriorly instead of anteriorly. Percentage increase of the (C-B)/A ratio in MO-27 and MO-ctl injected embryos or embryos co-injected with both MO-27 and MO-ptk2 compared to the ratio in wild-type embryos. Error bars represent SEM. n=40-60 embryos, **$p<0.01$ (student's t-test).

proliferation and differentiation of PCCs. This suggests that *miR-27* promotes a chondrogenic differentiation program regardless of the origin of the pre-chondrogenic progenitor cells. Biallelic knockout clones for the *miR-23a~27a~24-2* and *miR-23b~27b~24-1* clusters in ESCs demonstrated that these clusters are indispensable for ESC differentiation *in vitro* and *in vivo* (Ma et al., 2014). Our study shows that either *miR-27a* or *miR-27b* knockdown leads to severe craniofacial defects **(Fig. 7)**, consistent with the requirement for both isoforms in ESC differentiation and supporting the idea that both family members cooperate to control chondrogenic differentiation.

Although the role of *miR-27* in chondrogenesis has not been reported before, the *miR-23a~27a~24-2* cluster was implicated in skeletal development by negatively regulating *in vitro* osteogenic differentiation (Hassan et al., 2010). Interestingly, one of the most crucial bone-specific transcription factors, Runx2, was reported to suppress the transcription of the *miR-23a~27a~24-2* cluster early in osteogenesis, while in the final osteocyte stage of differentiation this cluster is upregulated and functions to attenuate continuing bone formation. These findings, along with our results demonstrating that *miR-27* is a positive regulator of chondrogenesis, suggest that *miR-27* plays a major role in the cell fate commitment program of skeletal stem cells.

miRNA knockdown and knockout experiments

Loss-of-function studies using morpholinos must be interpreted carefully with multiple controls to avoid possible off-target effects, as well as a reliable confirmation of morpholino efficacy. We have performed multiple control experiments following published guidelines such as the use of mismatch control morpholinos, targeting the same
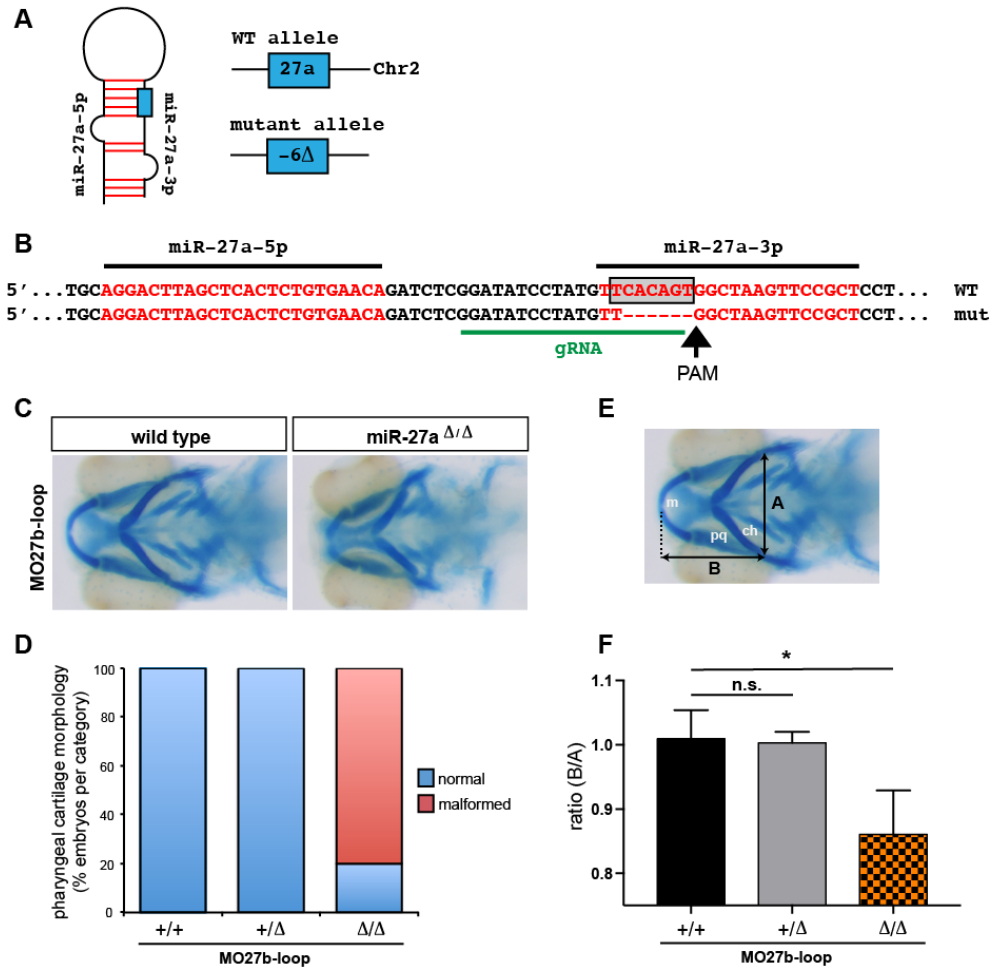
Figure 19   *miR-27a* **mutants have pharyngeal cartilage defects upon partial knock-down of *miR-27b*.**

(A) Schematic representation of the *miR-27a* precursor and generation of *miR-27a* mutants by CRISPR/Cas9. The blue box on the miRNA precursor represents the gRNA target region corresponding to the mature *miR-27a* seed. (B) The region of the *miR-27a* gene sequence that shows the CRISPR/Cas9 targeted region. *miR-27a-5p* and *miR-27a-3p* are shown in red. The seed region of mature *miR-27a* is shown in the grey box. The target region for the designed sgRNA is underlined in green. Arrow points to the PAM sequence. (C) Alcian blue staining of 4 dpf miR-27a$^{\Delta/\Delta}$ and WT siblings injected with 1.5ng of MO-27b loop at the one-cell stage. (D) Phenotypic categorization of the pharyngeal cartilage in 4dpf miR-27a$^{\Delta/\Delta}$, miR-27a$^{+/\Delta}$ and WT siblings injected with 1.5ng of MO-27b loop at the one-cell stage. n=20 for WTs, n=36 for miR-27a$^{+/\Delta}$ and n=20 in miR-27a$^{\Delta/\Delta}$. (E) Analysis of cartilage positions. Ventral view of head cartilage in wild-type embryos stained with alcian blue. A represents the distance between the palataquadrate (pq) and ceratohyal (ch) cartilage joints. B represents the distance from the anterior end of Meckel's cartilage (m) to the baseline. (F) The B/A ratio was calculated for quantitative analysis of anterior-posterior extension of the Meckel's cartilage. Error bars represent SEM. Statistical analysis was done using one-way ANOVA with Fisher's Least Significant Difference (LSD) test, *$p<0.05$.

57

gene with two morpholinos, testing dose dependent effects, and ensuring the efficacy of

knock downs (Eisen and Smith, 2008). In addition, the TUNEL assays showed that there

was no increase in apoptosis in pre-chondrogenic cells at the stage when pharyngeal arch

defects were detected suggesting that the morphant phenotype is not due to p53-induced

apoptosis (Robu et al., 2007). Due to the fact that MO-27 targets the mature full length

miR-27 RNA, we do not have a *miR-27* isoform that is immune to the MO which could

be used to rescue the morphant phenotype. However, and most importantly, we were

able to suppress the effects of *miR-27* knockdown by co-injection of morpholinos against

the *miR-27* target *ptk2aa*.

An ideal strategy to confirm morpholino associated phenotypes is to analyze

mutant alleles of the same gene. There have been concerns about the lack of concordance

between mutant and morphant phenotypes of the same genes in zebrafish (Kok et al.,

2015; Stainier et al., 2015). To address these concerns, we generated a *miR-27a* mutant

line (miR-27a$^{\Delta/\Delta}$) that carried a 6 bp deletion in the miRNA seed region using the

CRISPR/Cas9 system **(Fig. 19A,B)**. Analysis of F2 and F3 embryos of heterozygous

mutant parents either did not show any detectable craniofacial defects or the phenotypes

similar to the *miR27* morphants were observed with low penetrance in the homozygous

mutants. There could be multiple reasons for the discrepancy between the *miR-27*

morphants and the mutants. One possibility is genetic compensation upon CRISPR-

mediated mutation of the *miR-27a* gene, as has been reported recently, after other

CRISPR and TALEN mediated mutations (Blum et al., 2015; Rossi et al., 2015). The

candidate genes most likely contributing to the genetic compensation would be the other

members of *miR-27* family. Since we already showed that *miR-27b* is also required for

pharyngeal cartilage morphogenesis **(Fig. 7B)**, we hypothesized that *miR-27b* expression might compensate for the loss of *miR-27a* in *miR-27a$^{\Delta/\Delta}$* embryos. Injection of MO27b-loop at low concentration normally results in no detectable defects in the pharyngeal cartilage (Fig. S3B, Fig. S9C). However, we found that exclusively homozygous miR-27a$^{\Delta/\Delta}$ embryos are sensitized to limited loss of *miR-27b* knockdown compared to *miR-27a$^{+/\Delta}$* and WT siblings **(Fig. 19C-F)**. *miR-27b* knockdown with low doses of MO injection resulted in shorter pharyngeal elements, as shown by significant decreases in Meckel's extension compared to *miR-27a$^{+/\Delta}$* heterozygotes and WT siblings (Fig. S9E-F). This indicates that *miR-27b* can contribute to compensation of the *miR-27a* loss in miR-27a$^{\Delta/\Delta}$ embryos. However, there could also be other genes that compensate for the loss of *miR-27a,* including protein coding genes as well as other miRNAs. Most miRNAs target multiple mRNAs, it is unlikely that *ptk2aa (FAK)* is only targeted by *miR-27* family members, consistent with the finding that we were only able to partially suppress the severe ceratohyal positioning defect in the *miR-27* morphants by coincident *ptk2* knockdown. TargetScan predicts 7 miRNAs with significant seed matches that could target *ptk2.2* and could conceivably compensate for the loss of *miR-27* and retain proper regulation of *ptk2.2*. It remains to be determined whether any of these miRNAs are temporally and spatially expressed in a manner consistent with regulation of pharyngeal arch development.

While generation of 5 independent lines and crosses to generate a line lacking expression of all *miR-27* family members is beyond the scope of this report, we did attempt to utilize multiplex CRISPR/Cas9 using guide RNAs that target all *miR-27* family members in early embryos (Narayanan et al., 2016). Unfortunately, we did not

observe any resulting phenotypes at 4dpf, potentially due to the fact that the level of *miR-27* knockdown in early embryos was not sufficient, averaging less than 50%.
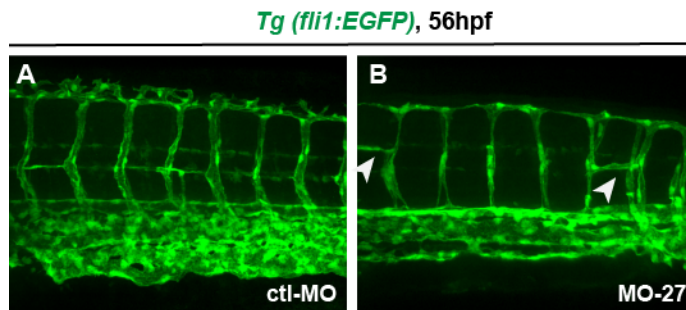
Figure 20 Vasculature defects in *miR-27* morphants.

Vasculature patterning in live *Tg(fli1a:eGFP)y1* embryos at 56 hpf. Embryos were injected with either MO-ctl or MO-27 at the single cell stage. Arrowheads indicate branching defects in the intersegmental vessels in *miR-27* morphants.

miR-27 regulates pharyngeal cartilage development through targeting FAK

miRNAs are well-known for their role in preventing translation and accelerating decay of target mRNAs, thereby providing a precise mechanism for spatiotemporal control of developmental processes (Krol et al., 2010; Zhao and Srivastava, 2007). Given that *miR-27* knockdown prevents chondrogenic differentiation, the target mRNA of *miR-27* would be hypothesized to be a negative regulator of PCC proliferation and differentiation. Here, we identify *ptk2aa (FAK)* as a novel *in vivo* target of *miR-27*. Ptk2aa and ptk2ab are paralogs of the zebrafish focal adhesion kinase (FAK) gene (Crawford et al., 2003; Henry et al., 2001). *ptk2ab* also carries two MREs for *miR-27* in its 3'UTR but our GFP reporter assays showed no detectable regulation of *ptk2ab* 3'UTR by *miR-27*. Importantly, we show that craniofacial cartilage defects can be partially rescued by *ptk2a* (FAK) knockdown (**Fig. 18**). This suggests that FAK accumulation is

required for proper chondrogenesis.

Potential roles of FAK during chondrogenic differentiation

Loss of *miR-27* does not prevent mesenchymal condensation of the PCCs (**Fig. 7**). However, PCC proliferation was significantly impaired in *miR-27* morphants during the condensation stage (**Fig. 13A,B**). We hypothesize that FAK accumulation due to *miR-27* knockdown does not affect condensation, but rather proliferation and differentiation of PCCs. A remaining question is whether in *miR-27* morphants, the effect of FAK accumulation during chondrogenesis is cell-autonomous. Previous studies have shown a cell-autonomous role of FAK on mesenchymal stem cells by performing *in vitro* chondrogenesis assays (Bursell et al., 2007; A. M. DeLise et al., 2000; Pala et al., 2008; Tang et al., 2013a). Conditional deletion of the membrane-anchored metalloproteinase MT1-MMP in mesenchymal progenitors caused a loss of β1 integrin/FAK signaling activation and thereby promoted differentiation towards the chondrogenic versus adipogenic or osteogenic lineages (Tang et al., 2013a). Similarly, using a micromass model of chondrogenesis with FAK$^{+/+}$ and FAK$^{-/-}$ embryonic fibroblasts, FAK signaling was reported as a negative regulator of chondrogenesis (Pala et al., 2008). Loss of FAK in embryonic mesenchymal cells resulted in a significant increase in chondrogenic differentiation along with a higher expression of chondrogenic genes compared to wild-type cells (Pala et al., 2008). Induction of chondrogenic differentiation observed in FAK null cells is strikingly similar to effects reported upon inhibition of other components in the FAK signaling pathway. For example, inhibition of the FAK interacting kinase Src and the RhoA/ROCK pathway downstream of FAK/Src complex resulted in cell

61

rounding and loss of stress fibers along with upregulation of chrondrogenic markers, Sox9, collagen type II and aggrecan during *in vitro* chondrogenesis (Bursell et al., 2007; Woods et al., 2005; Woods and Beier, 2006). All these findings demonstrate that FAK signaling suppresses chondrogenic differentiation with likely involvement of downstream RhoA/Rock signaling

An important role for FAK in focal adhesion complexes is to control mechanotransduction in cells that are subject to external mechanical forces or ECM remodeling (Eyckmans et al., 2011; Yim and Sheetz, 2012). Interestingly, mechanical stretching or ECM-mediated cell shape changes activate β1-integrin/FAK signaling and consequently inhibit chondrogenesis of mesenchymal stem cells (Onodera et al., 2005; Takahashi et al., 2003; Tang et al., 2013a; Woods et al., 2007). These studies support our hypothesis that *miR-27* regulates chondrogenesis in the pharyngeal arches by maintaining low levels of FAK.

miR-27 regulates differentiation programs in other tissue types

The *miR-23~27~24* cluster has been implicated as a positive regulator for mesoderm differentiation of embryonic stem cells (ESC) by directly targeting pluripotency-maintenance factors (Ma et al., 2014). We show that *miR-27* is also essential for development of specific mesoderm and neural crest-derived cell/tissue types *in vivo*. Previous reports showed that *miR-27* is required for angiogenesis, adipogenesis, and development of the embryonic vasculature consistent with phenotypes we observe upon knockdown of *miR-27* (Biyashev et al., 2012; Kang et al., 2013; Urbich et al., 2012; Zhou et al., 2011) (**Fig. 20**). Together, *miR-27* emerges as a key factor that negatively regulates the stemness of progenitor cells promoting the differentiation of multiple tissue

types.

Materials and Methods

Zebrafish husbandry and lines

Wild-type (AB) (Walker, 1999), *Tg(fli1a:eGFP)y1* (Lawson and Weinstein, 2002), *Tg(sox10(7.2):mRFP)vu234* (Kirby et al., 2006) lines were maintained at 28.5^{0}C on a 14:10 hour light:dark cycle. Embryos were raised in egg water (0.03% Instant Ocean) at 28.5^{0}C, staged by morphology (Kimmel et al., 1995) and hours post fertilization (hpf). For whole-mount immunohistochemistry and *in situ* hybridization analyses, embryos were raised in egg water supplemented with 0.003% N-phenylthiourea (PTU; Sigma-Aldrich) to prevent melanin formation. Zebrafish maintenance, embryo collection, and analyses were performed with the approval of the Vanderbilt University Institutional Animal Care and Use Committee (M/09/398).

Constructs

The *ptk2aa* (NM_198819.1) mRNA 3'UTR was amplified by RT-PCR using forward (5'- GGCGAATTCGACCTCCACACTGGCTGGATCATC-3') and reverse (5'-CGGCTCGACCTGAGCATTCGGTACACACTTTCTGTATTA-3') primers. *ptk2ab* (NM_131796.1) mRNA 3'UTR was amplified by RT-PCR using forward (5'-CGGACTAGTCTACTCACCCACCCTCACGTTAAGC-3') and reverse (5'-CGGCTCGAGTGCCTTGCTGTTAAACATCATTTGG-3') primers. Each 3'UTR was cloned downstream of the GFP coding sequence in the PCS2+ vector. miRNA

recognition elements (MREs) within the *ptk2aa* 3'UTR were deleted using the

QuikChange Lightning Site-Directed Mutagenesis Kit (Stratagene). The first MRE was

deleted using sense (5'- GAATAATAATACTGAAGCTGACGGAGGGCTGAGGTA -

3') and anti-sense (5'- TACCTCAGCCCTCCGTCAGCTTCAGTATTATTATTC -3')

primers. The second MRE was deleted using sense (5'-

CAAAATCAGTTCTATGGTGAAGGGGCGGGATTAAACAA -3') and anti-sense (5'-

TTGTTTAATCCCGCCCCTTCACCATAGAACTGATTTTG -3') primers. For the

ptk2aa in situ probe, a 1.1kb region was amplified by RT-PCR using forward (5'-

GTAGTAGGATCCTCAGAAACAGACGACTACGCA-3') and reverse (5'-

GTAGTACTCGAGTGGTTCCAGCTCTCAAGCG-3') primers containing BamHI and

XhoI sites for cloning into PCS2+. The *ptk2aa* coding region without the 3'UTR was

amplified by RT-PCR using forward (5'-

GTAGTAGAATTCCCTAGCGTACGGTAAAGGCA-3') and reverse (5'-

GTAGTACTCGAGAAGGGTGATGTTCCTCCGTG-3') primers and cloned into

PCS2+. For the reporter construct for MO-ptk2, GFP was amplified with a forward

primer carrying the MO binding site overlapping the *ptk2aa* translation start site (5'-

GTAGTAGGATCCAAGGCATGGCGACGGCATTCCTGGACATGGTGAGCAAGGG

CGAGG-3') and reverse (5'- GTAGTAGAATTCGCCTTCTAGAGCTCGTCCA -3')

primer and cloned into pCS2+.

512 pME-miR was a gift from Nathan Lawson (Addgene plasmid # 26032).

Around 300bp fragment spanning the *miR-27b* gene was amplified using genomic DNA

from 24 hpf old embryos and cloned into 512pME-miR using EcoRI restriction digestion

site. Hsp70l:miR27b-eGFP and sox10:miR27b-eGFP plasmids were generated using

pDestTol2CG2 vector, p5E-*hsp70l* (Kwan et al., 2007), p5E-*sox10* (Das and Crump, 2012), p3E-eGFPpA (Kwan et al., 2007) and assembled using the Multisite Gateway cloning system (Invitrogen).

Transgenesis

To generate the Tg*(hsp70l:miR27b-eGFP)* and Tg*(sox10:miR-27b-eGFP)* lines, the mixture of Tol2 mRNA (25pg) and plasmid (20pg) was injected into the single-cell stage embryos. Injected embryos were prescreened for GFP fluorescence and raised in egg water at 28^0C for five days before transferring them Aquatic Habitats system. Transgenic F1 lines were established by crossing founder and wild-type adults.

RNA synthesis

mRNAs were *in vitro* synthesized from linearized constructs using mMESSAGE mMACHINE® SP6 Transcription Kit (Life Technologies). Digoxigenin-UTP-labeled anti-sense RNA probes were *in vitro* synthesized from linearized constructs using either T7 or T3 RNA polymerases and DIG RNA labeling mix (Roche Applied Sciences). *In vitro* transcribed RNA was purified by NucAway[TM] Spin Columns (Life Technologies).

Morpholinos, Microinjections

Morpholinos were purchased from Gene Tools and their sequences are listed in **Table 1**. MO-27 was designed complementary to mature *miR-27a* and the MO-27a loop targets the Dicer cleavage site and the loop of the *miR-27a* precursor. MO-ptk2 was designed against the translation start site of ptk2aa. All injections were performed in fertilized 1-cell stage embryos. For reporter assays, GFP-ptk2aa3'UTR mRNA was injected at 150pg/embryo concentration either alone or with a synthetic *miR-27a* duplex

(Dharmacon) at 75pg/embryo. Double stranded mature *miR-27a* was synthesized with 3′-UU overhangs for the following target sequence: 5'-UUCACAGUGGCUAAGUUCCGCU-3'. MO-27 morpholinos were injected at 5ng/embryo concentration unless specified.

Table 1 List of morpholinos used in the study

Morpholino name	Sequence	
MO-standard control (MO-ctl)	5'-CCTCTTACCTCAGTTACAATTTATA-3'	
MO-27-4mis	5'-GCGCAACTTACCCAGTGTCAACA-3'	Alci
MO-27	5'-GCGGAACTTAGCCACTGTGAACA-3'	an
MO-27a loop	5'-TAGCCACTGTGAACATAGGATATCC-3'	Blue
MO-27b loop	5'-CTTAGCCACTGTGAACAAAGAGTTC-3'	Stai
MO-27c loop	5'-CCACTGTGAACATTGAAGTTCGATC-3'	ning
MO-ptk2	5'-TCCAGGAATGCCGTCGCCATGCCTT-3'	

Embryos were fixed with 4% phosphate-buffered paraformaldehyde (PFA) for 1 hour at room temperature. Fixed embryos were rinsed in PBS with 0.1% Tween-20 two times and rinsed in 50% EtOH for 10 minutes on a rocker. Embryos were then stained in 0.2% Alcian blue, 30mM MgCl2 in 75% EtOH overnight on a rocker and bleached with 1.5% H_2O_2 and 1% KOH for 20 minutes.

Generation of miRNA mutants by CRIPSR/Cas9

sgRNAs were designed using CRISPRscan (http://www.crisprscan.org). sgRNA and Cas9 mRNAs were prepared as described previously (Yin et al., 2015). The sgRNA target region for *miR-27a* gene was 5'-GGATATCCTATGTTCACAG-3'. WT embryos were injected at the one-cell stage with 300 ng/µL Cas9 mRNA and 50ng/ µL sgRNA.

Mutagenesis efficiency was confirmed by heteroduplex mobility assay analysis of the

PCR amplicon of the CRISPR targeted genomic region. F1 heterozygous mutant

embryos were obtained by crossing founder adults carrying germline *miR-27a* mutations

with WT adults. Indels in the *miR-27a* gene in the F1 adults were identified and a 6bp

deletion in the miRNA seed region was selected for further breeding.

qRT-PCR

Taqman small RNA assays (Life Technologies) were used to perform qRT-PCR

of the indicated miRNAs. 5ng of total RNA isolated from 50 pooled embryos at the

indicated stages were used per RT reaction and 1.33μl of 1:2 diluted resultant cDNA was

used in 10μl qPCR reaction in technical triplicates. qPCR reactions were conducted in

either 96-well plates using Bio-Rad CFX96 Real-time system or in 384-well plates using

Bio-Rad CFX384 Real-time System. All quantifications were normalized to an

endogenous U6 snRNA control. Fold changes were calculated using the $\Delta\Delta C(t)$ method,

where $\Delta = C(t)miRNA - C(t)U6\ snRNA$, and $\Delta\Delta C(t) = \Delta C(t)condition1 - \Delta C(t)$

condition2, and $FC = 2^{-\Delta\Delta C(t)}$. Taqman probe #: U6 snRNA: 001973; dre-miR-27a-3p:

007138_mat; dre-miR-27b: 008075_mat; dre-miR-27c: 006826_mat; dre-miR-27d:

003373_mat; dre-miR-27e: 007922_mat.

Immunoblotting and Northern Blots

Embryos were deyolked at the indicated time points and placed in RIPA buffer

with Complete Protease Inhibitor Cocktail (Roche 04693159001), followed by

homogenization with a pestle. Separation of total proteins and transfer was performed as

described (Olena et al., 2015). The following antibodies were used for western blots:

67

rabbit anti-GFP (1:1000, Torrey Pines), rabbit anti-α-tubulin (1:1000, Abcam), mouse anti-FAK (1:300, H-1 Santa Cruz Biotechnology), mouse anti-GAPDH (1:20,000, Ambion), anti-rabbit and anti-mouse HRP-conjugated secondary antibodies (1:5000, GE Healthcare). Quantification of band intensities was performed in ImageJ and intensities for each protein of interest were normalized to the loading control levels (either α-tubulin or gapdh). Data was represented as the mean for normalized band intensities from at least 3 independent pools of protein extract. Northern blots were performed as described (Flynt et al., 2007; Wei et al., 2013). Quantification of the band intensities was performed in ImageJ and intensities for *miR-27* were normalized to the loading control levels (*U6*).

In situ hybridization

Whole-mount *in situ* hybridization was performed as described (Thisse and Thisse, 2008). Embryos were hybridized to digoxygenin-UTP labeled RNA probes for *foxd3* (Kelsh et al., 2000), *sox10* (Dutton et al., 2001), *dlx2a* (Akimenko et al., 1994), *sox9a* (Chiang et al., 2001) and *col2a1* (Yan et al., 1995) at 70^0C in a hybridization solution containing 50% formamide. Hybridized probes were detected using anti-digoxigenin alkaline-phosphatase conjugated antibodies, followed by incubation with nitro blue tetrazolium chloride and 5-bromo-4-chloro-3-indolyl-phosphate (NBT/BCIP) solution (Roche Applied Sciences). Whole-mount miRNA *in situ* hybridization was performed as described (Olena et al., 2015) using miRCURY 5'- and 3'-DIG labeled LNA (locked nucleic acid) probes (Exiqon). LNA probe #: dre-miR-27a: 613249-360; dre-miR-27b: 613734-360; dre-miR-27c-3p: 613613-360.

Immunofluorescent staining

To visualize mature chondrocytes, anti-type II collagen (anti-Col2) antibodies and wheat germ agglutinin (WGA) were used for staining of sections. *Tg(fli1a:eGFP)y1* embryos at 61 hours post fertilization (hpf) were fixed in 4%PFA at 4^0C overnight, washed with PBT twice and permeabilized with proteinase K (10ug/ml) for 30min. Embryos were then incubated in blocking buffer (2mg/ml BSA, 2% donkey serum, 4% DMSO, 0.1% Triton-X in PBS) for 2 hours and stained with anti-GFP (1:500, A-11120 Invitrogen), anti-collagen type II (Col2) (1:200, Rockland) or WGA–Alexa-Fluor-555 conjugate (1:200, Molecular Probes) overnight at 4^0C, followed by Cy3-conjugated and Alexa Fluor 488-conjugated secondary antibody (1:100 and 1:200, Jackson Immuno) staining for 2 hours.

For phospho-histone 3 (pH3) staining, embryos were fixed, permeabilized as above, and incubated in blocking buffer (10mg/ml BSA, 2% donkey serum, 1%DMSO, 0.1% Triton-X in PBS). Embryos were then stained with anti-pH3 (1:200, 06-570 Millipore) in blocking buffer. For anti-fibronectin immunostainings, *Tg(fli1a:eGFP)y1* embryos were fixed, cryopreserved, and mounted in Cryomatrix (Thermo). 12μm thick cryosections were incubated in blocking buffer (1mg/ml BSA, 1%DMSO, 1% Triton-X in PBS) and then stained with anti-fibronectin (1:100, Sigma F-3648), Alexa 568 conjugate (Life Technologies, L32458) along with anti-GFP (1:500, Life Technologies, A11120) in blocking buffer.

To detect apoptosis, whole-mount TUNEL labeling was performed using an *in situ* Cell Death Detection Kit, TMR red (Roche), followed by anti-GFP (1:500, Torrey Pines Biolabs) staining.

Phospho-FAK pTyr397 (pFAK) staining was performed as described (Crawford et al., 2003; Koshida et al., 2005) using anti-pFAK [pY397] antibody (Invitrogen, 44-624G, originally from BioSource). This antibody was validated in zebrafish embryos previously by Western blotting and immunohistochemistry (Crawford et al., 2003; Henry et al., 2001). We also validated the specificity of the anti-pFAK [pY397] antibody by loss of pFAK signal in in MO-ptk2 embryos **(Fig. 15C)**. 12μm thick cryosections of *Tg(fli1a:eGFP)y1* embryos were incubated with anti-pFAK at 1:300 and anti-GFP (A-11120 Invitrogen) at 1:500, then stained with Cy3-conjugated and Alexa Fluor 488-conjugated secondary antibodies (1:100 and 1:200, Jackson Immuno) for 2 hours. For pFAK staining in wild-type embryos shown in Supplemental Figure 7C, embryos were stained with Alexa Fluor 488-conjugated phalloidin (1:100, Molecular Probes) and TO-PRO-3 (1:1000, Molecular Probes) along with the Cy3-conjugated secondary antibody for pFAK.

Imaging and Image processing

For time-lapse imaging, *Tg(fli1a:eGFP)y1* embryos were anesthetized at the indicated time points and mounted laterally in 0.6% agarose. Confocal stacks of the pharyngeal arch region were taken at 15 minutes intervals using a PerkinElmer spinning disk confocal microscope with a heating unit (PerkinElmer, 20X objective). For imaging of immunofluorescent stainings, either a PerkinElmer spinning disk confocal microscope or a META Zeiss LSM 510 Meta confocal microscope were used. Images were processed using either Volocity software (Improvision/PerkinElmer) or ImageJ software.

Cell counts and statistical analyses

For quantifying the pH3[+] and TUNEL^{+} cells in fli1a:eGFP[+] pharyngeal arches, cells positive for both GFP and marker of interest were counted, normalized to the whole area for fli1a:eGFP[+] arch region using ImageJ software. Data were represented as a mean for normalized counts for the marker of interest and statistical analyses was performed using a two-tailed Student's t-test.

Fluorescence intensity measurements are done using ImageJ software as described (Gavet and Pines, 2010). For each image, "integrated density", "area" and "mean gray value" of the fli1a:eGFP[+] region, as well as background were measured. Corrected fluorescence intensity of the selected region was calculated according to the formula: "Corrected fluorescence intensity= Integrated Density - (Area of selected region * mean fluorescence of background)". Data were represented as a mean of corrected fluorescence intensity for each experimental condition and statistical analyses were performed using a two-tailed Student's t-test.

CHAPTER III

miR-216-DOT1L REGULATORY AXIS IS NECESSARY AND SUFFICIENT FOR

MULLER GLIA REPROGRAMMING DURING RETINA REGENERATION

Nergis Kara[a], Kamya Rajaram[a], Anna Zhao, Dominic Didiano, Matthew Kent, Emily R.

Summerbell, James G. Patton[b]

---

[a] These authors contributed equally.
[b] N.K., K.R. and J.G.P. conceived and designed the experiments. N.K., K.R., A.Z., D.D., M.K.
and E.R.S. performed the experiments and analyzed the data. N.K. and J.G.P. wrote the
manuscript.

Introduction

A promising strategy to restore impaired vision due to degenerative retinal disorders is to induce endogenous repair mechanisms to regenerate lost cell types. Unfortunately, mammals are unable to spontaneously regenerate retinal neurons and instead, damage often induces reactive gliosis (Bringmann et al., 2009). However, retinal damage in teleost fish, including zebrafish, initiates a robust spontaneous regenerative response that restores both retinal structure and function (Goldman, 2014). Given that the cells and structure of the retina are highly conserved among vertebrates, understanding the molecular mechanisms that allow zebrafish to spontaneously regenerate damaged retinas is key to develop novel therapeutic strategies for retinal damage and disease in humans.

In zebrafish, Müller glia (MG) are the source of the regenerated neurons in the retina (R. L. Bernardos et al., 2007; Fausett and Goldman, 2006). After injury, MG dedifferentiate, undergo asymmetric cell division, and generate a population of proliferating neuronal progenitor cells (Nagashima et al., 2013; Ramachandran et al., 2010a; Thummel et al., 2008). MG-derived neural progenitors are able to differentiate into any of the lost retinal cell types and fully restore visual function in the zebrafish retina. Although many of the major cellular events and several differentially expressed genes have been identified, precise molecular mechanisms that regulate retina regeneration remain largely unknown (Goldman, 2014; Lenkowski and Raymond, 2014; Kamya Rajaram et al., 2014b).

Micro RNAs (miRNAs) are a family of highly conserved small noncoding RNAs that post transcriptionally regulate gene expression and play important roles in many

cellular processes during development and regeneration (Thatcher and Patton, 2010; Wienholds and Plasterk, 2005; Zhao and Srivastava, 2007). We recently showed that the major miRNA processing enzyme, Dicer, is required for retina regeneration in zebrafish and profiled dynamic miRNA expression patterns in the retina during regeneration induced by constant intense light damage (Kamya Rajaram et al., 2014a). Here, we report that *miR-216* acts a gatekeeper for MG reprogramming, maintaining MG in a quiescent state in undamaged retina. *miR-216* suppression is necessary and sufficient for MG dedifferentiation and proliferation. We identify the disruptor of telomeric silencing-1-like (Dot1l) as a *bona fide* target of *miR-216* and demonstrate that the *miR-216*/Dot1l regulatory axis mediates the initiation of retina regeneration through the Wnt/β-catenin pathway. Previous studies in multiple species have revealed that Dot1l is able to regulate transcription of Wnt-target genes by directly interacting with T-cell factor (TCF)/β-catenin complexes (Castaño Betancourt et al., 2012; Mahmoudi et al., 2010; Mohan et al., 2010). Our work uncovers for the first time the role of Dot1l downstream of *miR-216* in the context of retina regeneration and proliferation of Müller glia.

Results

miR-216 is suppressed in dedifferentiated MG during early retina regeneration

We previously demonstrated a general requirement for the Dicer-dependent miRNA biogenesis pathway during retina regeneration induced by constant intense light damage in adult zebrafish (Kamya Rajaram et al., 2014a). *miR-216* is a highly conserved
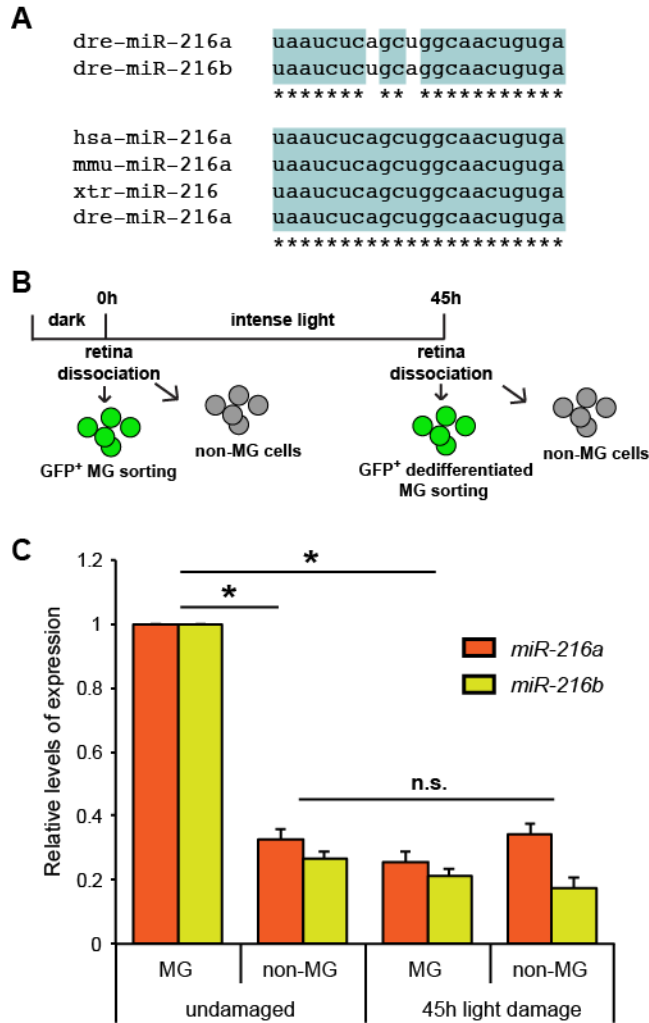
Figure 21   *miR-216* **is suppressed in Müller Glia during retina regeneration.**

(A) Alignment of the zebrafish *miR-216a-b* sequences by ClustalW2, with conserved regions highlighted in blue and indicated with stars. Alignment of *miR-216a* sequences from human (hsa), mouse (mmu), xtr (Xenopus), and dre (zebrafish). (B) Schematic for post-mitotic and dedifferentiated MG sorting. Adult zebrafish were dark adapted for 2 weeks and exposed to constant intense light lesioning for 45 hours. For post-mitotic MG isolation, GFP-positive cells were sorted from dark adapted *Tg(gfap:gfp)* retinas. For dedifferentiated MG isolation, GFP-positive cells were isolated from 45 hr light lesioned *Tg(1016tuba1a:GFP)* retinas. (C) Fold changes in *miR-216a* and *miR-216b* levels in FACS-purified MG were determined by qPCR. Both *miR-216a* and *miR-216b* are enriched in post-mitotic MG (GFP+) from undamaged retinas in *Tg(gfap:gfp)* fish. After 45h of light damage, *miR-216* is down-regulated ~5 fold in dedifferentiated MG (GFP+) in *Tg(1016tuba1a:gfp)* fish. *miR*-216 expression did not change in non-MG cells (GFP-) during regeneration. Shown are data from five independent experiments with three technical replicates of qPCR. MG were purified from 18 and 20 light damaged fish in each experiment. Error bars are SEM. * $p < 0.05$, ** $p < 0.01$. Two-way ANOVA with Fisher's LSD *post-hoc* test.

miRNA family **(Fig. 21A)** with previously characterized functions in gliogenesis during retina development (Olena et al., 2015). We sought to test whether *miR-216* might also regulate reprogramming of Müller glia during retina regeneration. First, we determined the expression levels of *miR-216a/b* in quiescent and proliferating MG, as well as non-MG cells in the retina. We used fluorescence activated cell sorting (FACS) to isolate GFP⁺ quiescent MG from undamaged Tg*(gfap:gfp)* retinas, GFP⁺ dedifferentiated and proliferating MG after 45 hours intense light damaged Tg*(1016tuba1a:gfp)* retinas (Bernardos and Raymond, 2006; Fausett and Goldman, 2006), and GFP⁻ cells from both sorts (non-MG) **(Fig.21B).** GFAP is expressed in quiescent MG, the Tg*(1016tuba1a:gfp)* transgenic line specifically marks dedifferentiated MG and MG-derived neural progenitors in actively regenerating retinas (Fausett and Goldman, 2006). Quantitative real-time PCR (qPCR) analysis showed that both *miR-216a* and *miR-216b* are significantly enriched in quiescent MG compared to non-MG cell population in the undamaged retinas **(Fig. 21C)**. However, *miR-216a/b* are significantly down regulated in dedifferentiated MG in regenerating retinas compared to quiescent MG. When we compared non-MG cell populations in undamaged and intense light damaged retinas, we did not detect any significant change in expression levels of *miR-216a/b*.

miR-216 suppression is required for MG dedifferentiation and proliferation

To test whether *miR-216* suppression is required for MG dedifferentiation and proliferation during retina regeneration, we performed over expression analysis of *miR-216*. We injected and electroporated *miR-216* or a control miRNA intravitreally into the eye of Tg*(tuba1a:gfp)* transgenic fish before intense light damage (0h) and assessed the

effects on MG dedifferentiation and proliferation at 45h of light exposure **(Fig. 22A)**.

While there were numerous GFP+ dedifferentiated MG in control miRNA injected
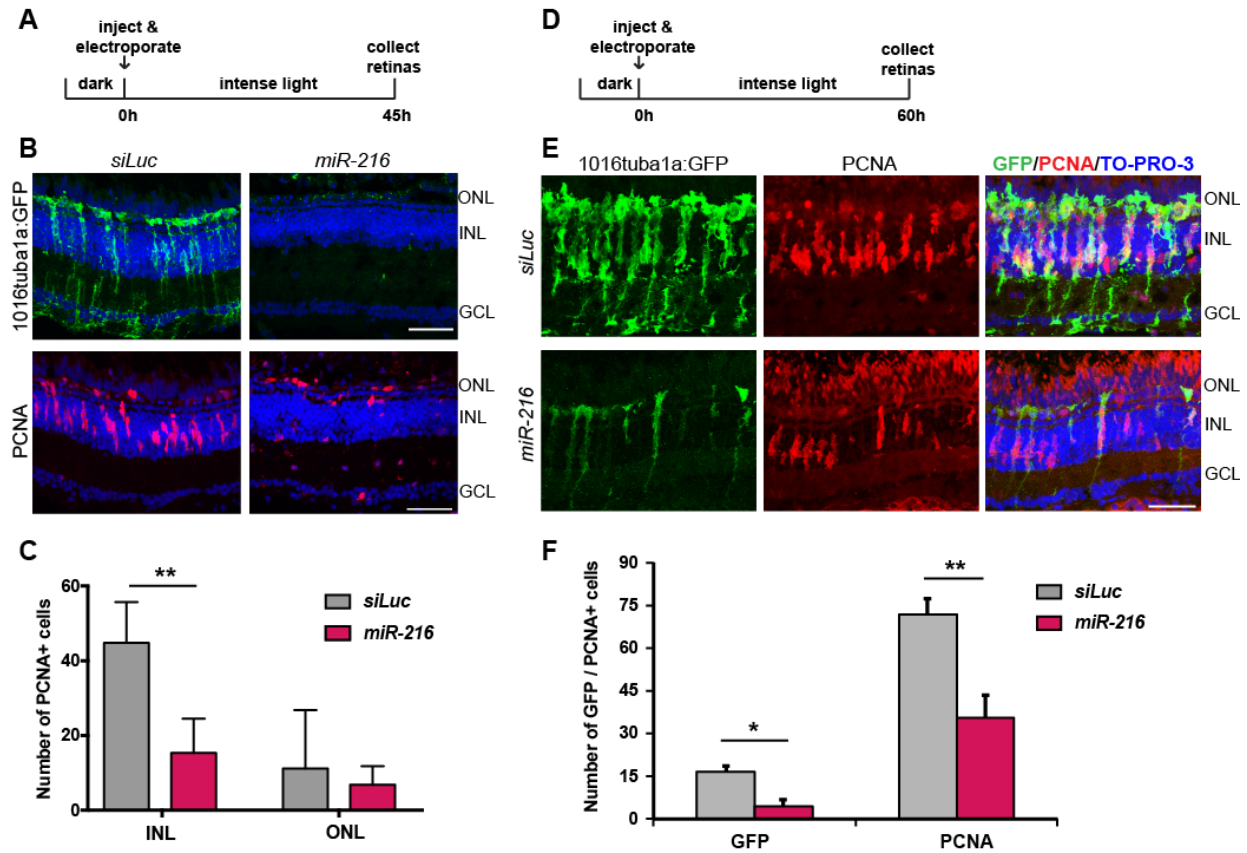
Figure 22   *miR-216* **gain-of-function impairs MG dedifferentiation and proliferation.**

(A) Experimental scheme. Control miRNA or *miR-216* was injected and electroporated into the left eyes of Tg(*1016tuba1a*:gfp) zebrafish before intense light exposure (0h). After 45h, retinas were collected, sectioned and immunostained using antibodies against GFP and PCNA. Nuclei were counterstained with TOPRO (blue). (B) *miR-216* gain-of-function abolished tuba1a:GFP transgene expression and significantly reduced the number of INL PCNA^{+} proliferating cells. (C) Quantification of PCNA^{+} cells in the INL and ONL. Data represent mean +/- s.e.m (n=5-6 fish); **, p<0.01 (Student's t-test). (D) Experimental scheme. (E) Quantification of total GFP[+] and PCNA^{+} cells. Data represent mean +/- s.e.m (n= 10 fish); * p<0.03 , ** p<0.003 (Student's t-test). ONL, Outer nuclear layer; INL, inner nuclear layer; GCL, ganglion cell layer. Scale bar 50um.

retinas at 45h of light damage, there was a striking absence of GFP+ dedifferentiated MG in *miR-216* overexpressing retinas **(Fig. 22B)**. We then analyzed the effect of *miR-216* overexpression on MG proliferation using proliferating cell nuclear antigen (PCNA) as a proliferation marker. Compared to control miRNA overexpressing retinas which had clusters of PCNA$^+$ cells in the inner nuclear layer (INL), excess *miR-216* resulted in significantly decreased numbers of proliferating MG **(Fig. 22C)**. Proliferation of rod progenitor cells in the outer nuclear (ONL) was not affected **(Fig. 22C)**.

Next we assessed β-catenin accumulation in MG, since it was previously shown that β-catenin accumulation as a result of Wnt signaling activation is necessary for MG dedifferentiation and proliferation (Ramachandran et al., 2011). Control miRNA overexpressing retinas expressed β-catenin in MG that co-localized with the PCNA$^+$ clusters (**Fig. 23B**), while *miR-216* overexpression resulted in complete loss of β-catenin staining in the INL. These results show that suppression of *miR-216* is required for the dedifferentiation and proliferation of MG during retina regeneration.
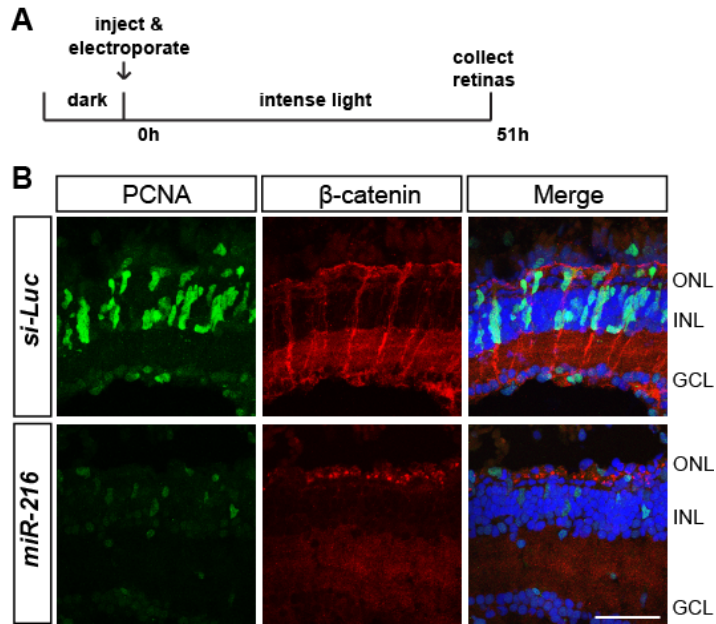
Figure 23   *miR-216* **gain-of-function impairs β-catenin accumulation in MG after intense light damage.**

(A) Experimental scheme. Control miRNA or *miR-216* was injected and electroporated into the left eyes of wild-type zebrafish before intense light exposure (0h). After 45h, retinas were collected, sectioned and immunostained using antibodies against β-catenin (red), PCNA (green). Nuclei were counterstained with TOPRO (blue). (B) β-catenin colocalized with PCNA+ proliferating MG after 45h of intense light damage. β-catenin accumulation was not detected in *miR-216* overexpressing retinas.

We then analyzed the effects of *miR-216* overexpression on MG proliferation at a later stage of retina regeneration (**Fig. 22D,E**). At 60 hours of intense light exposure, there were significantly less dedifferentiated MG marked by GFP, as well as PCNA[+] proliferating progenitors in the INL of *miR-216* overexpressing Tg(*tuba1a:GFP*) retinas compared to control (**Fig. 22E,F**). This suggests that the inhibitory effects of *miR-216* overexpression on the proliferation of MG and MG-derived progenitors are observed at later stages of regeneration, consistent with the model suppression of *miR-216* is a critical step in both the initiation of MG dedifferentiation and the generation of proliferating

progenitor cells during retina regeneration.

Dot1l is a direct target of miR-216 in vivo

To investigate the molecular mechanism through which *miR-216* regulates MG reprogramming, we used the target prediction algorithm TargetScanFish and narrowed down the list of candidate target genes based on their spatiotemporal expression using the RNA-seq transcriptome analysis in purified MG before and after retinal injury (unpublished data) (Lewis et al., 2005). Among the candidate targets, Dot1l emerged as a potential regulator of retina regeneration, since it was previously shown that it functions as an activator of canonical Wnt dependent transcription in zebrafish (Mahmoudi et al., 2010) and canonical Wnt activation is necessary for MG dedifferentiation and proliferation during retina regeneration (Ramachandran et al., 2011).

There are 3 miRNA recognition elements (MREs) for *miR-216* in the 3'UTR of *dot1l* mRNA (**Fig. 24A**). To test whether *miR-216* directly targets *dot1l*, we performed GFP reporter assays in embryos. We cloned the *dot1l* 3'UTR downstream of the GFP
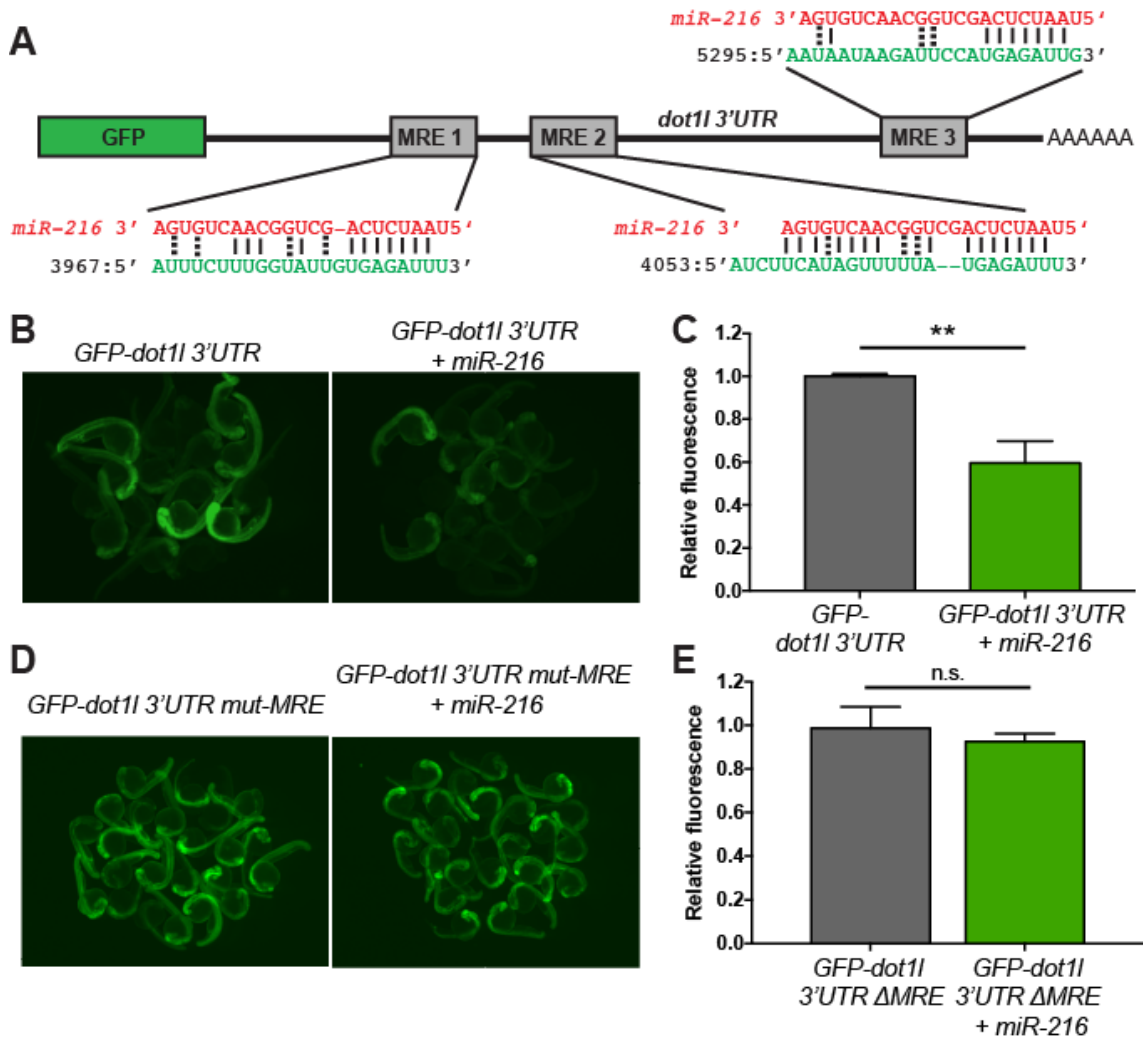
Figure 24   *Dot1l* **is a direct target of** *miR-216.*

(A) Schematic of the reporter mRNA consisting of the coding sequence of GFP fused to the *dot1l* 3'UTR. Three predicted miRNA recognition elements (MREs) are indicated. Predicted base-pairing between MREs (shown in green) and the *miR-216a* sequence (shown in red). (B) 1 dpf old embryos injected at the one-cell stage with 100pg of *GFP-dot1l 3'-UTR*, with or without 100pg of *miR-216*. GFP expression was apparent in embryos injected with *GFP-dot1l 3'-UTR* but was reduced in embryos co- injected with *miR-216*. (C) Quantification of relative fluorescence in 1dpf embryos injected with GFP reporter only or *miR-216* along with GFP reporter. (D) 1 dpf old embryos injected at the one-cell stage with 100pg of *GFP-dot1l 3'-UTR* carrying mutations in all *miR-216* MRE sites. Embryos were injected with the mutant reporter, either alone or co-injected with *miR-216*. (E) Quantification of relative fluorescence in 1dpf embryos injected with mutant GFP reporter alone, or with co-injection of *miR-216*.

coding sequence and in vitro transcribed reporter mRNAs. We then injected the reporter

mRNAs either alone or with co-injected *miR-216* mimics into 1-cell stage zebrafish

embryos. At 24 hours post fertilization (hpf), GFP expression levels were significantly

lower in the embryos co-injected with *miR-216* compared to the ones injected with only

the reporter mRNA (**Fig. 24B**). This indicates that *miR-216* can directly target the

3'UTR of the *dot1l* mRNA. To test whether this targeting is via the MREs predicted by

the target algorithm, we mutated the *miR-216* seed sites in all three MRE sites. Reporter

assays using the mutated reporter construct did not show any changes in the levels of

GFP fluorescence upon co-injection with *miR*-216 (**Fig. 24D,E**). This result shows that

dot1l mRNAs can be targeted by *miR-216* through the indicated MREs.

To determine the spatial expression pattern of Dot1l, we analyzed the expression

of Dot1l by immunohistochemistry and detected punctate localization of Dot1l protein in

tuba1a:GFP$^+$/PCNA$^+$ dedifferentiated and proliferating MG after 51h of light exposure

(**Fig. 25A**). Then, to analyze the changes in expression levels of *Dot1l*, we used FACS to

isolate quiescent MG in Tg(*gfap:gfp*) retinas and dedifferentiated MG in Tg(*tuba1a:gfp*)

retinas (**Fig. 25B**). qPCR analysis showed that there is ~2-fold upregulation in *dot1l*

transcripts in the dedifferentiated MG compared to post-mitotic MG (**Fig. 25C**). We did

not detect changes in *dot1l* expression in other retinal cells. Next, we investigated

whether *miR-216* is able to target endogenous *dot1l* in the retina during regeneration. We

injected and electroporated *miR-216* mimics into the dorsal retina and exposed the fish to

24h of constant intense light damage (**Fig. 25D**). We confirmed the increased levels of

miR-216 in miRNA mimic injected retinas (**Fig. 25F**). Increased *miR-216* levels led to a
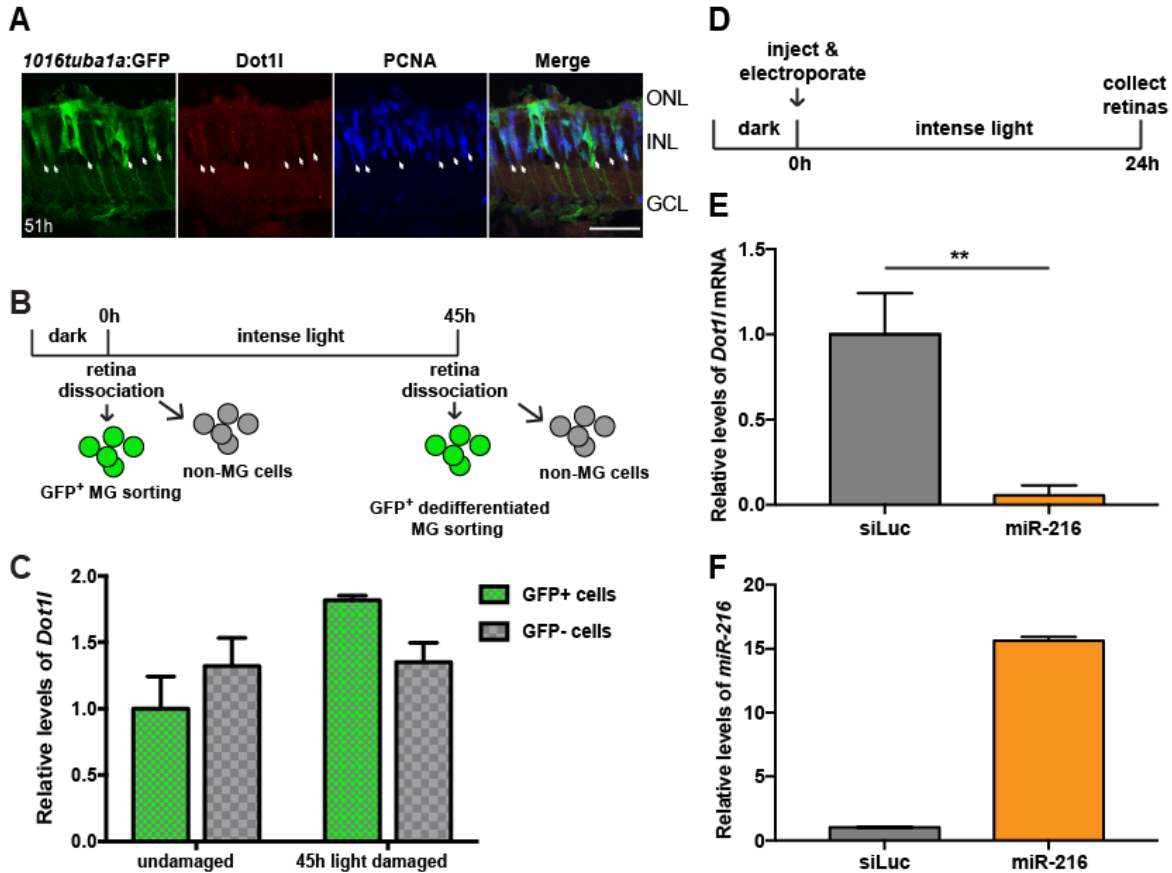
Figure 25 *miR-216* targets *Dot1l* in the retina during photoreceptor regeneration.

(A) Dot1l (red), GFP and PCNA (blue) immunostaining on 51 hr intense light lesioned Tg(1016tuba1a:gfp) retinas. Dot1l is expressed in proliferating MG. Arrows indicate some GFP[+]/PCNA[+] dedifferentiated MG that express Dot1l. (B) Schematic for post-mitotic and dedifferentiated MG sorting. For post-mitotic MG isolation, GFP^{+} cells were sorted from dark adapted undamaged *Tg(gfap:gfp)* retinas. For dedifferentiated MG isolation, GFP-positive cells were isolated from 45 hr light lesioned *Tg(1016tuba1a:GFP)* retinas. (C) Fold changes in *dot1l* levels in FACS-purified MG were determined by qPCR. After 45h of light damage, *dot1l* is up-regulated in dedifferentiated MG (GFP+) in *Tg(1016tuba1a:gfp)* fish. *Dot1l* expression did not change in non-MG cells (GFP-) during regeneration. Data represent mean +/- s.e.m from 15 undamaged fish and dedifferentiated MG were purified from 18 light damaged fish. (D) Experimental scheme. Wild-type adult zebrafish were dark adapted. Control miRNA or *miR-216* was injected and electroporated into the left eyes before intense light exposure. After 24 hours of light exposure, retinas were dissected for RNA isolation. (E) Fold changes in *dot1l* levels in *siLuc* or *miR-216* mimic electroporated retinas were quantified by qPCR. After 24h of light damage, *dot1l* is downregulated in *miR-216* overexpressing retinas ~20 fold. Data represent mean +/- s.e.m from 3 independent experiments. 6 retinas were pooled for RNA isolation in each experiment. ** $p<0.01$ (Student's t-test), p=0.0093. (F) Fold changes in *miR-216* levels in siLuc or *miR-216* mimic electroporated retinas were quantified by qPCR. *miR-216* levels were upregulated by 15-fold in *miR-216* mimic injected retinas compared to controls. Data represent mean +/- s.e.m from 6 retinas. ONL, outer nuclear layer; INL, inner nuclear layer; GCL, ganglion cell layer. Scale bar 50um.

significant decrease (~95%) in endogenous *dot1l* mRNA levels, as shown by the qPCR

analysis (**Fig. 25E**). Collectively, these results indicate that *miR-216* regulates *dot1l* in

the adult retina.

Dot1l is necessary for proliferation during retina regeneration

Given that excess *miR-216* inhibits the dedifferentiation and proliferation of MG,

we hypothesized that Dot1l would be required for the early phases of retina regeneration.

To analyze the loss-of-function of Dot1l during retina regeneration, we knocked down

Dot1l by injecting and electroporating previously characterized morpholinos (MOs)

against *dot1l* into the retina prior to intense light damage (Mahmoudi et al., 2010) (**Fig.**

26A). We used the Tg(*tuba1a:GFP*) transgenic line to assess the dedifferentiation of

MG, cell cycle re-entry of MG, and proliferation of MG-derived progenitors. At 45h of

constant intense light damage, there were significantly less dedifferentiated MG, as well

as decreased numbers of PCNA+ proliferating progenitors in retinas electroporated with

Dot1l MO (**Fig. 26B,C**). To test for specificity and possible off target effects of MOs, we

used a second Dot1l morpholino (MO-Dot1l-2) and again assessed the effect of Dot1l

knock-down in the regenerating retinas after intense light damage (**A.1A**). Dot1l-MO-2

injected retinas also displayed significantly reduced numbers of PCNA+ proliferating

neural progenitors at 45h of light damage (**A.1A**).

To test whether the requirement of Dot1l is through its histone methyltransferase

activity, we used a small molecule inhibitor of Dot1l catalytical activity, (iDot1l;

EPZ004777), that competitively binds to the S-adenosylmethionine-binding pocket of
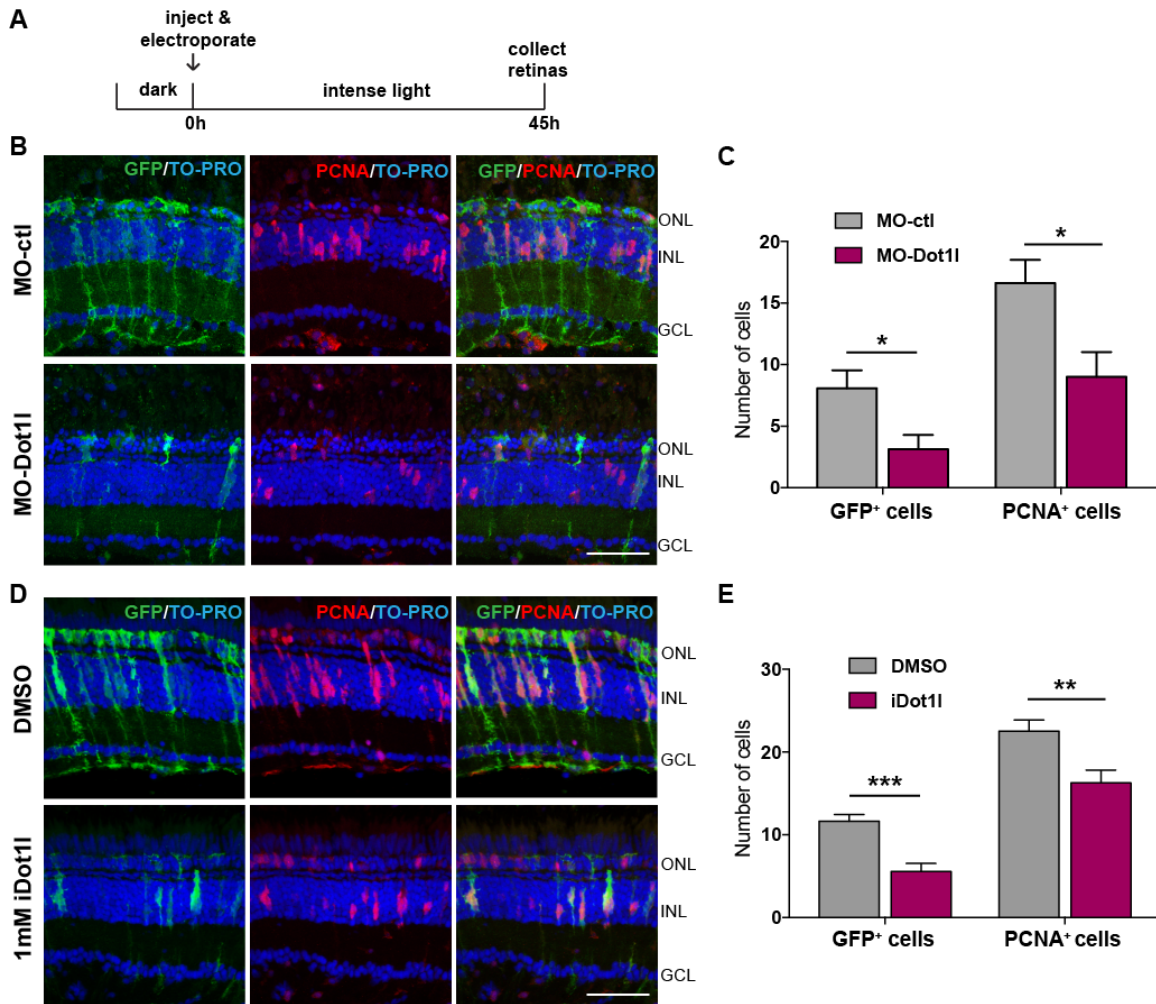
Figure 26   Dot1l is required for MG dedifferentiation and proliferation during retina regeneration.

(A) Experimental scheme. Control morpholino (MO) or Dot1l MO was injected and electroporated into the left eyes of Tg(*1016tuba1a*:gfp) zebrafish before intense light exposure (0h). After 45h, retinas were collected, sectioned and immunostained using antibodies against GFP, PCNA. Nuclei were counterstained with TOPRO (blue). (B) Dot1l loss-of-function reduced tuba1a:GFP transgene expression and the number of INL PCNA$^+$ proliferating cells. (C) Quantification of GFP$^+$ dedifferentiated MG and PCNA$^+$ proliferating progenitors in MO-ctl and MO-Dot1l electroporated retinas. Data represent mean +/- s.e.m (n= 5-6 fish); **, p<0.01 by two-tailed, Mann–Whitney U test. (D) Control vehicle (DMSO) or iDot1l (Dot1l inhibitor-EPZ004777) was injected intravitreally into the left eyes of Tg(*1016tuba1a*:gfp) zebrafish before intense light exposure (0h). After 45h, retinas were collected, sectioned and immunostained using antibodies against GFP, PCNA. Nuclei were counterstained with TOPRO (blue). (E) Quantification of total GFP$^+$ and PCNA$^+$ cells. Error bars represent mean +/- s.e.m (n=10 fish); *p=0.0111; ****$p < 0.0001$ by two-tailed, Mann–Whitney U test. ONL, Outer nuclear layer; INL, inner nuclear layer; GCL, ganglion cell layer. Scale bar 50um.

Dot1l (Daigle et al., 2011). Compared to the control vehicle injected retinas, intravitreal injection of iDot1l led to a significant reduction in the number of dedifferentiated MG, as well as the number of proliferating progenitors in the INL after 45h of intense light damage (**Fig. 26D,E**). Together, the knockdown experiments and pharmacologic inhibition experiments support the hypothesis that Dot1l is required for MG reprogramming acting as an epigenetic modifier required for dedifferentiation and proliferation of MG-derived neural progenitors during retina regeneration.

Suppression of miR-216 is sufficient for retina regeneration through targeting Dot1l

Next, we investigated whether *miR-216* down-regulation is sufficient to drive MG-dedifferentiation and the formation of neural progenitors. To test this, we suppressed the *miR-216* levels by injection and electroporation of antisense *miR-216* morpholinos (MO-216) in undamaged Tg(*tuba1a:gfp*) retinas. At 51 hours post injection (hpi), we assessed whether loss of *miR-216* function results in the initiation of a regenerative response similar to what happens after retinal damage (**Fig. 27A**). Surprisingly, while we did not detect any dedifferentiated GFP$^+$ MG in most of the control morpholino injected retinas, *miR-216* suppression resulted in a significant increase in the number of dedifferentiated MG in undamaged Tg(*tuba1a:gfp*) retinas (**Fig. 27B, C**). We also detected significantly higher numbers of proliferating PCNA$^+$ MG in *miR-216* suppressed retinas compared to control morpholino injected retinas (**Fig. 27B, D**).

We hypothesized that *miR-216* suppression stimulates MG proliferation through targeting Dot1l. Thus, co-suppressing Dot1l along with *miR-216* should block MG
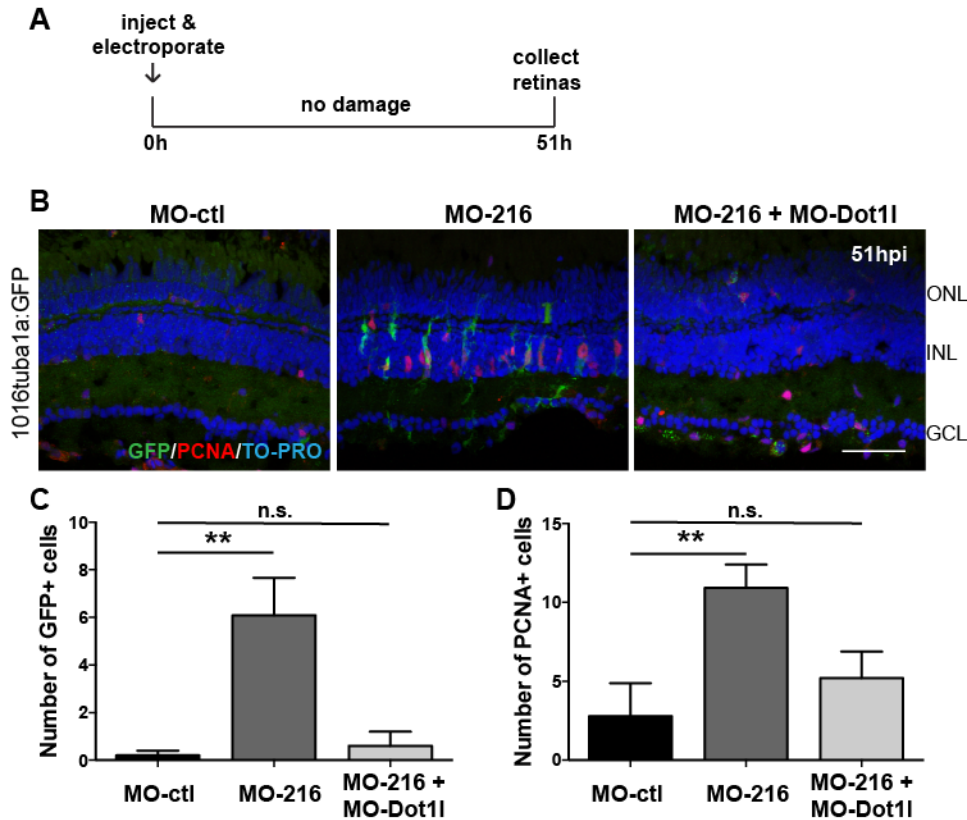
Figure 27   *miR-216* **suppression stimulates MG dedifferentiation and proliferation in the uninjured retina through regulating Dot1l.**

(A) Experimental scheme. Undamaged *Tg(1016tuba1a:gfp)* zebrafish were injected and electroporated with control MO (n=5), *miR-216* MO (n=6), or both (n=5). Eyes were collected at 51 h post-injection and immunostained using antibodies against GFP or PCNA. Nuclei were counterstained with TOPRO (blue). (B) *miR-216* MO significantly increased the number of PCNA$^+$ and GFP$^+$ cells in the INL, while there was no significant difference between *miR-216* MO + Dot1l MO co-injected eyes and control eyes. (C) Quantification of GFP$^+$ dedifferentiated MG and PCNA$^+$ proliferating progenitors in MO-ctl, MO-216 and MO-216 + MO-Dot1l electroporated retinas. The error bars represent mean ± s.e.m. ** $p < 0.01$, PCNA p-value=0.0098 and GFP p=0.0039 by one-way ANOVA with Dunnett's multiple comparisons test. ONL, Outer nuclear layer; INL, inner nuclear layer; GCL, ganglion cell layer. Scale bar 50um.

proliferation. To test this, we combined intravitreally injection and electroporation of

both Dot1l and *miR-216* morpholinos in uninjured Tg(*tuba1a:gfp*) retinas. Compared to

the control retinas, we no longer observed a significant increase in the number of

dedifferentiated and proliferating MG at 51 hours post injection (**Fig. 27B, D**). This

result demonstrates that *miR-216* must be downregulated to activate Dot1l during retina regeneration and that Dot1l is required for the initiation of MG proliferation.

Wnt/β-catenin signaling is required downstream of miR-216/Dot1l during retina regeneration

Dot1l is a histone methyltransferase responsible for H3K79me3 modification associated with gene activation (Feng et al., 2002; Shanower et al., 2005; Steger et al., 2008; Van Leeuwen et al., 2002). It was previously reported that Dot1l serves as a co-activator Wnt/β-catenin signaling (Mahmoudi et al., 2010; Mohan et al., 2010) which is known to be activated during retina regeneration and is required for the formation of MG-derived progenitors (Meyers et al., 2012; Ramachandran et al., 2011). Since our initial finding showed that *miR-216* suppression is necessary for MG-dependent retina regeneration, we wanted to test whether *miR-216* suppression is also required for the activation of Wnt/β-catenin signaling. We injected and electroporated *miR-216* mimics or control miRNAs in the retinas of adult wild-type fish prior to intense light damage (**Fig. 23A**). At 51h of light damage, β-catenin accumulation was clearly observed in MG associated with PCNA[+] neural progenitors in control retinas. However, no β-catenin accumulation was observed in *miR-216* overexpressing retinas (**Fig. 23B**). This led us to hypothesize that the *miR-216*/Dot1l regulatory pathway regulates retina regeneration through canonical Wnt signaling. We first tested whether the proliferation defects after knockdown of Dot1l could be rescued by activation of Wnt signaling. To activate Wnt signaling, we pharmacologically stabilized β-catenin using a glycogen synthase kinase-3β (GSK3β) inhibitor (Ramachandran et al., 2011). We intravitreally injected the GSK3β
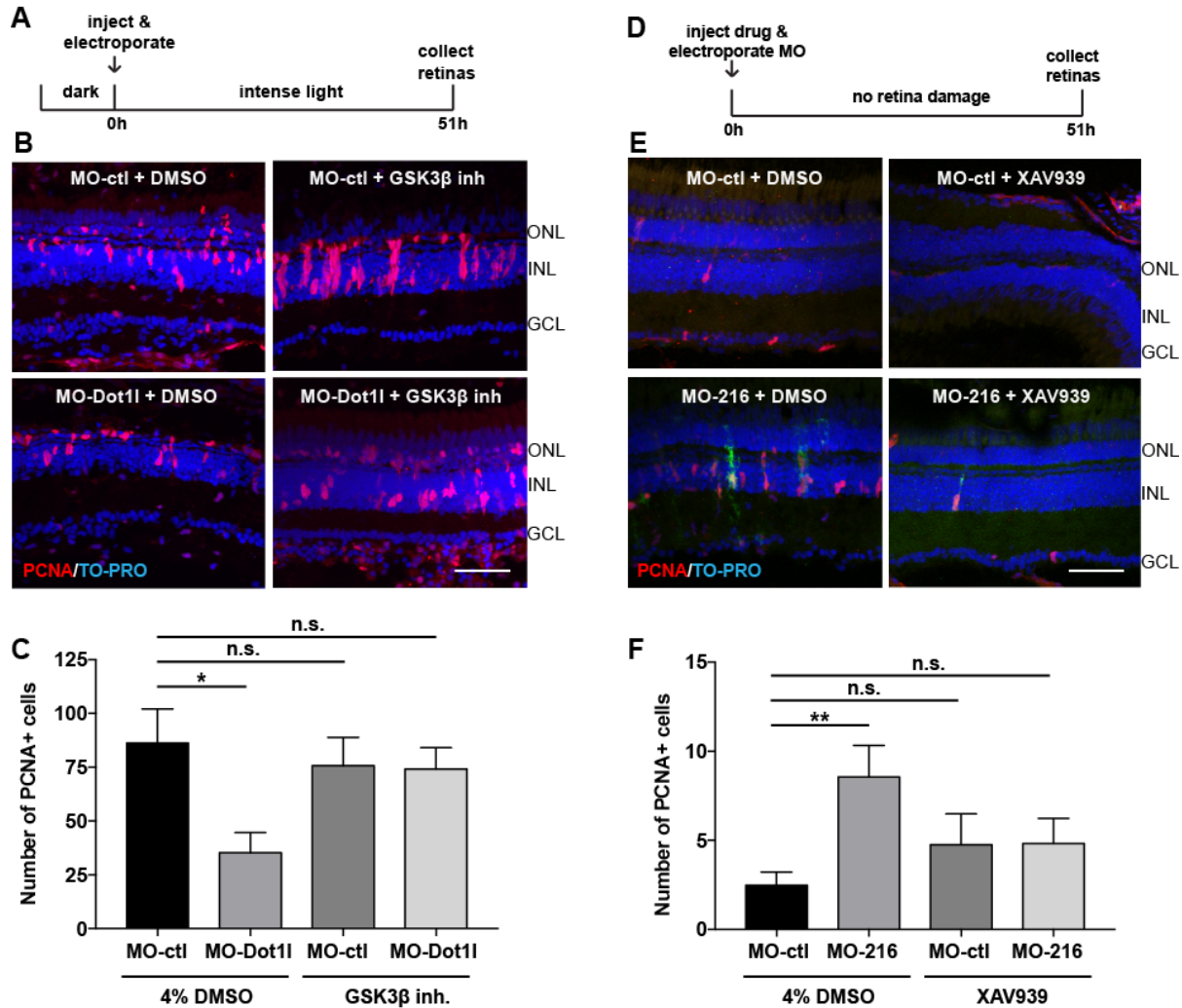
Figure 28 *miR-216* **and Dot1l regulate retinal regeneration through the Wnt/β-catenin pathway.**

(A) Experimental scheme. Control morpholino or Dot1l morpholino was injected and electroporated into the left eyes of wild-type zebrafish, followed by either 4% DMSO or GSK3β-inhibitor (1mM) before intense light exposure (0h). Eyes were collected after 51 hours of intense light lesion and immunostained using antibodies against PCNA. Nuclei were counterstained with TOPRO (blue). (B) Dot1l MO significantly decreased the number of PCNA^{+} cells in the INL, while there was no significant difference between Dot1l MO + GSK3β-inhibitor co-injected eyes and control eyes. (C) Quantification of PCNA[+] proliferating progenitors in MO-ctl+DMSO, MO-Dot1l+DMSO, MO-ctl+ GSK3β-inhibitor and MO-Dot1l + GSK3β-inhibitor electroporated retinas. Activation of Wnt signaling rescued the decrease in the number of proliferating progenitors upon Dot1l knockdown after 51 hours of intense light lesion. Error bars represent mean ± s.e.m. (n=9-11 fish). * $p < 0.05$, p-value=0.0167 (MO-ctl+DMSO vs MO-Dot1l+DMSO) by one-way ANOVA with Dunnett's multiple comparisons test. (D) Experimental scheme. Control morpholino or *miR-216* morpholino was injected and electroporated into the left eyes of Tg*(1016tuba1a:GFP)* zebrafish, followed by either 4%DMSO or XAV939(10μM). Eyes were collected at 51 h post-injection and immunostained using antibodies against GFP for dedifferentiated MG and PCNA for proliferating progenitors. Nuclei

were counterstained with TOPRO (blue). (E) Suppression of *miR-216* by MO-216 injection stimulates MG proliferation, however upon co-injection with XAV939 no significant increase in the number of proliferating progenitors was detected. (F) Quantification of PCNA$^+$ proliferating progenitors in MO-ctl+DMSO, MO-216+DMSO, MO-ctl+ XAV939 and MO-216 + XAV939 electroporated retinas. Inhibition of Wnt signaling reversed the increase in the number of progenitors upon *miR-216* knockdown after 51 hours of intense light lesion. Error bars represent mean ± s.e.m (n=18-21 fish). ** $p < 0.01$, p-value=0.0089 (MO-ctl+DMSO vs MO-216+DMSO) by one-way ANOVA with Dunnett's multiple comparisons test. ONL, Outer nuclear layer; INL, inner nuclear layer; GCL, ganglion cell layer. Scale bar 50um.

inhibitor or control vehicle (DMSO) with either control MOs or Dot1l MOs prior to

intense light damage (**Fig. 28A**). At 51h of light damage, Dot1l depletion resulted in

significantly decreased numbers of PCNA$^+$ proliferating progenitors compared to control

retinas (**Fig. 28B**). However, co-injection of Dot1l MOs and the GSK3β inhibitor

showed no defects in the number of neural progenitors. Of note, injection of the GSK3β

inhibitor alone did not elevate the regenerative response above that observed after intense

light damage. This suggests that Dot1l regulates MG proliferation through Wnt/ β-

catenin signaling during intense light damage induced retina regeneration.

Finally, we investigated whether *miR-216* depletion in undamaged retinas would

induce MG proliferation through modulating Wnt/ β-catenin signaling (**Fig. 28D**). We

pharmacologically inhibited canonical Wnt signaling by injecting XAV939, a tankyrase

inhibitor, which stabilizes Axin and eventually stimulates β-catenin degradation (Huang

et al., 2009). For this, we injected either XAV939 (10μM) or control vehicle (DMSO)

along with co-injection of either control or *miR-216* MO into undamaged retinas (**Fig.**

28D). Intravitreal injection of XAV939 at 10μM concentration was previously shown to

be sufficient to prevent injury dependent β-catenin accumulation in MG (Ramachandran

et al., 2011). As above, *miR-216* morpholino injection in undamaged retinas caused

spontaneous proliferation of MG as detected by the presence of significantly higher

numbers of PCNA+ proliferating cells in the INL at 51hpi (**Fig. 28E, F**). However, co-injection of XAV939 and MO-216 no longer caused any significant increase in the number PCNA+ proliferating cells compared to control MOs or DMSO injected retinas. These results demonstrate that Wnt/ β-catenin signaling is required for spontaneous MG proliferation initiated by depletion of *miR-216*.

Discussion

Müller glia (MG) dedifferentiation and re-entry into cell-cycle are key events during retina regeneration. In zebrafish, MG are capable of eliciting a robust regenerative response upon damage, while in mammals MG lack the spontaneous proliferative response and typcially become reactive and undergo hypertrophy (Bringmann et al., 2006). Understanding the molecular mechanisms of MG activation during regeneration is necessary to develop therapeutic strategies for retinal diseases in humans. Here, we identified a novel miRNA-mediated mechanism regulating initiation of retina regeneration in adult zebrafish. We show that suppression of *miR-216* in MG is required for dedifferentiation and proliferation upon constant intense light damage leading to de-repression of the H3K79 methyltransferase Dot1l which is required for regeneration. Furthermore, we demonstrate that *miR-216* and Dot1l regulate MG activation through Wnt/β-catenin signaling. Together, our data provide a novel mechanism through which *miR-216* serves a gatekeeper for MG dedifferentiation and proliferation by suppressing Dot1l during retina regeneration.

Although many individual miRNAs have been identified that regulate cell fate in

development and disease, only a few miRNAs have been shown to be functionally involved in modulating retina regeneration (Kamya Rajaram et al., 2014a, 2014b; Ramachandran et al., 2010c). We show that *miR-216* is expressed in quiescent MG in adult zebrafish retina and must be repressed to allow MG dedifferentiation and re-entry into cell cycle. Expression of miR-216 was not observed to change in non-MG cells of the retina. Interestingly, *miR-216* was first reported to modulate retinal gliogenesis by targeting *snx5* (sorting nexin 5) during development (Olena et al., 2015). *miR-216* is suppressed in the central retina to allow MG specification through activation of Notch signaling. In that model, *miR-216* targets *snx5* (sorting nexin 5) to block association of the Notch ligand Delta and prevent Delta endocytosis and thereby regulate Notch signaling. It predicts that *miR-216* functions in cells containing the Notch ligand Delta. Interestingly, we did not detect any significant changes in *snx5* expression levels in FACS-purified MG populations before and after intense light damage (data not shown). In addition, a previous study showed that while Notch receptors are present in proliferating neural progenitors, Notch ligands were detected in cells adjacent to the proliferating progenitors during retina regeneration (Wan et al., 2012b). Therefore, *miR-216* plays distinct roles during development versus regeneration regulating distinctly different targets.

Previous reports have shown that it is possible to stimulate MG proliferation in undamaged zebrafish retinas through manipulation of various factors such as tumor necrosis factor α (TNFα) (Nelson et al., 2013), GSK-3β (Ramachandran et al., 2011), leptin, interleukin-6 (IL-6) (Zhao et al., 2014) and γ-aminobutyric acid (GABA) (Rao et al., 2017). Although the interdependency of these factors is still to be determined, they

hold great promise as therapeutic agents to induce regenerative response in mammals. Here, we show that *miR-216* is an endogenous inhibitor of retina regeneration and suppression of *miR-216* is sufficient to induce a regenerative response in the absence of damage. This suggests that *miR-216* might be upstream of the many signaling pathways that are required for MG proliferation. Indeed, stimulation of MG proliferation upon suppression of *miR-216* was blocked by co-suppression of canonical Wnt signaling (**Fig. 28E, F**). In addition, excess *miR-216* levels resulted in loss of β-catenin accumulation in MG after intense light damage (**Fig. 23**). These findings suggest that *miR-216* serves as an inhibitory factor in quiescent MG that needs to be suppressed to turn on canonical Wnt signaling and allow MG to dedifferentiate and proliferate.

It is perhaps not surprising that epigenetic modifications accompany cell fate changes in MG during retina regeneration. Analysis of DNA methylation profiles in quiescent MG and MG-derived progenitors have shown that many pluripotency and regeneration-associated genes are hypomethylated during zebrafish retina regeneration (Powell et al., 2013). Interestingly, in mouse MG, these genes are also hypomethylated, suggesting that DNA methylation is not an epigenetic barrier for retina regeneration in mammals. Accessible chromatin in mouse mature MG decreases relatively rapidly, coincident with the loss of neurogenic capacity in postnatal development (Jorstad et al., 2017; Ueki et al., 2015). This suggests that changes in histone modifications may underlie MG reprogramming during retina regeneration in zebrafish but the precise chromatin modifying enzymes have remained unknown.

Our data support the hypothesis that *miR-216* regulates MG dedifferentiation and proliferation through targeting the H3K79 methyltransferase Dot1l. First, 3'UTR

reporter assays showed that *miR-216* targets the 3'UTR of Dot1l (**Fig. 24**). Second, we showed that Dot1l is upregulated in dedifferentiated MG compared to post-mitotic MG after 45hours of constant intense light damage (**Fig. 25A-C**). Third, morpholino knockdown and inhibition of Dot1l H3K79 methyltransferase activity showed that Dot1l upregulation is required for MG activation during early regeneration (**Fig. 26B-E**). Lastly, suppression of *miR-216* alone is sufficient to stimulate a regenerative response in the undamaged retina, while co-suppressing Dot1l prevented the MG proliferation.

Previous studies in multiple species have revealed that Dot1l is the only methyltransferase that catalyzes the histone H3-lysine 79 (H3K79) mono-, di-, and trimethylation (Feng et al., 2002; Jones et al., 2008; Shanower et al., 2005; Steger et al., 2008; Van Leeuwen et al., 2002). It has been proposed that Dot1l-mediated H3K79 methylation is associated with the transcription of Wnt-target genes, which is mediated by TCF transcription factors and the co-activator β-catenin (Clevers, 2006). A direct interaction between Dotl1l and β-catenin-dependent TCF4 complexes was identified in zebrafish intestinal stem cells, as well as in mouse small intestinal crypts (Mahmoudi et al., 2010). The hypothesis is that recruitment of Dot1l to Wnt target genes by β-catenin leads to H3K79 methylation and preferential activation of transcription of Wnt target genes. The interaction of Dot1l with β-catenin was confirmed in Drosophila embryos by demonstrating the presence of β-catenin within Dot1L-containing protein complexes and a requirement of H3K79me3 in regulating Wnt target genes (Mohan et al., 2010). Additionally, in a genome-wide association study (GWAS) a Dot1l polymorphism was linked to reduced risk for osteoarthritis. Further it was shown that Dot1l interacts with Tcf4 in articular chondrocytes and is required for Wnt-dependent chondrogenesis

(Castaño Betancourt et al., 2012). In zebrafish, retinal damage including both intense light and mechanical damage leads to activation of Wnt/ β-catenin signaling in MG (Meyers et al., 2012; Ramachandran et al., 2011). In this study, we showed that canonical Wnt signaling is required downstream of Dot1l activity during MG dedifferentiation and proliferation. Our data show that hyperactivation of Wnt signaling by stabilizing β-catenin alleviates the defects due to Dot1l knockdown during retina regeneration (**Fig. 28A, B**). Although this finding does not provide a direct interaction of Dot1l with β-catenin/Tcf4 components, it does support the model that Dot1l is an upstream regulator of β-catenin-dependent signaling during retina regeneration.

Together, our study reports the discovery of a novel *miR-216* mediated mechanism regulating the MG reprogramming in response to photoreceptor loss in adult zebrafish. Retinitis pigmentosa and age-related macular degeneration involve photoreceptor dysfunction that eventually leads to loss of vision. It will be interesting to test whether suppressing *miR-216* levels will induce mammalian MG proliferation and neural progenitor production.

Methods

Zebrafish husbandry and adult zebrafish light lesioning

Wild-type (AB) (Walker, 1999), T*g(1016tuba1a:gfp)* (Fausett and Goldman, 2006), *Tg(gfap:gfp)*[mi2001] (Bernardos and Raymond, 2006) lines were maintained at 28.5^0C on a 14:10 hour light:dark cycle. All experiments with zebrafish were performed with the approval of the Vanderbilt University Institutional Animal Care and Use

Committee. Adult zebrafish used for the experiments were between 5-12 months old.

Constant intense light lesioning to induce cone and rod photoreceptor cell death was

performed as previously described (Kamya Rajaram et al., 2014c). Briefly, adult fish

were dark adapted for 14 days, transferred to clear tanks placed between two fluorescent

lights with light intensity at ~20,000 lux for 16h-3days. The tank temperature was

maintained at 30- 33°C.

Fluorescence activated cell sorting (FACS)

FACS was used to isolate GFP+ and GFP- cells from the retinas of undamaged

Tg(*gfap:gfp*)[mi2001] and Tg(*1016tuba1a:gfp*) fish using BD FACSAria III (BD

Biosciences) at the VUMC Flow Cytometry Shared Resource. Retinas were dissociated

as previously described (Kamya Rajaram et al., 2014b) with the following changes. After

the retinas were dissected, they were collected in Leibovitz L-15 media (ThermoFisher

#21083-027) and treated with 1mg/ml hyaluronidase (Sigma #H3884) at room

temperature for 15 minutes on a rocker. Cells from the dissociated retinas were stained

with propidium iodide to detect dead cells. 12 adult fish were used for each FACS

experiment. As a quality control, sorted GFP+ cells were re-analyzed to check the purity

of the cell population by re-sorting.

RT-PCR

Total RNA was isolated from FAC-sorted cells using TRIzol-LS (ThermoFisher #

10296028). Taqman small RNA assays (Life Technologies) were used to perform qRT-

PCR of the indicated miRNAs. 5ng of total RNA was used per RT reaction and 1.33μl of

1:2 diluted resultant cDNA was used in 10μl qPCR reaction in technical triplicates.

qPCR reactions were conducted in either 96-well plates using Bio-Rad CFX96 Real-time system or in 384-well plates using Bio-Rad CFX384 Real-time System. All quantifications were normalized to an endogenous U6 snRNA control. Fold changes were calculated using the $\Delta\Delta C(t)$ method, where $\Delta = C(t)miRNA - C(t)U6$ snRNA, and $\Delta\Delta C(t) = \Delta C(t)condition1 - \Delta C(t)$ condition2, and $FC = 2-\Delta\Delta C(t)$. Taqman probe #: U6 snRNA: 001973; has-miR-216a:002220; hsa-miR-216b: 002326. For RT-PCR of mRNAs, RNA was DNase treated (TURBO DNAfree kit ThermoFisher #AM1907), converted to cDNA using Maxima first strand cDNA synthesis kit (Thermo Scientific) and qPCR was performed using SYBR Green (Biorad). All qPCR primers spanned exon-exon junctions (IDT). miRNA realtime PCR was perfomed using Taqman probes as per the manufacturer's instructions (Life Technologies). Relative RNA expression during regeneration were determined using the $\Delta\Delta Ct$ method and normalized to 18s rRNA levels and U6 snRNA levels for mRNAs and miRNAs respectively. Real time PCR was performed on a Biorad CFX 96 Real time system. The following primer sequences were used: dot1l-qpcr-fp: 5'- CATGATGCTGCACACGAAAT-3'; dot1l-qpcr-rp: 5'- TCTCGAAGCTCTTGGTGTCA-3'; 18srRNA-qpcr-fp: 5'- ACGCGAGATGGAGCAATAAC-3'; 18srRNA-qpcr-rp: 5'- CCTCGTTCATGGGAAACAGT-3'.

Plasmid construction and embryo injections

The *dot1l* 3'UTR was amplified from cDNA by PCR with the following primers: dot1l-3'utr-fp: 5'-AGACTTGAATTCCCTTCCAGGAACTGAGTTTAACC-3' dot1l-3'utr-rp: 5'- AGTCTGCTCGAGCAGCTCCACAGGTAAATGATCC-3'. The 3'UTR was cloned downstream of the GFP coding sequence in the PCS2+ vector. miRNA

recognition elements (MREs) within the *dot1l* 3'UTR were deleted using the

QuikChange Lightning Site-Directed Mutagenesis Kit (Stratagene). mRNAs were *in
vitro* synthesized from linearized constructs using mMESSAGE mMACHINE® SP6

Transcription Kit (Life Technologies). *In vitro* transcribed RNA was purified by

NucAway™ Spin Columns (Life Technologies). For reporter assays, GFP-dot1l-3'UTR

mRNA was injected at 100pg/embryo concentration either alone or with a synthetic *miR-
216a* duplex (Dharmacon) at 100pg/embryo.

Morpholino and miRNA mimic injection & electroporation

Lissamine tagged morpholinos (MOs) (Gene Tools) were injected intravitreally

and electroporated into adult zebrafish eyes prior to light lesioning as described

(Thummel et al., 2008b). The following 3'-Lissamine-tagged MOs were used: Gene

Tools standard control MO: 5'-CCTCTTACCTCAGTTACAATTTATA-3'; *Dot1*

MO: 5'-CCCAGCTATACACACAAAAAGCAGC-3'; Dot1l MO-2:

5'AAGAGAACATTTCTCACCTCCTGGT-3'; *miR-216a* MO: 5'-

TCACAGTTGCCAGCTGAGATTA-3'.

Duplex mature miRNAs (Thermo scientific) were injected and electroporated into eyes

prior to start of light lesioning as previously described (Rajaram, 2014b). Double

stranded mature miRNAs were synthesized with 3'- UU overhangs for the following

target sequences: *miR-216*: 5'-UAAUCUCAGCUGGCAACUGUGAUU-3' control: 5'-

AAAAACAUGCAGAAAAUGCUG-3' Electroporation was performed using the Gene

Pulser Xcell™ Electroporation Systems (Biorad).

Pharmacological treatment

To stimulate Wnt signaling, GSK-3β Inhibitor I (Calbiochem; CAS 327036-89-5) was intravitreally injected at 1mM in 4%DMSO. Wnt signaling was blocked by the tankyrase inhibitor/axin stabilizing agent XAV939 (Cayman chemical; 10mM stock in DMSO) intravitreally injected at 10μM in 4%DMSO. For catalytic inhibition of Dot1l, EPZ004777 (Calbiochem; CAS 1338466-77-5) was intravitreally injected.

Immunohistochemistry

Adult zebrafish eyes were collected and fixed in either 4% paraformaldehyde at 4^0C overnight or a fixant containing 9 parts 95% ethanol:1 part 37% formaldehyde (for dot1l IHC), cryoprotected in 30% sucrose/1X PBS before embedding. 10-12 micron sections were obtained using a cryostat (Leica), collected on charged Histobond slides (VWR), dried and stored at -80°C. For IHC, slides were warmed to room temperature, rehydrated in 1X PBS and blocked (3% Donkey serum, 0.1% TritonX-100 in 1X PBS) for 1–2h at room temperature before incubating with primary antibodies overnight at 4^0C. The following primary antibodies were used: mouse anti-PCNA monoclonal antibody (1:500, Sigma), anti-PCNA polyclonal antibody (1:500, Abcam), rabbit anti-GFP polyclonal antiserum (1:1000, Torrey Pines Biolabs), mouse anti-β-catenin antibody (1:500, BD Bioscience) and rabbit anti-dot1l polyclonal antibody (1:200, Bethyl labs). After primary antibody incubation, sections were washed and incubated with secondary antibody and nuclear stain TOPRO 3 (1:1000, Invitrogen) at room temperature. Secondary antibodies were donkey anti-mouse AF488 (1:200), donkey anti-mouse AF647 (1:200), donkey anti-mouse Cy-3 (1:100), donkey anti-rabbit Cy3 (1:100) and donkey anti-rabbit AF488 (1:200)(Jackson Immuno). Slides were washed, dried and

coverslipped with Vectashield (Vector labs). Antigen retrieval was performed for β-catenin and PCNA IHC as previously described (Kamya Rajaram et al., 2014b).

Imaging and image processing

For imaging of immunofluorescent staining, a META Zeiss LSM 510 Meta confocal microscope was used. Images were processed using ImageJ software 4.13. Fluorescence intensity measurements were done using ImageJ software (Gavet and Pines, 2010). For each image, "integrated density", "area" and "mean gray value" of the fli1a:eGFP+ region, as well as background, were measured. Corrected fluorescence intensity of the selected region was calculated according to the formula: "Corrected fluorescence intensity= Integrated Density - (Area of selected region * mean fluorescence of background)". Data were represented as a mean of corrected fluorescence intensity for each experimental condition and statistical analyses were performed using a two-tailed Student's t-test. For immunostaining and cell quantification, only retina sections that comprised optic nerves were used. All cell counts were done in the central-dorsal retina, at a linear distance of ~300 microns from the optic nerve. In all figures, data are represented as mean +/- standard error of the mean (s.e.m). Significance was calculated by the non-parametric Mann–Whitney U test for cell quantifications.

CHAPTER IV

TRANSCRIPTOME ANALYSIS OF MULLER GLIA REPROGRAMMING DURING CONSTANT INTENSE LIGHT DAMAGE INDUCED RETINA REGENERATION

Nergis Kara, Yongchao Dou, Bing Zhang and James G. Patton[a]

Introduction

Retinal degenerative diseases involving photoreceptor cell loss are among the most common eye-related disorders and currently lack therapeutic treatments that would endogenously replace lost neurons. Unlike mammals, zebrafish has a robust regenerative response upon retinal damage. During retina regeneration, Müller glia (MG) respond to retinal damage by undergoing a reprogramming event through which they re-enter the cell cycle, divide asymmetrically, and generate multipotent neural progenitor cells. Studies with various retinal damage models showed that MG-derived neural progenitor cells (NPCs) are capable of differentiating into any type of lost neuronal cells.

Limited neurogenic potential of mammalian MG is apparently possible but the numbers of NPCs and the cell types regenerated are very restricted. Strategies to induce reprogramming of mouse MG hold great potential as a therapeutic approach for retinal diseases. One strategy to induce MG reprogramming in mice is to overexpress proneural transcription factors, such as achaete-scute complex-like 1 (Ascl1). Ascl1 is one of the key regulators of MG dedifferentiation in zebrafish (Ramachandran et al., 2010b) and has been shown to induce expression of other genes and signaling pathways necessary for regeneration, including Lin28 (Ramachandran et al., 2010b), Myc (Ramachandran et al., 2010b), Insm1a (Ramachandran et al., 2012a), canonical Wnt (Ramachandran et al., 2012b, 2011) and Notch (Wan et al., 2012b). However, Ascl1 is not induced in the mouse retina upon injury, unlike zebrafish retina regeneration (Karl et al., 2008). Conditional expression of Ascl1 in mouse MG failed to induce the MG reprogramming in the mature retina, while in young mice up to two weeks old, limited neurogenic potential of MG was demonstrated (Ueki et al., 2015). Epigenetic modifications in the whole

102

retina, along with the forced expression of Ascl1, has also been used to induce MG

reprogramming (Jorstad et al., 2017). Intravitreal injection of the histone deacetylase

inhibitor trichostatin-A (TSA) enabled adult mice to generate neurons from MG upon

retinal injury. These reports demonstrate that other factors in addition to Ascl1 are

required to induce the neurogenic capacity of MG in mammalian retina. However,

therapeutic use of broad inhibitors of chromatin modifying enzymes such as TSA is

likely to be of little use due to genome-wide effects and induction of off target dormant

gene networks (Chang et al., 2012). Therefore, identification of the factors sufficient to

activate the regenerative potential of MG is crucial.

Zebrafish retina regeneration is an invaluable model to discover novel inductive

mechanisms of MG reprogramming. Although the number of regeneration-associated

factors and signaling pathways has expanded in the past decade, our understanding of

genome-wide transcriptional changes of MG reprogramming is limited. Here, I provide

high-throughput RNA-sequencing analysis of post-mitotic and dedifferentiated MG

during constant intense light damage-induced retina regeneration. My analysis identified

a list of differentially expressed genes, many of which have not been studied in

regeneration serving as a resource for further functional analysis to discover novel

molecular mechanisms for robust retina regeneration.

Results

FAC-sorting enriches for GFP-positive MG in the Tg(gfap:gfp) retinas

To identify differentially expressed genes during MG dedifferentiation, we used constant intense light lesioning to induce photoreceptor apoptosis in adult zebrafish retinas. Retinas from Tg(*gfap:gfp*) adult fish were collected before and after 37 hours of intense light damage. Tg(*gfap:gfp*) transgenic zebrafish express GFP in all MG driven by the GFAP (glial fibrillary acidic protein) promoter (Bernardos and Raymond, 2006). We used fluorescence activated cell sorting (FAC sorting) to enrich for populations of post-mitotic MG from undamaged MG, and dedifferentiated MG from intense light damaged retinas (**Fig. 29A**). To test whether our tissue dissociation protocol reliably yields single cells, we imaged dissociated retinal cells and confirmed the presence of single cells including GFP-positive (GFP$^+$) MG (**Fig. 29B**). Dissociated retinal cells were analyzed by flow cytometry (Fig. 1C) and live GFP$^+$ cells were FAC-sorted. The percentage of GFP$^+$ cells did not change (~15-16%) in undamaged and intense light damaged retinas. This confirms that at 37h of light damage, GFP fluorescence is retained in dedifferentiated MG of Tg(*gfap:gfp*) fish (K Rajaram et al., 2014). After FAC-sorting of MG, we re-analyzed the sorted cell population by flow cytometry (**Fig. 29D**). Our analysis showed that 85% of the cells were GFP$^+$ compared to 15% GFP$^+$ cells before sorting. This demonstrates that FAC-sorting can generate an enriched population of GFP$^+$ MG.
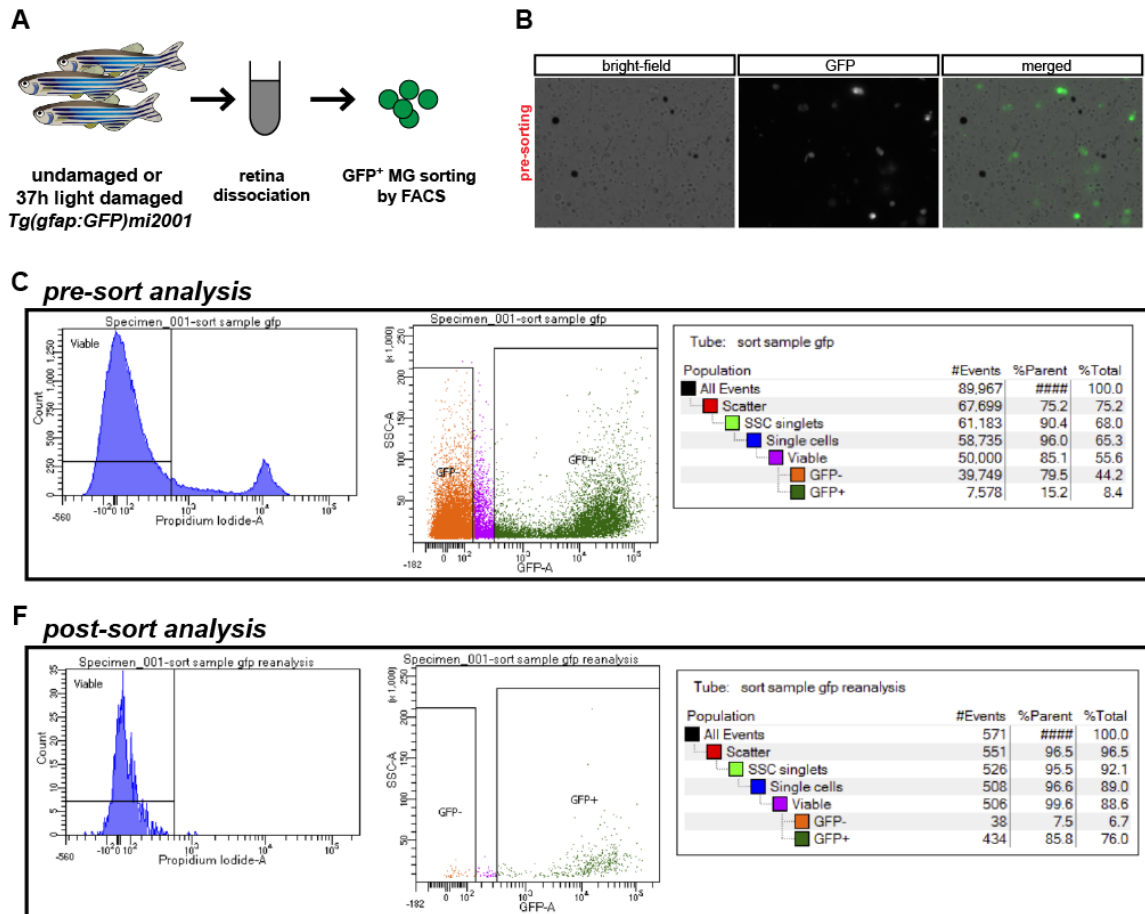
Figure 29   Fluorescence activated cell sorting of MG from dissociated retinas of Tg(gfap:gfp) yields enriched GFP$^+$ cells.

(A) Retinas from undamaged or intense light damaged (37h) Tg(*gfap:gfp*) fish were dissociated. (B) Bright-field and GFP fluorescence images of single cells dissociated from retinal tissues. (C) Flow cytometry analysis of retinal cells dissociated from 37h intense light damaged Tg(*gfap:gfp*) fish. Viable cells do not take up propidium iodide (PI-A). Intact viable cells were gated based on GFP fluorescence intensity. Gating was adjusted based on GFP$^-$ compensation control cells (not shown here). Percentages for each gated population are shown. 85% of the intact cells were alive, ~15% of the live intact cells were GFP$^+$. (F) Confirmation of the enrichment of GFP$^+$ cells by flow cytometry analysis. 99.6% of the intact cells were alive based on the percentage for PI-A negative population. 85.8% of the intact viable cells were GFP$^+$.

RNA-Seq analysis of Müller Glia during retina regeneration reveals dynamic transcriptome changes in response to intense light damage

To identify specific genes that are critical for MG dedifferentiation during regeneration of the intense light damaged retina, we performed high-throughput RNA-sequencing. We collected RNA and prepared sequencing libraries from FAC-sorted MG of Tg(*gfap:gfp*) retinas before light damage (0h) and after 37h of light damage (37h). 37h of intense light damage marks the time of cell cycle re-entry of the MG when MG dedifferentiate upon retinal damage (Kassen et al., 2007; K Rajaram et al., 2014). After mapping the reads to the zebrafish genome assembly (Zv9) and performing pairwise analyses between samples, two biological replicates of each time point showed very high correlation (r=0.98) (**Fig. 30A**). Using Principal Component Analysis (PCA), we determined that the mRNA profiles of MG from undamaged and intense light damaged retinas are distinct (**Fig. 30B**).

Differential gene expression analysis was performed comparing the transcriptome profiles of MG from undamaged and intense light damaged retinas (**Fig. 31**). We identified 3694 genes that were significantly up (1426/5641) or down (2268/5641) regulated (FDR≤0.01) by more than 2-fold in MG from 37h light damaged retinas compared to undamaged retinas. Our analysis confirmed differential expression of previously characterized regeneration associated genes (**Table 2**) (Kassen et al., 2007; Ramachandran et al., 2012c, 2010c; Thummel et al., 2010b; Veldman et al., 2010; Wan et al., 2012a; Zhao et al., 2014).

The top 20 up and down regulated genes identified many uncharacterized candidate factors involved in MG reprogramming (**Table 3 and 4**). To validate the
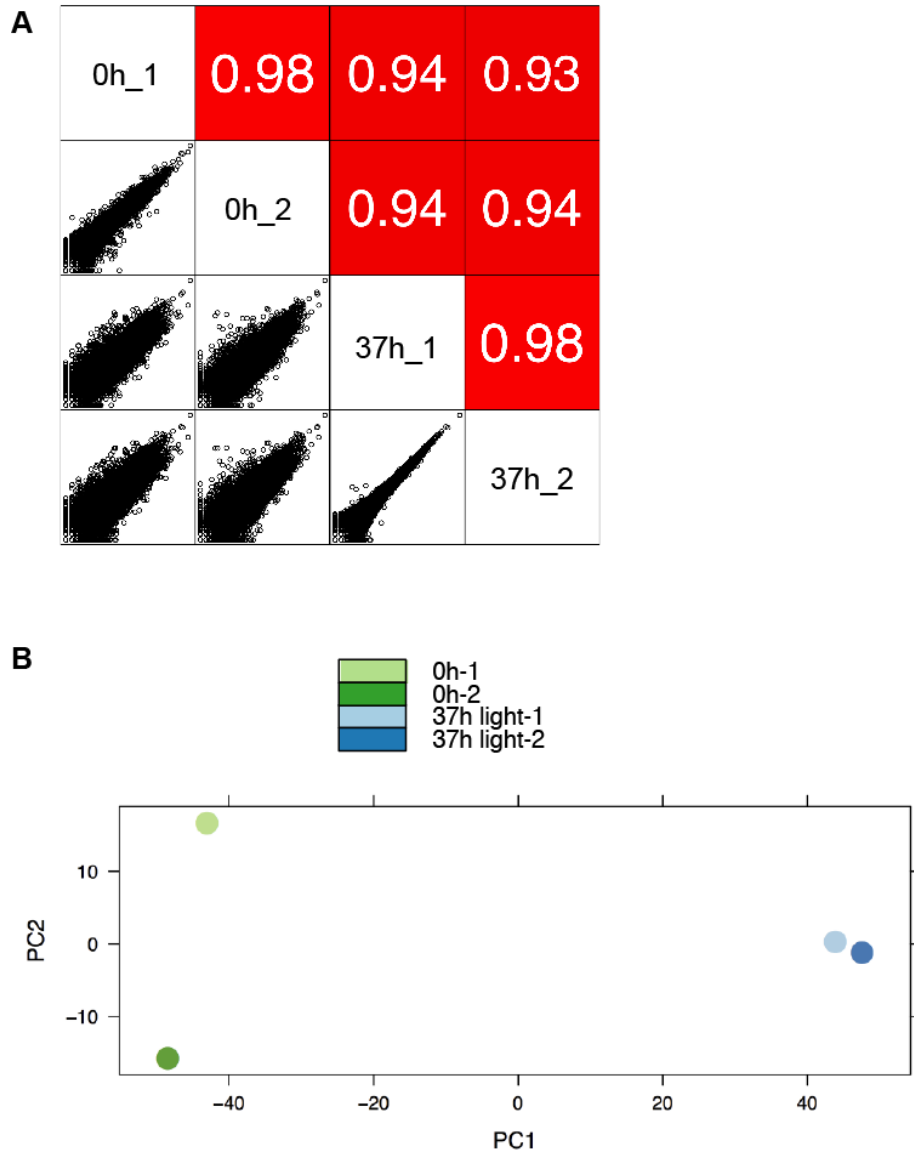
Figure 30 **Pairwise similarity and comparable principle component analysis (PCA) between the RNA-Seq samples.**

(A) Spearman correlation analysis was performed on all RNA-sequencing samples. Replicates of MG at 0h (0h_1 and 0h_2) and MG from 37h light damaged retinas (37h_1 and 37h_2) had higher correlations (r=0.98) compared to 0h vs 37h samples (r=0.94). (B) PCA analysis revealed that the transcriptome profiles of MG from undamaged retinas (0h) and light damaged retinas (37h) are distinct from each other.

sequencing results, we examined expression of four significantly up (stm, anxa2a, mmp9, ctgfa) and two significantly down (coch and dkk1b) regulated genes by qPCR. The

relative expression changes of these transcripts detected by qPCR agreed with those

revealed by RNA-seq analysis, although fold changes detected by qPCR were higher

(**Fig. 32**).
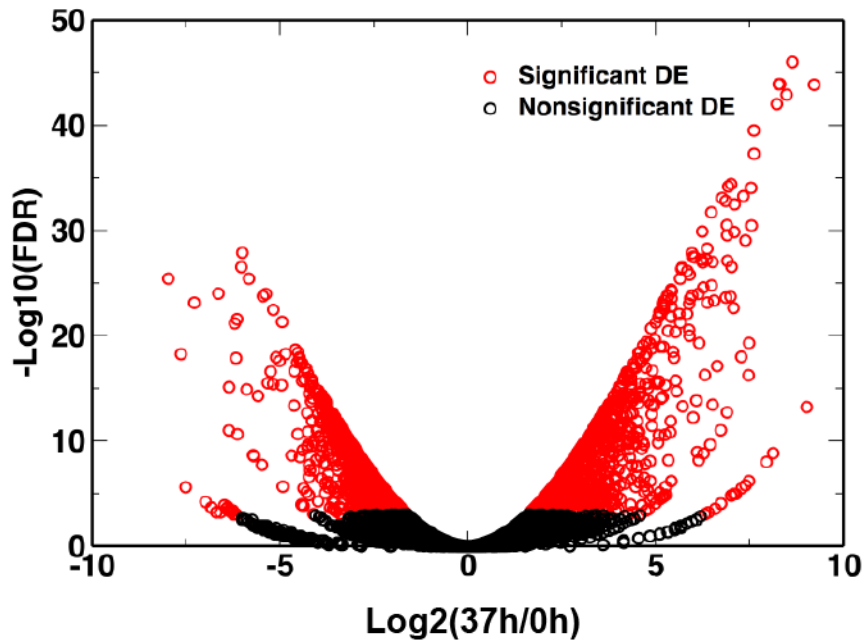
Figure 31   Volcano plot representation of differential expression analysis of genes in dedifferentiated MG (37h) vs post-mitotic MG.

Volcano plot showing genes significantly deregulated in dedifferentiated MG at 37h of constant intense light damage compared to post-mitotic MG from undamaged retinas (|logFC|≥1, FDR≤0.001).

Table 2. Differential expression of regeneration-associated genes

Gene Symbol	logFC[a]	FDR[b]
lin28a	8.49	1.24E-43
ascl1a	1.98	3.73E-05
hbegfa	4.55	4.17E-19
insm1a	-3.38	4.52E-12
il11a	5.85	7.09E-27
lepa	3.13	2.83E-08
lepb	8.23	9.58E-43
pcna	0.74	0.182
mycbp	1.58	0.001
tuba1a	1.10	0.031
pax6b	-1.06	0.038

[a] $\log_2$Fold Change=$\log_2$(37h MG/0h MG)
[b] False discovery rate

Table 3. Top 20 upregulated transcripts in MG from 37h light damaged retinas compared to MG prior to light damage (0h)

Gene symbol	Gene name	logFC[a]	logCPM[b]	PValue[c]	FDR[d]
stm	starmaker	8.64	9.36	3.39E-51	9.80E-47
anxa2a	annexin A2a	8.31	9.13	8.42E-49	1.22E-44
mmp9	matrix metallopeptidase a	8.28	9.26	1.28E-48	1.23E-44
clcf1	cardiotrophin-like cytokine factor 1	9.22	5.94	1.93E-48	1.39E-44
lin28a	lin-28 homolog A	8.49	6.63	2.15E-47	1.24E-43
lepb	leptin b	8.23	7.16	1.99E-46	9.58E-43
txn	thioredoxin	7.62	8.68	7.47E-44	3.08E-40
adamtsl7	ADAMTS-like 7	7.62	5.96	1.43E-41	5.15E-38
cyp27c1	cytochrome P450, family 27, subfamily C, polypeptide 1	7.01	6.65	1.22E-38	3.93E-35
tnfrsf11b	tumor necrosis factor receptor superfamily, member 11b	6.94	6.77	2.31E-38	6.66E-35
dkk1a	dickkopf WNT signaling pathway inhibitor 1a	7.54	4.66	3.40E-38	8.91E-35
si:ch73-65n21.2		7.34	4.14	2.31E-37	5.55E-34
adma	adrenomedullin a	6.77	7.36	3.78E-37	8.39E-34
adam8a	ADAM metallopeptidase domain 8a	6.87	5.90	7.74E-37	1.60E-33

Gene symbol	Gene name	logFC[a]	logCPM[b]	PValue[c]	FDR[d]
eva1bb	eva-1 homolog Bb	7.10	4.92	1.71E-36	3.29E-33
rgs5b	regulator of G protein signaling 5b	6.49	8.17	1.06E-35	1.91E-32
HPN	hepsin	6.90	3.81	1.86E-34	3.15E-31
ttc25	tetratricopeptide repeat domain 25	7.56	3.22	2.15E-34	3.45E-31

[a] log$_2$Fold Change=log$_2$(37h MG/0h MG)
[b] CPM=count per million
[c] uncorrected p-value
[d] False discovery rate

Table 4. Top 20 downregulated transcripts in MG from 37h light damages retinas compared to MG prior to light damage (0h)

Gene symbol	Gene name	logFC[a]	logCPM[b]	PValue[c]	FDR[d]
coch	coagulation factor C homolog	-6.00	6.70	1.08E-31	1.30E-28
stxbp6l	syntaxin binding protein 6	-6.02	4.75	3.53E-30	2.99E-27
FQ311879.2		-7.97	2.30	5.32E-29	3.80E-26
abi3bpb	ABI family member 3 (NESH) binding protein b	-5.83	4.75	5.36E-29	3.80E-26
opn1mw1	opsin 1 (cone pigments), medium-wave-sensitive 1	-6.64	2.70	1.56E-27	9.76E-25
dkk1b	dickkopf WNT signaling pathway inhibitor 1b	-5.37	7.24	1.79E-27	1.08E-24
serpinf1	serpin peptidase inhibitor, clade F (alpha-2 antiplasmin, pigment epithelium derived factor), member 1	-5.45	5.30	3.16E-27	1.76E-24
gal3st1b	galactose-3-O-sulfotransferase 1b	-7.28	2.15	1.55E-26	7.47E-24
cyp19a1b		-5.17	6.28	8.02E-26	3.46E-23
rsad2	radical S-adenosyl methionine domain containing 2	-6.14	2.39	7.03E-25	2.71E-22
slc2a1a	solute carrier family 2 (facilitated glucose transporter), member 1a	-4.94	9.41	1.28E-24	4.87E-22
zgc:152791		-6.20	2.28	1.85E-24	6.76E-22
PLEKHA4	pleckstrin homology domain containing, family A,member 4	-4.59	6.55	6.99E-22	2.15E-19
atp1b4	ATPase Na+/K+ transporting subunit beta 4	-4.51	8.94	1.35E-21	4.02E-19

cyp2n13	cytochrome P450, family 2, subfamily N, polypeptide 13	-4.85	3.29	1.88E-21	5.42E-19
si:dkey-9c18.3		-7.63	1.14	1.97E-21	5.64E-19
pcp4a	Purkinje cell protein 4a	-4.48	6.34	4.19E-21	1.16E-18
edn3b	endothelin 3b	-5.10	2.43	4.20E-21	1.16E-18
cacng1a	calcium channel, voltage-dependent gamma subunit 1a	-6.17	1.48	5.04E-21	1.36E-18
vegfab	vascular endothelial growth factor Ab	-4.48	5.65	5.86E-21	1.57E-18
clec11a	C-type lectin domain containing 11A	-5.01	2.57	9.51E-21	2.50E-18

[a] $\log_2$Fold Change=$\log_2$(37h MG/0h MG)
[b] CPM=count per million
[c] uncorrected p-value
[d] False discovery rate
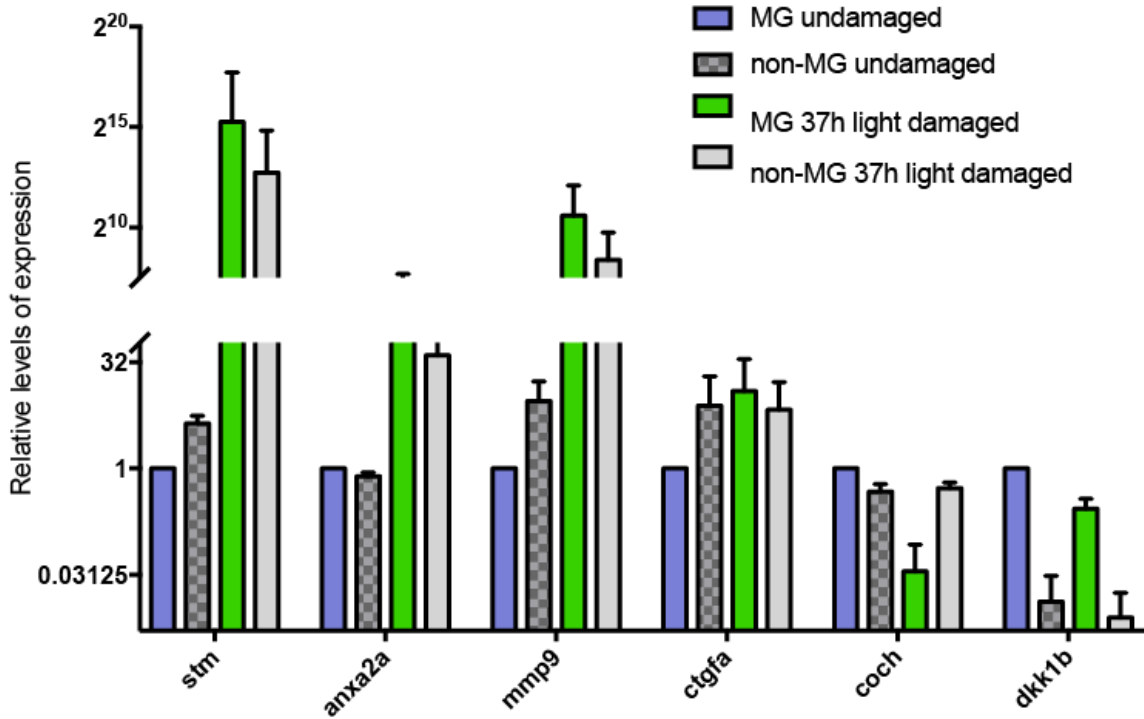
Figure 32. Validation of RNA-seq analysis.

Fold changes in selected gene expression levels in FACS-purified MG were determined by qPCR. *Stm, anxa2a, mmp9* and *ctgfa* were significantly upregulated in dedifferentiated MG (37h light damaged) compared to post-mitotic MG (undamaged). *Coch* and *dkk1b* were significantly downregulated in dedifferentiated MG (37h light damaged) compared to post-mitotic MG (undamaged). Data represent mean +/- s.e.m. from 3 independent experiments. P-values were calculated for each gene (MG 0h vs MG 37h light damaged comparison) by Student's t-test: stm $(5.16*10^{-6})$, anxa2a $(3.23*10^{-5})$, mmp9 $(2.19*10^{-6})$, coch $(0.7*10^{-3})$, dkk1b (0.002), ctgfa (0.001). y-axis in log2 scale.

Methods

Zebrafish husbandry and adult zebrafish light lesioning

Wild-type (AB) (Walker, 1999) and *Tg(gfap:gfp)^{mi2001}* (Bernardos and Raymond, 2006) lines were maintained at 28.5^{0}C on a 14:10 hour light:dark cycle. All experiments with zebrafish were performed with the approval of the Vanderbilt University

Institutional Animal Care and Use Committee. Adult zebrafish used for the experiments were between 5 months old. Constant intense light lesioning to induce cone and rod photoreceptor cell death was performed as previously described (Kamya Rajaram et al., 2014c). Briefly, adult fish were dark adapted for 14 days, transferred to clear tanks placed between two fluorescent lights with light intensity at ~20,000 lux for 37 hours. The tank temperature was maintained at 30- 33°C.

Retinal dissection and dissociation

FACS was used to isolate GFP+ and GFP- cells from the retinas of undamaged Tg(gfap:gfp)^{mi2001} fish using BD FACSAria III (BD Biosciences) at the VUMC Flow Cytometry Shared Resource. Retinas were dissociated as previously described (Kamya Rajaram et al., 2014b) with the following changes. After the retinas were dissected, they were collected in Leibovitz L-15 media (ThermoFisher #21083-027) and treated with 1mg/ml hyaluronidase (Sigma #H3884) at room temperature for 15 minutes on a rocker. Cells from the dissociated retinas were stained with propidium iodide to detect dead cells. 12 adult fish were used for each FACS experiment. 100μm nozzle was used for sorting. 70,000 cells were sorted into 700μl TRIzol-LS.

RNA purification, mRNA library preparation and sequencing

Total RNA was isolated from FAC-sorted cells using TRIzol-LS (ThermoFisher # 10296028). RNA pellets were resuspended in 20 of RNase-free water. The concentration and integrity of the extracted total RNA was analyzed by Qubit Fluorometer (Invitrogen) and Agilent 2100 Bioanalyzer (Applied Biosystems), respectively. RNA with RIN value with 7.0 or above were used for library preparation. Sequencing library preparations and

sequencing were performed by the VANTAGE at Vanderbilt University Medical Center using SMARTer low input RNA kit (Clontech), utilizing the polyA tail for initial priming. High throughput RNA sequencing was perfomed on four libraries in total, multiplexed in one lane of the Illumina HiSeq2500. On average 150 million 75 bp paired-end reads were generated for each group.

Read mapping and differential expression analysis

The quality of the reads was assessed before and after trimming with FastQC (v0.11.2). Reads were mapped to the zebrafish genome Zv9 using tophat2 (v2.0.13) with bowtie2 (v2.2.3). Htseq-count (v0.6.1p1) was used for gene-level counting. edgeR was used for differential expression analysis and PCA analysis. The cutoffs for log2 fold change (log2FC) and FDR are |log2FC|≥1 and FDR≤0.001.

qRT-PCR analysis

For RT-PCR of mRNAs, RNA was DNase treated (TURBO DNAfree kit ThermoFisher #AM1907), converted to cDNA using Maxima first strand cDNA synthesis kit (Thermo Scientific) and qPCR was performed using SYBR Green (Biorad). All qPCR primers spanned exon-exon junctions (IDT) (**Table 5**). Relative RNA expression during regeneration were determined using the ΔΔCt method and normalized to 18s rRNA. Real time PCR was performed on a Biorad CFX 96 Real time system.

Table 5 Q-PCR primers used for the validation of RNA-seq

Primer name	Sequence (5'-3')
Q-stm-F	GTCCAGCTTCAGACCAGCTT
Q-stm-R	CGGAACAAACACTGTCCGGG
Q-anxa2a-F	CATTGCTGAGCACACAAAGGG
Q-anxa2a-R	AGTCTAAGCGAGTGCGTGTT
Q-mmp9-F	CACACAGGGAGACGCTCATT
Q-mmp9-R	TAGCGGGTTTGAATGGCTGG
Q-coch-F	GGTGTTTGTTGATGGGTGGC
Q-coch-R	TCCTTGCACACTGCCTTTCT
Q-dkk1b-F	AATGACCCTGACATGATTCAGC
Q-dkk1b-R	AGGCTTGCAGATTTTGGACC
Q-ctgfa-F	TTCTTAAGATGGGCTGTGGCT
Q-ctgfa-R	GGTCGCAAACATCTCGTTCTG

CHAPTER V

SUMMARY AND CONCLUSIONS

Significance

Since the seminal discovery of the first miRNA, *lin-4*, in *C. elegans* in 1993, over 30,000 miRNAs are identified in over 200 species (Griffiths-Jones et al., 2006). Discoveries in function and biogenesis of miRNAs along with other small noncoding RNAs, redefined the biology of gene regulation. These discoveries have broadened the view of RNA from the original "central dogma of molecular biology" in which RNA was mostly thought to serve a messenger role that mediates the flow of information from DNA to proteins. Additionally, advances in high-throughput sequencing that identified miRNA populations and mapped their genomic loci helped refute the "junk DNA hypothesis" which proposed that more than 80% of the genome is non-functional (Gerstein et al., 2007; Landgraf et al., 2007; Ohno, 1972).

miRNAs are involved in nearly all developmental and pathological processes (Ambros, 2003; Chen et al., 2005; Lagos-Quintana et al., 2003; Pasquinelli et al., 2000). In early miRNA studies, miRNAs were proposed to resemble to adjustable resistor, a rheostat, as in an electric circuit (Bartel and Chen, 2004). This analogy was made based on the cases where miRNA target sites have combinatorial effects and protein levels of target mRNA decrease, but are not totally extinguished. This proposed model suggested that miRNAs are only micromanagers of gene expression, mostly fine-tuning protein

levels. However, the strong phenotypes achieved upon loss-of-function of major

components of the miRNA biogenesis pathway and/or individual miRNAs have

demonstrated that miRNAs can indeed function as crucial developmental switches

(Bernstein et al., 2003; Flynt et al., 2007; Giraldez et al., 2006; Li et al., 2011b; Stefani

and Slack, 2008; Suh et al., 2010; Wang et al., 2007).

Despite the vast number of identified miRNAs with corresponding expression

patterns, very few have actually been fully functionally characterized. Unlike plant

miRNAs binding to their target mRNAs with perfect complementarity, metazoan

miRNAs most commonly form imperfect base pairs with target sequences. Although

binding through the seed sequence is an important determinant, other factors such as

RNA secondary structure, positions of the miRNA binding sites, 3'UTR sequence

features surrounding target sites may also affect miRNA:mRNA interactions (Bartel,

2009). These variable together create difficulty developing in silico target identification

algorithms for animal miRNAs. Identifying the targets of individual miRNAs requires

precise temporal and spatial analyses along with genetic manipulation of individual

miRNA expression.

Summary of Results

Research presented in this dissertation identified novel regulatory functions for

miR-27 in craniofacial development and *miR-216a* in retina regeneration. I demonstrated

that *miR-27* is a highly enriched miRNA in the pharyngeal arches and required for

craniofacial chondrogenesis. *miR-27* loss-of-function led to nearly complete loss of

pharyngeal cartilage. I demonstrated that the *miR-27* loss-of-function phenotype is due to attenuation of proliferation and blocking differentiation of cranial neural crest cells. I identified focal adhesion kinase (FAK) as a direct target of *miR-27* and a regulator of pharyngeal arch morphogenesis in pharyngeal arches. *miR-27* suppresses FAK levels on the pharyngeal arch primordia, thus regulating chondrogenic differentiation. For *miR-216a,* I discovered that it functions during Müller glia dedifferentiation and proliferation during retina regeneration in adult zebrafish. Cell type-specific gene expression analyses and in vivo manipulation of miRNA levels showed that *miR-216a* suppression is necessary and sufficient for MG proliferation. The H3K79 methyltransferase, Dot1l is a target of *miR-216* and is required for retina regeneration. Altogether, these two studies demonstrate a requirement for miRNAs controlling cell fate changes during development and regeneration. Lastly, I completed MG-specific transcriptome analysis during the early phases of retina regeneration, thus serving as an invaluable resource to discover novel cell-autonomous factors that initiate the MG dedifferentiation and proliferation.

Discussion and Future Directions

Role of miR-27 in pharyngeal arch morphogenesis

Vertebrate cranial neural crest (CNC) cells are a multipotent cell population that can differentiate into cartilage, bone, neurons, pigment cells and glia (Baroffio et al., 1991). I discovered that *miR-27* is involved in chondrogenic differentiation of CNCs. Previous studies provided evidence for a global miRNA requirement for skeletal development in mice using conditional deletion of Dicer in either NC cells or early

chondrocytes in craniofacial cartilage (Kobayashi et al., 2008; Zehir et al., 2010). Blocking the miRNA biogenesis pathway with Dicer deletion led to loss of the majority of NC-derived craniofacial cartilage and bone. Although these findings underlined the requirement for miRNAs in cartilage and bone development, only a few individual miRNAs were identified that regulate chondrocyte formation (Eberhart et al., 2008; Nakamura et al., 2011; Ning et al., 2013; Sheehy et al., 2010).

I discovered *ptk2aa (FAK)* is a novel *in vivo* target of *miR-27*. First, using GFP reporter assays, I showed that *miR-27* is able to target two MREs on the 3'UTR of *fak* mRNA. FAK protein levels change upon overexpression and knock down of *miR-27*. Lastly, co-suppression of FAK in *miR-27* morphants was able to partially rescue the pharyngeal arch defects in the embryos. Together, these findings support the model in which *miR-27* regulates chondrogenic differentiation by suppressing FAK levels in CNCs.

Interestingly, a potential role for FAK in chondrogenesis was reported previously, using in vitro assays (Bursell et al., 2007; a. M. DeLise et al., 2000; Pala et al., 2008; Tang et al., 2013b). These reports provided evidence that supports a mechanism in which FAK signaling suppresses chondrogenic differentiation with likely involvement of downstream RhoA/Rock signaling. I tested a direct involvement of FAK in chondrogenic differentiation by overexpressing *pktk2aa* in embryos following two strategies, either injecting *ptk2aa* mRNA into single cell embryos, or performing mosaic analysis by conditionally expressing *ptk2aa* in CNCs. Ubiquitous overexpression of *ptk2aa* led to early defects in embryogenesis preventing downstream analysis at later stages when pharyngeal arches form. In the second strategy, limited expression in only a

119

few single cells that were overexpressing FAK prevented analysis of chondrocyte-specific ECM markers. In the future, it will be useful to generate conditional alleles for both temporal and spatial analysis of FAK overexpression using the Cre/loxP system. This strategy will allow analysis of potential cell-autonomous roles for FAK in CNCs *in vivo*.

Role of miR-216a in MG dedifferentiation and proliferation during retina regeneration

MG dedifferentiation and proliferation underlies the unique regenerative capacity of zebrafish retinas. Mammalian MG respond to retinal damage by undergoing reactive gliosis resulting in glial scars, rather than initiating a regenerative response. Understanding the molecular mechanisms of MG function during retina regeneration is crucial for developing new therapeutic approaches.

I discovered a *miR-216* mediated mechanism that initiates MG reprogramming during retina regeneration. Analysis of gene expression of purified MG populations before and after intense light damage showed that *miR-216a* is significantly downregulated in dedifferentiated MG. To test if suppression of *miR-216a* is required for retina regeneration, gain-of-function analysis of *miR-216a* was performed. Using the Tg(*tuba1a:GFP*) line in which transgene expression is turned on specifically in dedifferentiated MG, *miR-216a* overexpression resulted in decreased numbers of dedifferentiated and proliferating MG. Interestingly, I demonstrated that *miR-216* suppression is sufficient to stimulate MG dedifferentiation and cell-cycle re-entry in the absence of damage. While only a few individual miRNAs involved in retina regeneration have been identified (Kaur et al., 2018; Kamya Rajaram et al., 2014b, 2014a;

Ramachandran et al., 2010a), my finding serves as the discovery of the first miRNA solely regulating MG dedifferentiation.

Using lineage tracing methods and various retinal damage models in zebrafish, previous reports showed that MG-derived NPCs are multipotent and able to differentiate into any cell type in the retina (Rebecca L Bernardos et al., 2007; Fausett and Goldman, 2006). Future work is needed to provide greater insight into the dedifferentiation of MG upon *miR-216a* suppression in the absence of damage. Although I was able to show a significant increase in proliferating MG and dedifferentiation of MG through the activation of the *tuba1a* reporter, the neurogenic potential of the newly generated neural progenitor cells (NPCs) remains unknown.

Epigenetic Regulation of MG dedifferentiation

During development, as pluripotent stem cells differentiate into 'multipotent' adult stem cells and then to fully differentiated 'unipotent' cells, lineage-specific epigenetic modifications lead to the restriction of transcriptional circuits and fixation of the lineage fate. This constitutes one of the reasons why differentiated cells only inefficiently reprogram to a more potent cell type as in nuclear reprogramming and transdifferentiation experiments (Takahashi and Yamanaka, 2006; Wernig et al., 2007; Zhou et al., 2008). Further studies on nuclear reprogramming of somatic cells showed that epigenetic modifications constitute one of the major roadblocks to efficient reprogramming experiments and manipulation of the levels of certain chromatin modifying enzymes can help to increase the efficiency of cell fate changes (Onder et al., 2012; Pasque et al., 2011; Rais et al., 2013). In this context, epigenetic mechanisms are

121

likely involved in MG dedifferentiation during retina regeneration. Analysis of DNA methylation status of pluripotency and regeneration-associated genes in post-mitotic and dedifferentiated MG demonstrated that that there is no significant change in DNA methylation status on regeneration-associated genes (Powell et al., 2013, 2012). The transcriptional regulatory regions of regeneration and pluripotency-associated genes such as Ascl1a, Hb-egfa, lin28, Oct4 and Sox2 have low methylation levels. Interestingly, mouse MG exhibited the same hypomethylated pattern on the same genes (Powell et al., 2013). Therefore, the lost regenerative capacity of MG cannot be based on mechanisms involving DNA methylation. This suggests the involvement of post-translational histone modifications and chromatin modifiers during retina regeneration.

The findings presented in this thesis suggest a mechanism by which *miR-216* regulates MG dedifferentiation and proliferation through targeting the H3K79 methyltransferase Dot1l. *miR-216* targets the 3'UTR of *dot1l* by GFP reporter assays and Dot1l levels are affected upon *miR-216* gain-of-function. Gene expression analysis in purified post-mitotic and dedifferentiated MG showed that Dot1l is upregulated in dedifferentiated MG. Loss-of-function analyses of Dot1l through either morpholino knockdown or inhibition by enzymatic activity, demonstrated that Dot1l is required for MG dedifferentiation and proliferation. In addition, I provided *in vivo* evidence for the regulation of Dot1l by *miR-216* during the process of MG proliferation. While suppression of *miR-216* alone was sufficient to stimulate a regenerative response in the undamaged retina, co-suppression of Dot1l prevented MG proliferation.

Future work is needed to analyze the potential regulation H3K79 methylation levels by Dot1l in MG during retina regeneration. Given that H3K79 methylation is

generally associated with actively transcribed genes (Feng et al., 2002; Jones et al., 2008; Shanower et al., 2005; Steger et al., 2008), one hypothesis is that Dot1l is required for maintaining the expression of regeneration-associated genes in dedifferentiating MG. Previous reports demonstrated that Dot1l-mediated H3K79 methylation is associated with the transcription of Wnt-target genes, mediated by TCF transcription factors and the co-activator β-catenin (Castaño Betancourt et al., 2012; Clevers, 2006; Mahmoudi et al., 2010; Mohan et al., 2010). Additionally, a direct interaction between Dot1l and β-catenin was identified in zebrafish and mouse intestinal stem cells (Mahmoudi et al., 2010). In this thesis, I provide evidence that canonical Wnt signaling is required downstream of Dot1l during retina regeneration. Stabilization of β-catenin through small molecule inhibitor of GSK3β was able to rescue the proliferation defects due to Dot1l knockdown. Although this supports that Dot1l is an upstream regulator of β-catenin-dependent signaling during retina regeneration, more work is needed to show that Dot1l mediates H3K79 methylation on canonical Wnt target genes in MG. Generation of zebrafish Dot1l specific antibodies will enable chromatin immunoprecipitation (ChIP) experiments to test the interaction of Dot1l with regulatory DNA regions of Wnt-target genes. In addition, ChIP-sequencing for H3K79 in purified MG population would provide genome-wide enrichment sites for the Dot1l-mediated histone modification and other potential downstream targets for Dot1l that might be involved in retina regeneration.

Conclusion

In conclusion, work presented in this thesis demonstrates that miRNAs are key players in cell-fate transitions during pharyngeal arch morphogenesis in embryos and retina regeneration in adult zebrafish. Spatiotemporal expression of miRNAs is critical for both normal differentiation, as well as reprogramming upon tissue damage. This work emphasizes that miRNAs have key instructive roles in development and regeneration, rather than being just micromanagers of gene expression.

A. Supplemental Figures

A.1. Time-lapse imaging of the pharyngeal arches in *Tg(fli1a:eGFP)y1* embryos injected with MO-ctl at the single cell stage. Imaging was performed starting at 30hpf till 48hpf. Anterior is to the left. (included in online version of the paper http://dx.doi.org/10.1016/j.ydbio.2017.06.013)

A.2. Time-lapse imaging of the pharyngeal arches in *Tg(fli1a:eGFP)y1* embryos injected with MO-27 at the single cell stage. Imaging was performed starting at 30hpf till 48hpf. Anterior is to the left. (included in online version of the paper, http://dx.doi.org/10.1016/j.ydbio.2017.06.013)
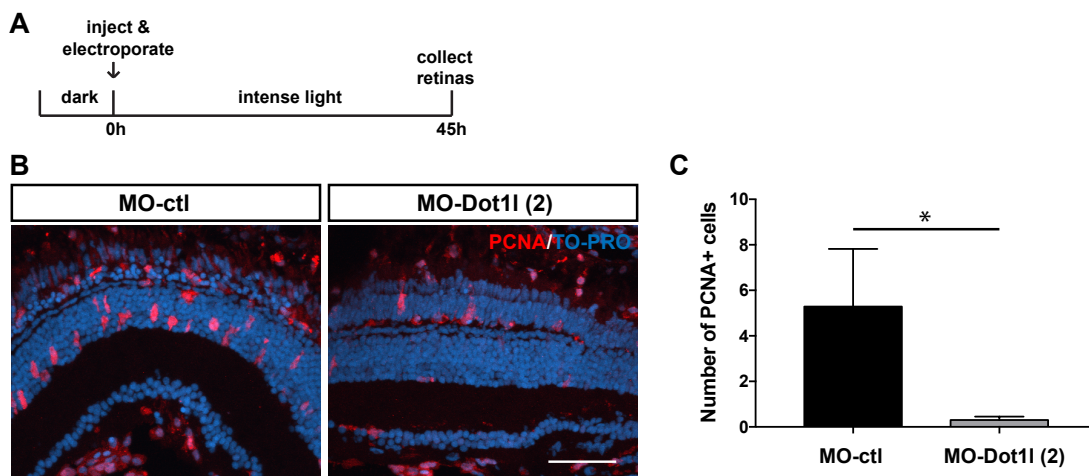
A.3.

Dot1l knock-down by an alternative morpholino injection inhibits MG proliferation during retina regeneration.

(A) Experimental scheme. Control morpholino or a second independent Dot1l morpholino (Dot1l-MO-2) was injected and electroporated into the left eyes of Tg(*1016tuba1a*:gfp) zebrafish before intense light exposure (0h). After 45h, retinas were collected, sectioned and immunostained using antibodies against GFP, PCNA. Nuclei were counterstained with TOPRO (blue). (B) Dot1l loss-of-function reduced the number of INL PCNA$^+$ proliferating cells. (C) Quantification of PCNA$^+$ proliferating progenitors in MO-ctl and MO-Dot1l electroporated retinas. Data represent mean +/- s.e.m (n= 7-10 fish); *, $p<0.05$ by two-tailed Student's t-test. ONL, Outer nuclear layer; INL, inner nuclear layer; GCL, ganglion cell layer. Scale bar 50um.

A.2
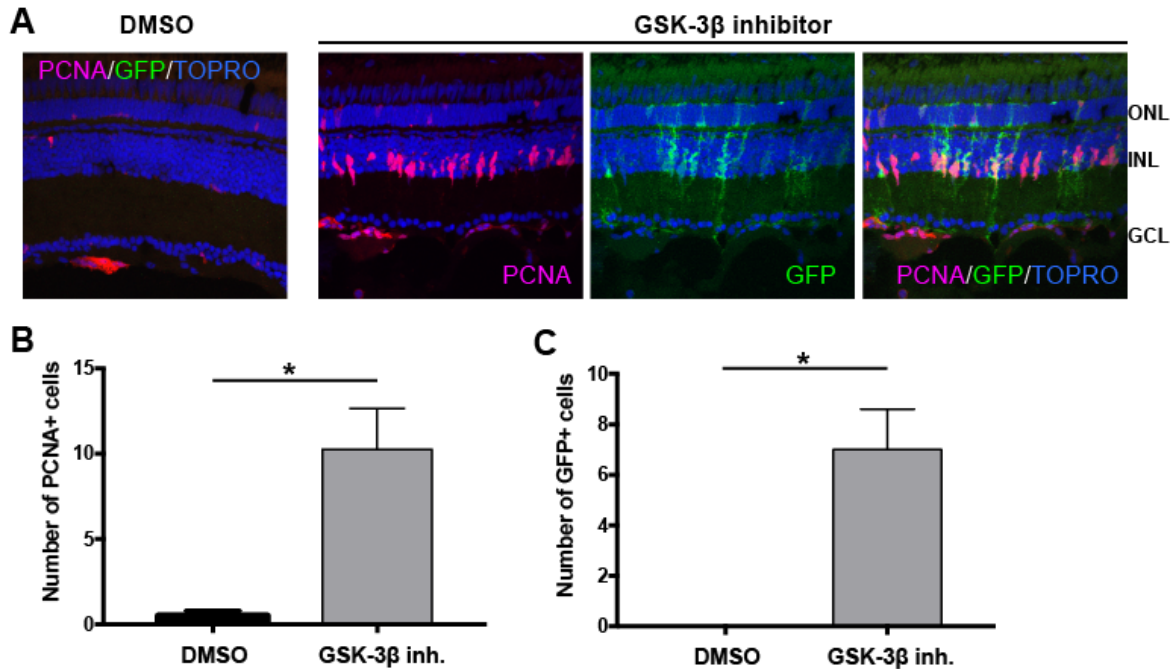
β-catenin stabilization stimulates MG dedifferentiation and proliferation.

 (A) Tg(*1016tuba1a:gfp*) adult fish were intravitreally injected with 1mM GSK-3β inhibitor (n=8) or control vehicle (DMSO) (n=4). Eyes were collected 51h post injection and sectioned retinas were immunostained using antibodies against GFP for dedifferentiated MG and PCNA for proliferating progenitors. Nuclei were counterstained with TOPRO (blue). (B) Quantification of PCNA$^+$ proliferating progenitors and (C) GFP$^+$ dedifferentiated MG in control vehicle and GSK-3β inhibitor injected retinas. Data represent mean +/- s.e.m (n= 4-8 fish); *, $p<0.05$ by two-tailed, Mann–Whitney *U* test. ONL, Outer nuclear layer; INL, inner nuclear layer; GCL, ganglion cell layer.

REFERENCES

Akimenko, M.A., Ekker, M., Wegner, J., Lin, W., Westerfield, M., 1994. Combinatorial expression of three zebrafish genes related to distal-less: part of a homeobox gene code for the head. J. Neurosci. 14, 3475–3486.

Allison, W.T., Barthel, L.K., Skebo, K.M., Takechi, M., Kawamura, S., Raymond, P. a, 2010. Ontogeny of cone photoreceptor mosaics in zebrafish. J. Comp. Neurol. 518, 4182–95. doi:10.1002/cne.22447

Alvarez-Garcia, I., Miska, E.A., 2005. MicroRNA functions in animal development and human disease. Development 132, 4653–62. doi:10.1242/dev.02073

Ambros, V., 2003. MicroRNA pathways in flies and worms: growth, death, fat, stress, and timing. Cell 113, 673–6.

Ameres, S.L., Zamore, P.D., 2013. Diversifying microRNA sequence and function. Nat. Rev. Mol. Cell Biol. 14, 475–488. doi:10.1038/nrm3611

Amiel, J., de Pontual, L., Henrion-Caude, A., 2012. miRNA, Development and Disease. pp. 1–36. doi:10.1016/B978-0-12-404742-6.00001-6

Ang, C.E., Wernig, M., 2014. Induced neuronal reprogramming. J. Comp. Neurol. 522, 2877–2886. doi:10.1002/cne.23620

Ason, B., Darnell, D.K., Wittbrodt, B., Berezikov, E., Kloosterman, W.P., Wittbrodt, J., Antin, P.B., Plasterk, R.H.A., 2006. Differences in vertebrate microRNA expression. Proc. Natl. Acad. Sci. U. S. A. 103, 14385–9. doi:10.1073/pnas.0603529103

Baroffio, A., Dupin, E., Le Douarin, N.M., 1991. Common precursors for neural and mesectodermal derivatives in the cephalic neural crest. Development 112, 301–305.

Barrero, M.J., Boué, S., Izpisúa Belmonte, J.C., 2010. Epigenetic mechanisms that regulate cell identity. Cell Stem Cell 7, 565–70. doi:10.1016/j.stem.2010.10.009

Bartel, D.P., 2009. MicroRNAs: target recognition and regulatory functions. Cell 136, 215–33. doi:10.1016/j.cell.2009.01.002

Bartel, D.P., Chen, C.-Z., 2004. Micromanagers of gene expression: the potentially widespread influence of metazoan microRNAs. Nat. Rev. Genet. 5, 396–400. doi:10.1038/nrg1328

Bassett, E. a, Wallace, V. a, 2012. Cell fate determination in the vertebrate retina. Trends Neurosci. 35, 565–73. doi:10.1016/j.tins.2012.05.004

Bazzini, A.A., Lee, M.T., Giraldez, A.J., 2012. Ribosome profiling shows that miR-430 reduces translation before causing mRNA decay in zebrafish. Science 336, 233–7. doi:10.1126/science.1215704

Becker, T., Wullimann, M.F., Becker, C.G., Bernhardt, R.R., Schachner, M., 1997. Axonal

regrowth after spinal cord transection in adult zebrafish. J. Comp. Neurol. 377, 577–95.

Bernardos, R.L., Barthel, L.K., Meyers, J.R., Raymond, P. a, 2007. Late-stage neuronal progenitors in the retina are radial Müller glia that function as retinal stem cells. J. Neurosci. 27, 7028–40. doi:10.1523/JNEUROSCI.1624-07.2007

Bernardos, R.L., Barthel, L.K., Meyers, J.R., Raymond, P.A., 2007. Late-Stage Neuronal Progenitors in the Retina Are Radial Muller Glia That Function as Retinal Stem Cells. J. Neurosci. 27, 7028–7040. doi:10.1523/JNEUROSCI.1624-07.2007

Bernardos, R.L., Raymond, P. a, 2006. GFAP transgenic zebrafish. Gene Expr. Patterns 6, 1007–13. doi:10.1016/j.modgep.2006.04.006

Berninger, B., Costa, M.R., Koch, U., Schroeder, T., Sutor, B., Grothe, B., Gotz, M., 2007. Functional Properties of Neurons Derived from In Vitro Reprogrammed Postnatal Astroglia. J. Neurosci. 27, 8654–8664. doi:10.1523/JNEUROSCI.1615-07.2007

Bernstein, B.E., Birney, E., Dunham, I., Green, E.D., Gunter, C., Snyder, M., 2012. An integrated encyclopedia of DNA elements in the human genome. Nature 489, 57–74. doi:10.1038/nature11247

Bernstein, B.E., Kamal, M., Lindblad-Toh, K., Bekiranov, S., Bailey, D.K., Huebert, D.J., McMahon, S., Karlsson, E.K., Kulbokas, E.J., Gingeras, T.R., Schreiber, S.L., Lander, E.S., 2005. Genomic maps and comparative analysis of histone modifications in human and mouse. Cell 120, 169–81. doi:10.1016/j.cell.2005.01.001

Bernstein, B.E., Meissner, A., Lander, E.S., 2007. The mammalian epigenome. Cell 128, 669–81. doi:10.1016/j.cell.2007.01.033

Bernstein, E., Caudy, A.A., Hammond, S.M., Hannon, G.J., 2001. Role for a bidentate ribonuclease in the initiation step of RNA interference. Nature 409, 363–6. doi:10.1038/35053110

Bernstein, E., Kim, S.Y., Carmell, M.A., Murchison, E.P., Alcorn, H., Li, M.Z., Mills, A.A., Elledge, S.J., Anderson, K. V, Hannon, G.J., 2003. Dicer is essential for mouse development. Nat. Genet. 35, 215–7. doi:10.1038/ng1253

Bi, W., Deng, J.M., Zhang, Z., Behringer, R.R., de Crombrugghe, B., 1999. Sox9 is required for cartilage formation. Nat. Genet. 22, 85–89. doi:10.1038/8792

Biyashev, D., Veliceasa, D., Topczewski, J., Topczewska, J.M., Mizgirev, I., Vinokour, E., Reddi, A.L., Licht, J.D., Revskoy, S.Y., Volpert, O. V., 2012. miR-27b controls venous specification and tip cell fate. Blood 119, 2679–2687. doi:10.1182/blood-2011-07-370635

Blum, M., De Robertis, E.M., Wallingford, J.B., Niehrs, C., 2015. Morpholinos: Antisense and Sensibility. Dev. Cell 35, 145–149. doi:10.1016/j.devcel.2015.09.017

Boyer, L. a, Plath, K., Zeitlinger, J., Brambrink, T., Medeiros, L. a, Lee, T.I., Levine, S.S., Wernig, M., Tajonar, a, Ray, M.K., Bell, G.W., Otte, a P., Vidal, M., Gifford, D.K., Young, R. a, Jaenisch, R., 2006. Polycomb complexes repress developmental regulators in murine embryonic stem cells. Nature 441, 349–353. doi:10.1038/nature04733

Bracken, a P., 2006. Genome-wide mapping of Polycomb target genes unravels their roles in cell fate transitions. Genes Dev. 20, 1123–1136. doi:10.1101/gad.381706

Braisted, J.E., Essman, T.F., Raymond, P. a, 1994. Selective regeneration of photoreceptors in goldfish retina. Development 120, 2409–19.

Bringmann, A., Iandiev, I., Pannicke, T., Wurm, A., Hollborn, M., Wiedemann, P., Osborne, N.N., Reichenbach, A., 2009. Cellular signaling and factors involved in Müller cell gliosis: neuroprotective and detrimental effects. Prog. Retin. Eye Res. 28, 423–51. doi:10.1016/j.preteyeres.2009.07.001

Bringmann, A., Pannicke, T., Grosche, J., Francke, M., Wiedemann, P., Skatchkov, S.N., Osborne, N.N., Reichenbach, A., 2006. Müller cells in the healthy and diseased retina. Prog. Retin. Eye Res. 25, 397–424. doi:10.1016/j.preteyeres.2006.05.003

Bringmann, A., Reichenbach, A., 2009. Müller cells 1083–1093.

Bursell, L., Woods, A., James, C.G., Pala, D., Leask, A., Beier, F., 2007. Src kinase inhibition promotes the chondrocyte phenotype. Arthritis Res. Ther. 9, R105. doi:10.1186/ar2308

Cai, X., Hagedorn, C.H., Cullen, B.R., 2004. Human microRNAs are processed from capped, polyadenylated transcripts that can also function as mRNAs. RNA 10, 1957–66. doi:10.1261/rna.7135204

Campos, E.I., Reinberg, D., 2009. Histones: annotating chromatin. Annu. Rev. Genet. 43, 559–99. doi:10.1146/annurev.genet.032608.103928

Castaño Betancourt, M.C., Cailotto, F.F., Kerkhof, H.J., Cornelis, F.M.F., Doherty, S. a, Hart, D.J., Hofman, A., Luyten, F.P., Maciewicz, R. a, Mangino, M., Metrustry, S., Muir, K., Peters, M.J., Rivadeneira, F., Wheeler, M., Zhang, W., Arden, N., Spector, T.D., Uitterlinden, A.G., Doherty, M., Lories, R.J.U., Valdes, A.M., van Meurs, J.B.J., Castaño, M.C., 2012. Genome-wide association and functional studies identify the DOT1L gene to be involved in cartilage thickness and hip osteoarthritis. Proc. Natl. Acad. Sci. 109, 8218–8223. doi:10.1073/pnas.1119899109/-/DCSupplemental.www.pnas.org/cgi/doi/10.1073/pnas.1119899109

Castro, D.S., Martynoga, B., Parras, C., Ramesh, V., Pacary, E., Johnston, C., Drechsel, D., Lebel-Potter, M., Garcia, L.G., Hunt, C., Dolle, D., Bithell, A., Ettwiller, L., Buckley, N., Guillemot, F., 2011. A novel function of the proneural factor Ascl1 in progenitor proliferation identified by genome-wide characterization of its targets. Genes Dev. 25, 930–945. doi:10.1101/gad.627811

Chang, J., Varghese, D.S., Gillam, M.C., Peyton, M., Modi, B., Schiltz, R.L., Girard, L., Martinez, E.D., 2012. Differential response of cancer cells to HDAC inhibitors trichostatin A and depsipeptide. Br. J. Cancer 106, 116–25. doi:10.1038/bjc.2011.532

Chen, P.Y., Manninga, H., Slanchev, K., Chien, M., Russo, J.J., Ju, J., Sheridan, R., John, B., Marks, D.S., Gaidatzis, D., Sander, C., Zavolan, M., 2005. The developmental miRNA profiles of zebrafish as determined by small RNA cloning 1288–1293. doi:10.1101/gad.1310605.The

Chiang, E.F., Pai, C.I., Wyatt, M., Yan, Y.L., Postlethwait, J., Chung, B., 2001. Two sox9 genes on duplicated zebrafish chromosomes: expression of similar transcription activators in distinct sites. Dev. Biol. 231, 149–163. doi:10.1006/dbio.2000.0129

Chong, M.M.W., Zhang, G., Cheloufi, S., Neubert, T.A., Hannon, G.J., Littman, D.R., 2010.

Canonical and alternate functions of the microRNA biogenesis machinery. Genes Dev. 24, 1951–60. doi:10.1101/gad.1953310

Chuang, J.C., Raymond, P. a, 2002. Embryonic origin of the eyes in teleost fish. Bioessays 24, 519–29. doi:10.1002/bies.10097

Clevers, H., 2006. Wnt/beta-catenin signaling in development and disease. Cell 127, 469–80. doi:10.1016/j.cell.2006.10.018

Couly, G.F., Coltey, P.M., Le Douarin, N.M., 1993. The triple origin of skull in higher vertebrates: a study in quail-chick chimeras. Development 117, 409–429.

Crawford, B.D., Henry, C.A., Clason, T.A., Becker, A.L., Hille, M.B., 2003. Activity and distribution of paxillin, focal adhesion kinase, and cadherin indicate cooperative roles during zebrafish morphogenesis. Mol. Biol. Cell 14, 3065–3081. doi:10.1091/mbc.E02-08-0537

Curado, S., Anderson, R.M., Jungblut, B., Mumm, J., Schroeter, E., Stainier, D.Y.R., 2007. Conditional targeted cell ablation in zebrafish: a new tool for regeneration studies. Dev. Dyn. 236, 1025–35. doi:10.1002/dvdy.21100

Czech, B., Zhou, R., Erlich, Y., Brennecke, J., Binari, R., Villalta, C., Gordon, A., Perrimon, N., Hannon, G.J., 2009. Hierarchical rules for Argonaute loading in Drosophila. Mol. Cell 36, 445–56. doi:10.1016/j.molcel.2009.09.028

Daigle, S.R., Olhava, E.J., Therkelsen, C.A., Majer, C.R., Sneeringer, C.J., Song, J., Johnston, L.D., Scott, M.P., Smith, J.J., Xiao, Y., Jin, L., Kuntz, K.W., Chesworth, R., Moyer, M.P., Bernt, K.M., Tseng, J.-C., Kung, A.L., Armstrong, S.A., Copeland, R.A., Richon, V.M., Pollock, R.M., 2011. Selective Killing of Mixed Lineage Leukemia Cells by a Potent Small-Molecule DOT1L Inhibitor. Cancer Cell 20, 53–65. doi:10.1016/j.ccr.2011.06.009

Das, A., Crump, J.G., 2012. Bmps and Id2a act upstream of twist1 to restrict ectomesenchyme potential of the cranial neural crest. PLoS Genet. 8. doi:10.1371/journal.pgen.1002710

de Vries, S.E.J., Baccus, S. a, Meister, M., 2011. The projective field of a retinal amacrine cell. J. Neurosci. 31, 8595–604. doi:10.1523/JNEUROSCI.5662-10.2011

Del Bene, F., Wehman, A.M., Link, B. a, Baier, H., 2008. Regulation of neurogenesis by interkinetic nuclear migration through an apical-basal notch gradient. Cell 134, 1055–65. doi:10.1016/j.cell.2008.07.017

DeLise, a. M., Fischer, L., Tuan, R.S., 2000. Cellular interactions and signaling in cartilage development. Osteoarthr. Cartil. 8, 309–334. doi:10.1053/joca.1999.0306

DeLise, A.M., Stringa, E., Woodward, W.A., Mello, M.A., Tuan, R.S., 2000. Embryonic limb mesenchyme micromass culture as an in vitro model for chondrogenesis and cartilage maturation. Methods Mol. Biol. 137, 359–375. doi:10.1385/1-59259-066-7:359

Denli, A.M., Tops, B.B.J., Plasterk, R.H.A., Ketting, R.F., Hannon, G.J., 2004. Processing of primary microRNAs by the Microprocessor complex. Nature 432, 231–5. doi:10.1038/nature03049

Dion, M.F., Altschuler, S.J., Wu, L.F., Rando, O.J., 2005. Genomic characterization reveals a simple histone H4 acetylation code. Proc. Natl. Acad. Sci. U. S. A. 102, 5501–6.

doi:10.1073/pnas.0500136102

Djuranovic, S., Nahvi, A., Green, R., 2012. miRNA-mediated gene silencing by translational repression followed by mRNA deadenylation and decay. Science 336, 237–40. doi:10.1126/science.1215691

Doench, J.G., Sharp, P.A., 2004. Specificity of microRNA target selection in translational repression. Genes Dev. 18, 504–11. doi:10.1101/gad.1184404

Dutton, K.A., Pauliny, A., Lopes, S.S., Elworthy, S., Carney, T.J., Rauch, J., Geisler, R., Haffter, P., Kelsh, R.N., 2001. Zebrafish colourless encodes sox10 and specifies non-ectomesenchymal neural crest fates. Development 128, 4113–4125.

Eberhart, J.K., He, X., Swartz, M.E., Yan, Y.-L., Song, H., Boling, T.C., Kunerth, A.K., Walker, M.B., Kimmel, C.B., Postlethwait, J.H., 2008. MicroRNA Mirn140 modulates Pdgf signaling during palatogenesis. Nat. Genet. 40, 290–298. doi:10.1038/ng.82

Eggers, E., Lukasiewicz, P., 2011. Multiple pathways of inhibition shape bipolar cell responses in the retina. Vis. Neurosci. 28, 95–108. doi:10.1017/S0952523810000209.Multiple

Eisen, J.S., Smith, J.C., 2008. Controlling morpholino experiments: don't stop making antisense. Development 135, 1735–1743. doi:10.1242/dev.001115

Ernst, J., Kheradpour, P., Mikkelsen, T.S., Shoresh, N., Ward, L.D., Epstein, C.B., Zhang, X., Wang, L., Issner, R., Coyne, M., Ku, M., Durham, T., Kellis, M., Bernstein, B.E., 2011. Mapping and analysis of chromatin state dynamics in nine human cell types. Nature 473, 43–9. doi:10.1038/nature09906

Eyckmans, J., Boudou, T., Yu, X., Chen, C.S., 2011. A Hitchhiker's Guide to Mechanobiology. Dev. Cell. doi:10.1016/j.devcel.2011.06.015

Fadool, J.M., Dowling, J.E., 2008. Zebrafish: a model system for the study of eye genetics. Prog. Retin. Eye Res. 27, 89–110. doi:10.1016/j.preteyeres.2007.08.002

Fausett, B. V, Goldman, D., 2006. A role for alpha1 tubulin-expressing Müller glia in regeneration of the injured zebrafish retina. J. Neurosci. 26, 6303–13. doi:10.1523/JNEUROSCI.0332-06.2006

Fausett, B. V, Gumerson, J.D., Goldman, D., 2008. The proneural basic helix-loop-helix gene ascl1a is required for retina regeneration. J. Neurosci. 28, 1109–17. doi:10.1523/JNEUROSCI.4853-07.2008

Fawcett, J.W., Asher, R. a, 1999. The glial scar and central nervous system repair. Brain Res. Bull. 49, 377–91.

Feng, Q., Wang, H., Ng, H.H., Erdjument-Bromage, H., Tempst, P., Struhl, K., Zhang, Y., 2002. Methylation of H3-lysine 79 is mediated by a new family of HMTases without a SET domain. Curr. Biol. 12, 1052–1058. doi:10.1016/S0960-9822(02)00901-6

Fimbel, S.M., Montgomery, J.E., Burket, C.T., Hyde, D.R., 2007. Regeneration of inner retinal neurons after intravitreal injection of ouabain in zebrafish. J. Neurosci. 27, 1712–24. doi:10.1523/JNEUROSCI.5317-06.2007

Flores, M.V., Tsang, V.W.K., Hu, W., Kalev-Zylinska, M., Postlethwait, J., Crosier, P., Crosier,

K., Fisher, S., 2004. Duplicate zebrafish runx2 orthologues are expressed in developing skeletal elements. Gene Expr. Patterns 4, 573–581. doi:10.1016/j.modgep.2004.01.016

Flynt, A.S., Li, N., Thatcher, E.J., Solnica-Krezel, L., Patton, J.G., 2007. Zebrafish miR-214 modulates Hedgehog signaling to specify muscle cell fate. Nat. Genet. 39, 259–263. doi:10.1038/ng1953

Flynt, A.S., Thatcher, E.J., Burkewitz, K., Li, N., Liu, Y., Patton, J.G., 2009. miR-8 microRNAs regulate the response to osmotic stress in zebrafish embryos. J. Cell Biol. 185, 115–27. doi:10.1083/jcb.200807026

Friedman, R.C., Farh, K.K.-H., Burge, C.B., Bartel, D.P., 2009. Most mammalian mRNAs are conserved targets of microRNAs. Genome Res. 19, 92–105. doi:10.1101/gr.082701.108

Gallina, D., Todd, L., Fischer, A.J., 2013. A comparative analysis of Müller glia-mediated regeneration in the vertebrate retina. Exp. Eye Res. 1–10. doi:10.1016/j.exer.2013.06.019

Gao, L., McBeath, R., Chen, C.S., 2010. Stem cell shape regulates a chondrogenic versus myogenic fate through rac1 and N-cadherin. Stem Cells 28, 564–572. doi:10.1002/stem.308

Gaspar-Maia, A., Alajem, A., Polesso, F., Sridharan, R., Mason, M.J., Heidersbach, A., Ramalho-Santos, J., McManus, M.T., Plath, K., Meshorer, E., Ramalho-Santos, M., 2009. Chd1 regulates open chromatin and pluripotency of embryonic stem cells. Nature 460, 863–8. doi:10.1038/nature08212

Gavet, O., Pines, J., 2010. Progressive Activation of CyclinB1-Cdk1 Coordinates Entry to Mitosis. Dev. Cell 18, 533–543. doi:10.1016/j.devcel.2010.02.013

Gerstein, M.B., Bruce, C., Rozowsky, J.S., Zheng, D., Du, J., Korbel, J.O., Emanuelsson, O., Zhang, Z.D., Weissman, S., Snyder, M., 2007. What is a gene, post-ENCODE? History and updated definition. Genome Res. 17, 669–81. doi:10.1101/gr.6339607

Ghildiyal, M., Xu, J., Seitz, H., Weng, Z., Zamore, P.D., 2010. Sorting of Drosophila small silencing RNAs partitions microRNA* strands into the RNA interference pathway. RNA 16, 43–56. doi:10.1261/rna.1972910

Gifford, C. a, Ziller, M.J., Gu, H., Trapnell, C., Donaghey, J., Tsankov, A., Shalek, A.K., Kelley, D.R., Shishkin, A. a, Issner, R., Zhang, X., Coyne, M., Fostel, J.L., Holmes, L., Meldrim, J., Guttman, M., Epstein, C., Park, H., Kohlbacher, O., Rinn, J., Gnirke, A., Lander, E.S., Bernstein, B.E., Meissner, A., 2013. Transcriptional and Epigenetic Dynamics during Specification of Human Embryonic Stem Cells. Cell 153, 1149–1163. doi:10.1016/j.cell.2013.04.037

Giraldez, A.J., Cinalli, R.M., Glasner, M.E., Enright, A.J., Thomson, J.M., Baskerville, S., Hammond, S.M., Bartel, D.P., Schier, A.F., 2005. MicroRNAs regulate brain morphogenesis in zebrafish. Science 308, 833–838. doi:10.1126/science.1109020

Giraldez, A.J., Mishima, Y., Rihel, J., Grocock, R.J., Van Dongen, S., Inoue, K., Enright, A.J., Schier, A.F., 2006. Zebrafish MiR-430 promotes deadenylation and clearance of maternal mRNAs. Science 312, 75–9. doi:10.1126/science.1122689

Goldman, D., 2014. Müller glial cell reprogramming and retina regeneration. Nat. Rev. Neurosci. 15, 431–442. doi:10.1038/nrn3723

Goldshmit, Y., Sztal, T.E., Jusuf, P.R., Hall, T.E., Nguyen-Chi, M., Currie, P.D., 2012. Fgf-dependent glial cell bridges facilitate spinal cord regeneration in zebrafish. J. Neurosci. 32, 7477–92. doi:10.1523/JNEUROSCI.0758-12.2012

Gorlin, R.J., Stefan, L.L., Cohen, M.M., 1990. Syndromes of the Head and Neck, 3rd ed. ed. Oxford University Press, New York. doi:http://dx.doi.org/10.1097/00006534

Gorsuch, R. a, Hyde, D.R., 2013. Regulation of Müller glial dependent neuronal regeneration in the damaged adult zebrafish retina. Exp. Eye Res. 1–10. doi:10.1016/j.exer.2013.07.012

Gregory, R.I., Yan, K.-P., Amuthan, G., Chendrimada, T., Doratotaj, B., Cooch, N., Shiekhattar, R., 2004. The Microprocessor complex mediates the genesis of microRNAs. Nature 432, 235–40. doi:10.1038/nature03120

Griffiths-Jones, S., Grocock, R.J., van Dongen, S., Bateman, A., Enright, A.J., 2006. miRBase: microRNA sequences, targets and gene nomenclature. Nucleic Acids Res. 34, D140-4. doi:10.1093/nar/gkj112

Grishok, A., Pasquinelli, A.E., Conte, D., Li, N., Parrish, S., Ha, I., Baillie, D.L., Fire, A., Ruvkun, G., Mello, C.C., 2001. Genes and mechanisms related to RNA interference regulate expression of the small temporal RNAs that control C. elegans developmental timing. Cell 106, 23–34.

Guo, Z., Zhang, L., Wu, Z., Chen, Y., Wang, F., Chen, G., 2014. In vivo direct reprogramming of reactive glial cells into functional neurons after brain injury and in an Alzheimer's disease model. Cell Stem Cell 14, 188–202. doi:10.1016/j.stem.2013.12.001

Ha, M., Kim, V.N., 2014. Regulation of microRNA biogenesis. Nat. Rev. Mol. Cell Biol. 15, 509–524. doi:10.1038/nrm3838

Haase, A.D., Jaskiewicz, L., Zhang, H., Lainé, S., Sack, R., Gatignol, A., Filipowicz, W., 2005. TRBP, a regulator of cellular PKR and HIV-1 virus expression, interacts with Dicer and functions in RNA silencing. EMBO Rep. 6, 961–7. doi:10.1038/sj.embor.7400509

Hall, B.K., Miyake, T., 2000. All for one and one for all: Condensations and the initiation of skeletal development. BioEssays 22, 138–147. doi:10.1002/(SICI)1521-1878(200002)22:2<138::AID-BIES5>3.0.CO;2-4

Hall, B.K., Miyake, T., 1995. Divide, accumulate, differentiate: Cell condensation in skeletal development revisited. Int. J. Dev. Biol. 39, 881–893.

Han, J., Lee, Y., Yeom, K.-H., Kim, Y.-K., Jin, H., Kim, V.N., 2004. The Drosha-DGCR8 complex in primary microRNA processing. Genes Dev. 18, 3016–27. doi:10.1101/gad.1262504

Hassan, M.Q., Gordon, J. a R., Beloti, M.M., Croce, C.M., van Wijnen, A.J., Stein, J.L., Stein, G.S., Lian, J.B., 2010. A network connecting Runx2, SATB2, and the miR-23a~27a~24-2 cluster regulates the osteoblast differentiation program. Proc. Natl. Acad. Sci. U. S. A. 107, 19879–19884. doi:10.1073/pnas.1007698107

Henry, C. a, Crawford, B.D., Yan, Y.L., Postlethwait, J., Cooper, M.S., Hille, M.B., 2001. Roles for zebrafish focal adhesion kinase in notochord and somite morphogenesis. Dev. Biol. 240, 474–487. doi:10.1006/dbio.2001.0467

Hitchcock, P.F., Lindsey Myhr, K.J., Easter, S.S., Mangione-Smith, R., Jones, D.D., 1992. Local regeneration in the retina of the goldfish. J. Neurobiol. 23, 187–203. doi:10.1002/neu.480230209

Hochmann, S., Kaslin, J., Hans, S., Weber, A., Machate, A., Geffarth, M., Funk, R.H.W., Brand, M., 2012. Fgf signaling is required for photoreceptor maintenance in the adult zebrafish retina. PLoS One 7, e30365. doi:10.1371/journal.pone.0030365

Hongs, L., Schrothp, G.P., Matthew, H.R., Yaus, P., Bradbyrysliii, E.M., 1993. Studies of the DNA Binding Properties of Histone H4 Amino Terminus.

Honjo, M., Tanihara, H., Kido, N., Inatani, M., Okazaki, K., Honda, Y., 2000. Expression of Ciliary Neurotrophic Factor Activated by Acid – Induced Neuronal Death 41, 552–560.

Huang, S.-M.A., Mishina, Y.M., Liu, S., Cheung, A., Stegmeier, F., Michaud, G.A., Charlat, O., Wiellette, E., Zhang, Y., Wiessner, S., Hild, M., Shi, X., Wilson, C.J., Mickanin, C., Myer, V., Fazal, A., Tomlinson, R., Serluca, F., Shao, W., Cheng, H., Shultz, M., Rau, C., Schirle, M., Schlegl, J., Ghidelli, S., Fawell, S., Lu, C., Curtis, D., Kirschner, M.W., Lengauer, C., Finan, P.M., Tallarico, J.A., Bouwmeester, T., Porter, J.A., Bauer, A., Cong, F., 2009. Tankyrase inhibition stabilizes axin and antagonizes Wnt signalling. Nature 461, 614–20. doi:10.1038/nature08356

Huntzinger, E., Izaurralde, E., 2011. Gene silencing by microRNAs: contributions of translational repression and mRNA decay. Nat. Rev. Genet. 12, 99–110. doi:10.1038/nrg2936

Hutvágner, G., McLachlan, J., Pasquinelli, A.E., Bálint, E., Tuschl, T., Zamore, P.D., 2001. A cellular function for the RNA-interference enzyme Dicer in the maturation of the let-7 small temporal RNA. Science 293, 834–8. doi:10.1126/science.1062961

Jadhav, A.P., Roesch, K., Cepko, C.L., 2009. Development and neurogenic potential of Müller glial cells in the vertebrate retina. Prog. Retin. Eye Res. 28, 249–62. doi:10.1016/j.preteyeres.2009.05.002

Johns, P., Fernald, R., 1981. Genesis of rods in teleost fish retina. Nature 293, 141–142.

Johns, P.R., 1982. Formation of photoreceptors in larval and adult goldfish. J. Neurosci. 2, 178–198.

Johns, P.R., Easter, S.S., 1977. Growth of the Adult Goldfish Eye. II. Increase in retinal cell number. J. Comp. Neurol. 176, 331–341.

Jones, B., Su, H., Bhat, A., Lei, H., Bajko, J., Hevi, S., Baltus, G.A., Kadam, S., Zhai, H., Valdez, R., Gonzalo, S., Zhang, Y., Li, E., Chen, T., 2008. The histone H3K79 methyltransferase Dot1L is essential for mammalian development and heterochromatin structure. PLoS Genet. 4. doi:10.1371/journal.pgen.1000190

Jorstad, N.L., Wilken, M.S., Grimes, W.N., Wohl, S.G., Vandenbosch, L.S., Yoshimatsu, T., Wong, R.O., Rieke, F., Reh, T.A., 2017. Stimulation of functional neuronal regeneration from Müller glia in adult mice. Nature 548, 103–107. doi:10.1038/nature23283

Julian, D., Ennis, K., Korenbrot, J.I., 1998. Birth and fate of proliferative cells in the inner nuclear layer of the mature fish retina. J. Comp. Neurol. 394, 271–82.

Kaneko, B.Y.A., 1970. Physiological and morphological identification of horizontal, bipolar and

amacrine cells in goldfish retina. J. Physiol. 207, 623–633.

Kanellopoulou, C., Muljo, S.A., Kung, A.L., Ganesan, S., Drapkin, R., Jenuwein, T., Livingston, D.M., Rajewsky, K., 2005. Dicer-deficient mouse embryonic stem cells are defective in differentiation and centromeric silencing. Genes Dev. 19, 489–501. doi:10.1101/gad.1248505

Kang, T., Lu, W., Xu, W., Anderson, L., Bacanamwo, M., Thompson, W., Chen, Y.E., Liu, D., 2013. MicroRNA-27 (miR-27) targets prohibitin and impairs adipocyte differentiation and mitochondrial function in human adipose-derived stem cells. J. Biol. Chem. 288, 34394–34402. doi:10.1074/jbc.M113.514372

Karl, M.O., Hayes, S., Nelson, B.R., Tan, K., Buckingham, B., Reh, T. a, 2008. Stimulation of neural regeneration in the mouse retina. Proc. Natl. Acad. Sci. U. S. A. 105, 19508–13. doi:10.1073/pnas.0807453105

Kassen, S.C., Ramanan, V., Montgomery, J.E., T Burket, C., Liu, C.-G., Vihtelic, T.S., Hyde, D.R., 2007. Time course analysis of gene expression during light-induced photoreceptor cell death and regeneration in albino zebrafish. Dev. Neurobiol. 67, 1009–31. doi:10.1002/dneu.20362

Kaur, S., Gupta, S., Chaudhary, M., Khursheed, M.A., Mitra, S., Kurup, A.J., Ramachandran, R., 2018. let-7 MicroRNA-Mediated Regulation of Shh Signaling and the Gene Regulatory Network Is Essential for Retina Regeneration. Cell Rep. 23, 1409–1423. doi:10.1016/j.celrep.2018.04.002

Kelsh, R.N., Dutton, K., Medlin, J., Eisen, J.S., 2000. Expression of zebrafish fkd6 in neural crest-derived glia. Mech. Dev. 93, 161–164. doi:10.1016/S0925-4773(00)00250-1

Ketting, R.F., Fischer, S.E., Bernstein, E., Sijen, T., Hannon, G.J., Plasterk, R.H., 2001. Dicer functions in RNA interference and in synthesis of small RNA involved in developmental timing in C. elegans. Genes Dev. 15, 2654–9. doi:10.1101/gad.927801

Khvorova, A., Reynolds, A., Jayasena, S.D., 2003. Functional siRNAs and miRNAs exhibit strand bias. Cell 115, 209–16.

Kim, Y.-K., Wee, G., Park, J., Kim, J., Baek, D., Kim, J.-S., Kim, V.N., 2013. TALEN-based knockout library for human microRNAs. Nat. Struct. Mol. Biol. 20, 1458–64. doi:10.1038/nsmb.2701

Kimmel, C.B., Ballard, W.W., Kimmel, S.R., Ullmann, B., Schilling, T.F., 1995. Stages of embryonic development of the zebrafish. Dev. Dyn. 203, 253–310. doi:10.1002/aja.1002030302

Kirby, B.B., Takada, N., Latimer, A.J., Shin, J., Carney, T.J., Kelsh, R.N., Appel, B., 2006. In vivo time-lapse imaging shows dynamic oligodendrocyte progenitor behavior during zebrafish development. Nat. Neurosci. 9, 1506–1511. doi:10.1038/nn1803

Kiriakidou, M., Nelson, P.T., Kouranov, A., Fitziev, P., Bouyioukos, C., Mourelatos, Z., Hatzigeorgiou, A., 2004. A combined computational-experimental approach predicts human microRNA targets. Genes Dev. 18, 1165–78. doi:10.1101/gad.1184704

Kloosterman, W.P., Lagendijk, A.K., Ketting, R.F., Moulton, J.D., Plasterk, R.H.A., 2007.

Targeted Inhibition of miRNA Maturation with Morpholinos Reveals a Role for miR-375 in Pancreatic Islet Development. PLoS Biol. 5, e203. doi:10.1371/journal.pbio.0050203

Kloosterman, W.P., Plasterk, R.H.A., 2006. The diverse functions of microRNAs in animal development and disease. Dev. Cell 11, 441–50. doi:10.1016/j.devcel.2006.09.009

Kloosterman, W.P., Wienholds, E., de Bruijn, E., Kauppinen, S., Plasterk, R.H.A., 2006. In situ detection of miRNAs in animal embryos using LNA-modified oligonucleotide probes. Nat. Methods 3, 27–9. doi:10.1038/nmeth843

Knopf, F., Hammond, C., Chekuru, A., Kurth, T., Hans, S., Weber, C.W., Mahatma, G., Fisher, S., Brand, M., Schulte-Merker, S., Weidinger, G., 2011. Bone regenerates via dedifferentiation of osteoblasts in the zebrafish fin. Dev. Cell 20, 713–24. doi:10.1016/j.devcel.2011.04.014

Kobayashi, T., Lu, J., Cobb, B.S., Rodda, S.J., McMahon, A.P., Schipani, E., Merkenschlager, M., Kronenberg, H.M., 2008. Dicer-dependent pathways regulate chondrocyte proliferation and differentiation. Proc. Natl. Acad. Sci. U. S. A. 105, 1949–1954. doi:10.1073/pnas.0707900105

Kok, F.O., Shin, M., Ni, C.-W., Gupta, A., Grosse, A.S., van Impel, A., Kirchmaier, B.C., Peterson-Maduro, J., Kourkoulis, G., Male, I., DeSantis, D.F., Sheppard-Tindell, S., Ebarasi, L., Betsholtz, C., Schulte-Merker, S., Wolfe, S.A., Lawson, N.D., 2015. Reverse Genetic Screening Reveals Poor Correlation between Morpholino-Induced and Mutant Phenotypes in Zebrafish. Dev. Cell 32, 97–108. doi:10.1016/j.devcel.2014.11.018

Kolb, H., Nelson, R., Ahnelt, P., Cuenca, N., 2001. Cellular organization of the vertebrate retina, in: Progress in Brain Research.

Kornberg, R.D., 1974. Chromatin structure: a repeating unit of histones and DNA. Science 184, 868–71.

Kornberg, R.D., Thomas, J.O., 1974. Chromatin structure; oligomers of the histones. Science 184, 865–8.

Koshida, S., Kishimoto, Y., Ustumi, H., Shimizu, T., Furutani-Seiki, M., Kondoh, H., Takada, S., 2005. Integrinα5-dependent fibronectin accumulation for maintenance of somite boundaries in zebrafish embryos. Dev. Cell 8, 587–598. doi:10.1016/j.devcel.2005.03.006

Kouzarides, T., 2007. Chromatin modifications and their function. Cell 128, 693–705. doi:10.1016/j.cell.2007.02.005

Kozhemyakina, E., Lassar, a. B., Zelzer, E., 2015. A pathway to bone: signaling molecules and transcription factors involved in chondrocyte development and maturation. Development 142, 817–831. doi:10.1242/dev.105536

Krol, J., Loedige, I., Filipowicz, W., 2010. The widespread regulation of microRNA biogenesis, function and decay. Nat. Rev. Genet. 11, 597–610. doi:10.1038/nrg2843

Kwan, K.M., Fujimoto, E., Grabher, C., Mangum, B.D., Hardy, M.E., Campbell, D.S., Parant, J.M., Yost, H.J., Kanki, J.P., Chien, C.-B., 2007. The Tol2kit: A multisite gateway-based construction kit forTol2 transposon transgenesis constructs. Dev. Dyn. 236, 3088–3099. doi:10.1002/dvdy.21343

Lagos-Quintana, M., Rauhut, R., Meyer, J., Borkhardt, A., Tuschl, T., 2003. New microRNAs from mouse and human. RNA 9, 175–9.

Lahne, M., Li, J., Marton, R.M., Hyde, D.R., 2015. Actin-Cytoskeleton- and Rock-Mediated INM Are Required for Photoreceptor Regeneration in the Adult Zebrafish Retina. J. Neurosci. 35, 15612–34. doi:10.1523/JNEUROSCI.5005-14.2015

Lamba, D., Karl, M., Reh, T., 2008. Neural regeneration and cell replacement: a view from the eye. Cell Stem Cell 2, 538–49. doi:10.1016/j.stem.2008.05.002

Landgraf, P., Rusu, M., Sheridan, R., Sewer, A., Iovino, N., Aravin, A., Pfeffer, S., Rice, A., Kamphorst, A.O., Landthaler, M., Lin, C., Socci, N.D., Hermida, L., Fulci, V., Chiaretti, S., Foà, R., Schliwka, J., Fuchs, U., Novosel, A., Müller, R.-U., Schermer, B., Bissels, U., Inman, J., Phan, Q., Chien, M., Weir, D.B., Choksi, R., De Vita, G., Frezzetti, D., Trompeter, H.-I., Hornung, V., Teng, G., Hartmann, G., Palkovits, M., Di Lauro, R., Wernet, P., Macino, G., Rogler, C.E., Nagle, J.W., Ju, J., Papavasiliou, F.N., Benzing, T., Lichter, P., Tam, W., Brownstein, M.J., Bosio, A., Borkhardt, A., Russo, J.J., Sander, C., Zavolan, M., Tuschl, T., 2007. A mammalian microRNA expression atlas based on small RNA library sequencing. Cell 129, 1401–14. doi:10.1016/j.cell.2007.04.040

Lauberth, S.M., Nakayama, T., Wu, X., Ferris, A.L., Tang, Z., Hughes, S.H., Roeder, R.G., 2013. H3K4me3 interactions with TAF3 regulate preinitiation complex assembly and selective gene activation. Cell 152, 1021–36. doi:10.1016/j.cell.2013.01.052

Lawson, N.D., Weinstein, B.M., 2002. In vivo imaging of embryonic vascular development using transgenic zebrafish. Dev. Biol. 248, 307–318. doi:10.1006/dbio.2002.0711

Le Douarin, N.M., Creuzet, S., Couly, G., Dupin, E., 2004. Neural crest cell plasticity and its limits. Development 131, 4637–4650. doi:10.1242/dev.01350

Lee, R.C., Feinbaum, R.L., Ambros, V., 1993. The C. elegans heterochronic gene lin-4 encodes small RNAs with antisense complementarity to lin-14. Cell 75, 843–54.

Lee, R.T.H., Knapik, E.W., Thiery, J.P., Carney, T.J., 2013. An exclusively mesodermal origin of fin mesenchyme demonstrates that zebrafish trunk neural crest does not generate ectomesenchyme. Development 140, 2923–32. doi:10.1242/dev.093534

Lee, T.I., Jenner, R.G., Boyer, L. a, Guenther, M.G., Levine, S.S., Kumar, R.M., Chevalier, B., Johnstone, S.E., Cole, M.F., Isono, K., Koseki, H., Fuchikami, T., Abe, K., Murray, H.L., Zucker, J.P., Yuan, B., Bell, G.W., Herbolsheimer, E., Hannett, N.M., Sun, K., Odom, D.T., Otte, A.P., Volkert, T.L., Bartel, D.P., Melton, D. a, Gifford, D.K., Jaenisch, R., Young, R. a, 2006. Control of developmental regulators by Polycomb in human embryonic stem cells. Cell 125, 301–13. doi:10.1016/j.cell.2006.02.043

Lee, Y., Ahn, C., Han, J., Choi, H., Kim, J., Yim, J., Lee, J., Provost, P., Rådmark, O., Kim, S., Kim, V.N., 2003. The nuclear RNase III Drosha initiates microRNA processing. Nature 425, 415–9. doi:10.1038/nature01957

Lee, Y., Jeon, K., Lee, J.-T., Kim, S., Kim, V.N., 2002. MicroRNA maturation: stepwise processing and subcellular localization. EMBO J. 21, 4663–70.

Lee, Y., Kim, M., Han, J., Yeom, K.-H., Lee, S., Baek, S.H., Kim, V.N., 2004. MicroRNA genes are transcribed by RNA polymerase II. EMBO J. 23, 4051–60.

doi:10.1038/sj.emboj.7600385

Lenkowski, J.R., Raymond, P.A., 2014. Müller glia: Stem cells for generation and regeneration of retinal neurons in teleost fish. Prog. Retin. Eye Res. 40, 94–123. doi:10.1016/j.preteyeres.2013.12.007

Lewis, B.P., Burge, C.B., Bartel, D.P., 2005. Conserved seed pairing, often flanked by adenosines, indicates that thousands of human genes are microRNA targets. Cell 120, 15–20. doi:10.1016/j.cell.2004.12.035

Lewis, B.P., Shih, I., Jones-Rhoades, M.W., Bartel, D.P., Burge, C.B., 2003. Prediction of mammalian microRNA targets. Cell 115, 787–98.

Li, N., Wei, C., Olena, A.F., Patton, J.G., 2011a. Regulation of endoderm formation and left-right asymmetry by miR-92 during early zebrafish development. Development 138, 1817–26. doi:10.1242/dev.056697

Li, N., Wei, C., Olena, A.F., Patton, J.G., 2011b. Regulation of endoderm formation and left-right asymmetry by miR-92 during early zebrafish development. Development 138, 1817–1826. doi:10.1242/dev.056697

Liu, C.L., Kaplan, T., Kim, M., Buratowski, S., Schreiber, S.L., Friedman, N., Rando, O.J., 2005. Single-nucleosome mapping of histone modifications in S. cerevisiae. PLoS Biol. 3, e328. doi:10.1371/journal.pbio.0030328

Lombardo, F., 1972. Andamento e localizzazione della mitosi durante la rigenerazione della retina di un Teleosteo adulto (Time course and localization of mitoses during regneration of the retina an adult teleost). Accad. Lincei-Rediconti Sci. Fis. Mat. Nat. Ser. 8, 323–327.

Lombardo, F., 1968. La rigenerazione della retina negli adulti di un Teleosteo (Regeneration of the retina in an adult Teleost). Accad. Lincei-Rendiconti Sci. Fis. Mat. Nat. Sr. 8, 631–635.

Luger, K., Rechsteiner, T.J., Flaus, a J., Waye, M.M., Richmond, T.J., 1997. Characterization of nucleosome core particles containing histone proteins made in bacteria. J. Mol. Biol. 272, 301–11. doi:10.1006/jmbi.1997.1235

Lumsden, A., Sprawson, N., Graham, A., 1991. Segmental origin and migration of neural crest cells in the hindbrain region of the chick embryo. Development 113, 1281–1291.

Lund, E., Güttinger, S., Calado, A., Dahlberg, J.E., Kutay, U., 2004. Nuclear export of microRNA precursors. Science 303, 95–8. doi:10.1126/science.1090599

Ma, Y., Yao, N., Liu, G., Dong, L., Liu, Y., Zhang, M., Wang, F., Wang, B., Wei, X., Dong, H., Wang, L., Ji, S., Zhang, J., Wang, Y., Huang, Y., Yu, J., 2014. Functional screen reveals essential roles of miR- 27 a / 24 in differentiation of embryonic stem cells 1–19.

Macosko, E.Z., Basu, A., Satija, R., Nemesh, J., Shekhar, K., Goldman, M., Tirosh, I., Bialas, A.R., Kamitaki, N., Martersteck, E.M., Trombetta, J.J., Weitz, D.A., Sanes, J.R., Shalek, A.K., Regev, A., McCarroll, S.A., 2015. Highly parallel genome-wide expression profiling of individual cells using nanoliter droplets. Cell 161, 1202–1214. doi:10.1016/j.cell.2015.05.002

Maherali, N., Ahfeldt, T., Rigamonti, A., Utikal, J., Cowan, C., Hochedlinger, K., 2008. A high-efficiency system for the generation and study of human induced pluripotent stem cells. Cell

Stem Cell 3, 340–5. doi:10.1016/j.stem.2008.08.003

Mahmoudi, T., Boj, S.F., Hatzis, P., Li, V.S.W., Taouatas, N., Vries, R.G.J., Teunissen, H., Begthel, H., Korving, J., Mohammed, S., Heck, A.J.R., Clevers, H., 2010. The leukemia-associated Mllt10/Af10-Dot1l are Tcf4/β-catenin coactivators essential for intestinal homeostasis. PLoS Biol. 8. doi:10.1371/journal.pbio.1000539

Maier, W., Wolburg, H., 1979. Regeneration of the Goldfish Retina After Exposure to Different Doses of Ouabain. Cell tissue Res. 202, 99–118.

Mansour, A.A., Gafni, O., Weinberger, L., Zviran, A., Ayyash, M., Rais, Y., Krupalnik, V., Zerbib, M., Amann-Zalcenstein, D., Maza, I., Geula, S., Viukov, S., Holtzman, L., Pribluda, A., Canaani, E., Horn-Saban, S., Amit, I., Novershtern, N., Hanna, J.H., 2012. The H3K27 demethylase Utx regulates somatic and germ cell epigenetic reprogramming. Nature 488, 409–13. doi:10.1038/nature11272

Masland, R.H., 2012. The neuronal organization of the retina. Neuron 76, 266–80. doi:10.1016/j.neuron.2012.10.002

Masland, R.H., 2001. Neuronal diversity in the retina. Curr. Opin. Neurobiol. 11, 431–6.

McBride, S.H., Knothe Tate, M.L., 2008. Modulation of stem cell shape and fate A: the role of density and seeding protocol on nucleus shape and gene expression. Tissue Eng. Part A 14, 1561–1572. doi:10.1089/ten.tea.2008.0112

Megee, P.C., Morgan, B. a, Smith, M.M., 1995. Histone H4 and the maintenance of genome integrity. Genes Dev. 9, 1716–1727. doi:10.1101/gad.9.14.1716

Mensinger, a F., Powers, M.K., 1999. Visual function in regenerating teleost retina following cytotoxic lesioning. Vis. Neurosci. 16, 241–51.

Meyers, J.R., Hu, L., Moses, A., Kaboli, K., Papandrea, A., Raymond, P. a, 2012. β-catenin/Wnt signaling controls progenitor fate in the developing and regenerating zebrafish retina. Neural Dev. 7, 30. doi:10.1186/1749-8104-7-30

Mikkelsen, T.S., Ku, M., Jaffe, D.B., Issac, B., Lieberman, E., Giannoukos, G., Alvarez, P., Brockman, W., Kim, T.-K., Koche, R.P., Lee, W., Mendenhall, E., O'Donovan, A., Presser, A., Russ, C., Xie, X., Meissner, A., Wernig, M., Jaenisch, R., Nusbaum, C., Lander, E.S., Bernstein, B.E., 2007. Genome-wide maps of chromatin state in pluripotent and lineage-committed cells. Nature 448, 553–60. doi:10.1038/nature06008

Mitra, S.K., Hanson, D.A., Schlaepfer, D.D., 2005. Focal adhesion kinase: in command and control of cell motility. Nat. Rev. Mol. Cell Biol. 6, 56–68. doi:10.1038/nrm1549

Mohan, M., Herz, H.M., Takahashi, Y.H., Lin, C., Lai, K.C., Zhang, Y., Washburn, M.P., Florens, L., Shilatifard, A., 2010. Linking H3K79 trimethylation to Wnt signaling through a novel Dot1-containing complex (DotCom). Genes Dev. 24, 574–589. doi:10.1101/gad.1898410

Moss, J.B., Koustubhan, P., Greenman, M., Parsons, M.J., Walter, I., Moss, L.G., 2009. Regeneration of the Pancreas in Adult Zebrafish. Diabetes 58, 1844–1851. doi:10.2337/db08-0628.

Murchison, E.P., Stein, P., Xuan, Z., Pan, H., Zhang, M.Q., Schultz, R.M., Hannon, G.J., 2007.

Critical roles for Dicer in the female germline. Genes Dev. 21, 682–93. doi:10.1101/gad.1521307

Murciano, A., Zamora, J., López-Sánchez, J., Frade, J.M., 2002. Interkinetic nuclear movement may provide spatial clues to the regulation of neurogenesis. Mol. Cell. Neurosci. 21, 285–300.

Nagashima, M., Barthel, L.K., Raymond, P.A., 2013. A self-renewing division of zebrafish Muller glial cells generates neuronal progenitors that require N-cadherin to regenerate retinal neurons. Development 140, 4510–4521. doi:10.1242/dev.090738

Nakamura, Y., Inloes, J.B., Katagiri, T., Kobayashi, T., 2011. Chondrocyte-specific microRNA-140 regulates endochondral bone development and targets Dnpep to modulate bone morphogenetic protein signaling. Mol. Cell. Biol. 31, 3019–3028. doi:10.1128/MCB.05178-11

Nakatani, Y., Kawakami, A., Kudo, A., 2007. Cellular and molecular processes of regeneration , with special emphasis on fish fins 145–154. doi:10.1111/j.1440-169x.2007.00917.x

Narayanan, A., Hill-Teran, G., Moro, A., Ristori, E., Kasper, D.M., A. Roden, C., Lu, J., Nicoli, S., 2016. In vivo mutagenesis of miRNA gene families using a scalable multiplexed CRISPR/Cas9 nuclease system. Sci. Rep. 6, 32386. doi:10.1038/srep32386

Negishi, K., Stell, W.K., Teranishi, T., Karkhanis, a, Owusu-Yaw, V., Takasaki, Y., 1991. Induction of proliferating cell nuclear antigen (PCNA)-immunoreactive cells in goldfish retina following intravitreal injection with 6-hydroxydopamine. Cell. Mol. Neurobiol. 11, 639–59.

Nelson, C.M., Ackerman, K.M., O'Hayer, P., Bailey, T.J., Gorsuch, R. a, Hyde, D.R., 2013. Tumor Necrosis Factor-Alpha Is Produced by Dying Retinal Neurons and Is Required for Muller Glia Proliferation during Zebrafish Retinal Regeneration. J. Neurosci. 33, 6524–39. doi:10.1523/JNEUROSCI.3838-12.2013

Newman, E., Reichenbach, a, 1996. The Müller cell: a functional element of the retina. Trends Neurosci. 19, 307–12.

Ning, G., Liu, X., Dai, M., Meng, A., Wang, Q., 2013. MicroRNA-92a Upholds Bmp Signaling by Targeting noggin3 during Pharyngeal Cartilage Formation. Dev. Cell 24, 283–295. doi:10.1016/j.devcel.2012.12.016

Ohno, S., 1972. So much "junk" DNA in our genome. Brookhaven Symp. Biol. 23, 366–70.

Okamura, K., Liu, N., Lai, E.C., 2009. Distinct mechanisms for microRNA strand selection by Drosophila Argonautes. Mol. Cell 36, 431–44. doi:10.1016/j.molcel.2009.09.027

Olena, A.F., Rao, M.B., Thatcher, E.J., Wu, S.-Y., Patton, J.G., 2015. miR-216a regulates snx5, a novel notch signaling pathway component, during zebrafish retinal development. Dev. Biol. 400, 72–81. doi:10.1016/j.ydbio.2015.01.016

Olins, A.L., Olins, D.E., 1974. Spheroid Chromatin Units (v Bodies). Science 183, 330–332.

Onder, T.T., Kara, N., Cherry, A., Sinha, A.U., Zhu, N., Bernt, K.M., Cahan, P., Mancarci, O.B., Unternaehrer, J., Gupta, P.B., Lander, E.S., Armstrong, S.A., Daley, G.Q., 2012. Chromatin-modifying enzymes as modulators of reprogramming. Nature 483, 598–602.

doi:10.1038/nature10953

Onodera, K., Takahashi, I., Sasano, Y., Bae, J.W., Mitani, H., Kagayama, M., Mitani, H., 2005. Stepwise mechanical stretching inhibits chondrogenesis through cell-matrix adhesion mediated by integrins in embryonic rat limb-bud mesenchymal cells. Eur. J. Cell Biol. 84, 45–58. doi:10.1016/j.ejcb.2004.09.004

Ooto, S., Akagi, T., Kageyama, R., Akita, J., Mandai, M., Honda, Y., Takahashi, M., 2004. Potential for neural regeneration after neurotoxic injury in the adult mammalian retina. Proc. Natl. Acad. Sci. U. S. A. 101, 13654–9. doi:10.1073/pnas.0402129101

Osakada, F., Ooto, S., Akagi, T., Mandai, M., Akaike, A., Takahashi, M., 2007. Wnt signaling promotes regeneration in the retina of adult mammals. J. Neurosci. 27, 4210–9. doi:10.1523/JNEUROSCI.4193-06.2007

Otteson, D.C., D'Costa, a R., Hitchcock, P.F., 2001. Putative stem cells and the lineage of rod photoreceptors in the mature retina of the goldfish. Dev. Biol. 232, 62–76. doi:10.1006/dbio.2001.0163

Otteson, D.C., Hitchcock, P.F., 2003. Stem cells in the teleost retina: persistent neurogenesis and injury-induced regeneration. Vision Res. 43, 927–936. doi:10.1016/S0042-6989(02)00400-5

Pala, D., Kapoor, M., Woods, A., Kennedy, L., Liu, S., Chen, S., Bursell, L., Lyons, K.M., Carter, D.E., Beier, F., Leask, A., 2008. Focal adhesion kinase/Src suppresses early chondrogenesis: Central role of CCN2. J. Biol. Chem. 283, 9239–9247. doi:10.1074/jbc.M705175200

Parsons, J.T., 2003. Focal adhesion kinase: the first ten years. J. Cell Sci. 116, 1409–1416. doi:10.1242/jcs.00373

Pasque, V., Jullien, J., Miyamoto, K., Halley-Stott, R.P., Gurdon, J.B., 2011. Epigenetic factors influencing resistance to nuclear reprogramming. Trends Genet. 27, 516–25. doi:10.1016/j.tig.2011.08.002

Pasquinelli, A.E., Reinhart, B.J., Slack, F., Martindale, M.Q., Kuroda, M.I., Maller, B., Hayward, D.C., Ball, E.E., Degnan, B., Müller, P., Spring, J., Srinivasan, A., Fishman, M., Finnerty, J., Corbo, J., Levine, M., Leahy, P., Davidson, E., Ruvkun, G., 2000. Conservation of the sequence and temporal expression of let-7 heterochronic regulatory RNA. Nature 408, 86–9. doi:10.1038/35040556

Poché, R. a, Reese, B.E., 2009. Retinal horizontal cells: challenging paradigms of neural development and cancer biology. Development 136, 2141–51. doi:10.1242/dev.033175

Pokholok, D.K., Harbison, C.T., Levine, S., Cole, M., Hannett, N.M., Lee, T.I., Bell, G.W., Walker, K., Rolfe, P.A., Herbolsheimer, E., Zeitlinger, J., Lewitter, F., Gifford, D.K., Young, R. a, 2005. Genome-wide map of nucleosome acetylation and methylation in yeast. Cell 122, 517–27. doi:10.1016/j.cell.2005.06.026

Pollak, J., Wilken, M.S., Ueki, Y., Cox, K.E., Sullivan, J.M., Taylor, R.J., Levine, E.M., Reh, T.A., 2013. ASCL1 reprograms mouse Muller glia into neurogenic retinal progenitors. Development 140, 2619–2631. doi:10.1242/dev.091355

Poss, K.D., Wilson, L.G., Keating, M.T., 2002. Heart regeneration in zebrafish. Science 298,

2188–90. doi:10.1126/science.1077857

Powell, C., Elsaeidi, F., Goldman, D., 2012. Injury-dependent Müller glia and ganglion cell reprogramming during tissue regeneration requires Apobec2a and Apobec2b. J. Neurosci. 32, 1096–109. doi:10.1523/JNEUROSCI.5603-11.2012

Powell, C., Grant, A.R., Cornblath, E., Goldman, D., 2013. Analysis of DNA methylation reveals a partial reprogramming of the Muller glia genome during retina regeneration. Proc. Natl. Acad. Sci. 110, 19814–19819. doi:10.1073/pnas.1312009110

Qin, Z., Kidd, A.R., Thomas, J.L., Poss, K.D., Hyde, D.R., Raymond, P. a, Thummel, R., 2011. FGF signaling regulates rod photoreceptor cell maintenance and regeneration in zebrafish. Exp. Eye Res. 93, 726–34. doi:10.1016/j.exer.2011.09.003

Quintero, H., Gómez-Montalvo, A.I., Lamas, M., 2016. MicroRNA changes through Müller glia dedifferentiation and early/late rod photoreceptor differentiation. Neuroscience 316, 109–21. doi:10.1016/j.neuroscience.2015.12.025

Rais, Y., Zviran, A., Geula, S., Gafni, O., Chomsky, E., Viukov, S., Mansour, A.A., Caspi, I., Krupalnik, V., Zerbib, M., Maza, I., Mor, N., Baran, D., Weinberger, L., Jaitin, D. a., Lara-Astiaso, D., Blecher-Gonen, R., Shipony, Z., Mukamel, Z., Hagai, T., Gilad, S., Amann-Zalcenstein, D., Tanay, A., Amit, I., Novershtern, N., Hanna, J.H., 2013. Deterministic direct reprogramming of somatic cells to pluripotency. Nature 502, 65–70. doi:10.1038/nature12587

Rajaram, K., Harding, R.L., Bailey, T., Patton, J.G., Hyde, D.R., 2014a. Dynamic miRNA expression patterns during retinal regeneration in zebrafish: Reduced dicer or miRNA expression suppresses proliferation of Müller Glia-derived neuronal progenitor cells. Dev. Dyn. 243, 1591–1605. doi:10.1002/dvdy.24188

Rajaram, K., Harding, R.L., Hyde, D.R., Patton, J.G., 2014b. MiR-203 regulates progenitor cell proliferation during adult zebrafish retina regeneration. Dev. Biol. 392, 393–403. doi:10.1016/j.ydbio.2014.05.005

Rajaram, K., Summerbell, E.R., Patton, J.G., 2014c. Technical brief: Constant intense light exposure to lesion and initiate regeneration in normally pigmented zebrafish. Mol. Vis. 20, 1075–84.

Rajaram, K., Summerbell, E.R., Patton, J.G., 2014. Technical brief: Constant intense light exposure to lesion and initiate regeneration in normally pigmented zebrafish. Mol Vis 20, 1075–1084.

Ramachandran, R., Fausett, B. V., Goldman, D., 2010a. Ascl1a regulates Müller glia dedifferentiation and retinal regeneration through a Lin-28-dependent, let-7 microRNA signalling pathway. Nat. Cell Biol. 12, 1101–1107. doi:10.1038/ncb2115

Ramachandran, R., Fausett, B. V, Goldman, D., 2010b. Ascl1a regulates Müller glia dedifferentiation and retinal regeneration through a Lin-28-dependent, let-7 microRNA signalling pathway. Nat. Cell Biol. 12, 1101–7. doi:10.1038/ncb2115

Ramachandran, R., Fausett, B. V, Goldman, D., 2010c. Ascl1a regulates Müller glia dedifferentiation and retinal regeneration through a Lin-28-dependent, let-7 microRNA signalling pathway. Nat. Cell Biol. 12, 1101–7. doi:10.1038/ncb2115

Ramachandran, R., Zhao, X.-F., Goldman, D., 2012a. Insm1a-mediated gene repression is essential for the formation and differentiation of Müller glia-derived progenitors in the injured retina. Nat. Cell Biol. 14, 1013–23. doi:10.1038/ncb2586

Ramachandran, R., Zhao, X.-F., Goldman, D., 2012b. Insm1a-mediated gene repression is essential for the formation and differentiation of Müller glia-derived progenitors in the injured retina. Nat. Cell Biol. 14, 1013–23. doi:10.1038/ncb2586

Ramachandran, R., Zhao, X.-F., Goldman, D., 2012c. Insm1a-mediated gene repression is essential for the formation and differentiation of Müller glia-derived progenitors in the injured retina. Nat. Cell Biol. 14, 1013–23. doi:10.1038/ncb2586

Ramachandran, R., Zhao, X.-F., Goldman, D., 2011. Ascl1a/Dkk/ -catenin signaling pathway is necessary and glycogen synthase kinase-3 inhibition is sufficient for zebrafish retina regeneration. Proc. Natl. Acad. Sci. 108, 15858–15863. doi:10.1073/pnas.1107220108

Rao, M.B., Didiano, D., Patton, J.G., 2017. Neurotransmitter-Regulated Regeneration in the Zebrafish Retina. Stem Cell Reports 8, 831–842. doi:10.1016/j.stemcr.2017.02.007

Raymond, P. a, Barthel, L.K., Bernardos, R.L., Perkowski, J.J., 2006. Molecular characterization of retinal stem cells and their niches in adult zebrafish. BMC Dev. Biol. 6, 36. doi:10.1186/1471-213X-6-36

Raymond, P. a, Barthel, L.K., Rounsifer, M.E., Sullivan, S. a, Knight, J.K., 1993. Expression of rod and cone visual pigments in goldfish and zebrafish: a rhodopsin-like gene is expressed in cones. Neuron 10, 1161–74.

Raymond, P. a, Reifler, M.J., Rivlin, P.K., 1988. Regeneration of goldfish retina: rod precursors are a likely source of regenerated cells. J. Neurobiol. 19, 431–63. doi:10.1002/neu.480190504

Raymond, P. a, Rivlin, P.K., 1987. Germinal cells in the goldfish retina that produce rod photoreceptors. Dev. Biol. 122, 120–38.

Reichenbach, A., Bringmann, A., 2013. New functions of Müller cells. Glia 61, 651–78. doi:10.1002/glia.22477

Reichenbach, A., Bringmann, A., 2010a. Müller Cells in the Healthy and Diseased Retina. Springer New York, New York, NY. doi:10.1007/978-1-4419-1672-3_2

Reichenbach, A., Bringmann, A., 2010b. Müller Cells in the Diseased Retina. Springer New York, New York, NY. doi:10.1007/978-1-4419-1672-3

Robu, M.E., Larson, J.D., Nasevicius, A., Beiraghi, S., Brenner, C., Farber, S.A., Ekker, S.C., 2007. p53 activation by knockdown technologies. PLoS Genet. 3, 787–801. doi:10.1371/journal.pgen.0030078

Rodriguez, A., Griffiths-Jones, S., Ashurst, J.L., Bradley, A., 2004. Identification of mammalian microRNA host genes and transcription units. Genome Res. 14, 1902–10. doi:10.1101/gr.2722704

Rossi, A., Kontarakis, Z., Gerri, C., Nolte, H., Hölper, S., Krüger, M., Stainier, D.Y.R., 2015. Genetic compensation induced by deleterious mutations but not gene knockdowns. Nature 524, 230–233. doi:10.1038/nature14580

Roush, S., Slack, F.J., 2008. The let-7 family of microRNAs. Trends Cell Biol. 18, 505–16. doi:10.1016/j.tcb.2008.07.007

Schilling, T.F., Kimmel, C.B., 1994. Segment and cell type lineage restrictions during pharyngeal arch development in the zebrafish embryo. Development 120, 483–494.

Schwarz, D.S., Hutvágner, G., Du, T., Xu, Z., Aronin, N., Zamore, P.D., 2003. Asymmetry in the assembly of the RNAi enzyme complex. Cell 115, 199–208.

Shanower, G.A., Muller, M., Blanton, J.L., Honti, V., Gyurkovics, H., Schedl, P., 2005. Characterization of the grappa gene, the Drosophila Histone H3 lysine 79 methyltransferase. Genetics 169, 173–184. doi:10.1534/genetics.104.033191

Sheehy, N.T., Cordes, K.R., White, M.P., Ivey, K.N., Srivastava, D., 2010. The neural crest-enriched microRNA miR-452 regulates epithelial-mesenchymal signaling in the first pharyngeal arch. Development 137, 4307–4316. doi:10.1242/dev.052647

Sherpa, T., Fimbel, S.M., Mallory, D.E., Maaswinkel, H., Spritzer, S.D., Sand, J.A., Li, L., Hyde, D.R., Stenkamp, D.L., 2008. Ganglion cell regeneration following whole-retina destruction in zebrafish. Dev. Neurobiol. 68, 166–81. doi:10.1002/dneu.20568

Shogren-knaak, A.M., Ishii, H., Sun, J., Pazin, M.J., James, R., Peterson, C.L., 2006. Histone H4-K16 Acetylation Controls Chromatin Structure and Protein Interactions. Science (80-.). 311, 844–847.

Singh, P., Schwarzbauer, J.E., 2014. Fibronectin matrix assembly is essential for cell condensation during chondrogenesis 4420–4428. doi:10.1242/jcs.150276

Solomon, S.G., Lennie, P., 2007. The machinery of colour vision. Nat. Rev. Neurosci. 8, 276–86. doi:10.1038/nrn2094

Stainier, D.Y.R., Kontarakis, Z., Rossi, A., 2015. Making Sense of Anti-Sense Data. Dev. Cell 32, 7–8. doi:10.1016/j.devcel.2014.12.012

Stefani, G., Slack, F.J., 2008. Small non-coding RNAs in animal development. Nat. Rev. Mol. Cell Biol. 9, 219–230. doi:10.1038/nrm2347

Steger, D.J., Lefterova, M.I., Ying, L., Stonestrom, A.J., Schupp, M., Zhuo, D., Vakoc, A.L., Kim, J.-E., Chen, J., Lazar, M.A., Blobel, G.A., Vakoc, C.R., 2008. DOT1L/KMT4 Recruitment and H3K79 Methylation Are Ubiquitously Coupled with Gene Transcription in Mammalian Cells. Mol. Cell. Biol. 28, 2825–2839. doi:10.1128/MCB.02076-07

Stenkamp, D.L., 2011. The rod photoreceptor lineage of teleost fish. Prog. Retin. Eye Res. 30, 395–404. doi:10.1016/j.preteyeres.2011.06.004

Stenkamp, D.L., 2007. Neurogenesis in the fish retina. Int. Rev. Cytol. 259, 173–224. doi:10.1016/S0074-7696(06)59005-9

Suh, N., Baehner, L., Moltzahn, F., Melton, C., Shenoy, A., Chen, J., Blelloch, R., 2010. MicroRNA function is globally suppressed in mouse oocytes and early embryos. Curr. Biol. 20, 271–7. doi:10.1016/j.cub.2009.12.044

Takahashi, I., Onodera, K., Sasano, Y., Mizoguchi, I., Bae, J.-W., Mitani, H., Kagayama, M., Mitani, H., 2003. Effect of stretching on gene expression of beta1 integrin and focal

adhesion kinase and on chondrogenesis through cell-extracellular matrix interactions. Eur. J. Cell Biol. 82, 182–192. doi:10.1078/0171-9335-00307

Takahashi, K., Yamanaka, S., 2006. Induction of pluripotent stem cells from mouse embryonic and adult fibroblast cultures by defined factors. Cell 126, 663–76. doi:10.1016/j.cell.2006.07.024

Tang, Y., Rowe, R.G., Botvinick, E., Kurup, A., Putnam, A., Seiki, M., Weaver, V., Keller, E., Goldstein, S., Dai, J., Begun, D., Saunders, T., Weiss, S.J., 2013a. MT1-MMP-Dependent Control of Skeletal Stem Cell Commitment via a β1-Integrin/YAP/TAZ Signaling Axis. Dev. Cell 25, 402–416. doi:10.1016/j.devcel.2013.04.011

Tang, Y., Rowe, R.G., Botvinick, E.L., Kurup, A., Putnam, A.J., Seiki, M., Weaver, V.M., Keller, E.T., Goldstein, S., Dai, J., Begun, D., Saunders, T., Weiss, S.J., 2013b. Article MT1-MMP-Dependent Control of Skeletal Stem Cell Commitment via a b 1-Integrin / YAP / TAZ Signaling Axis. Dev. Cell 25, 402–416. doi:10.1016/j.devcel.2013.04.011

Telese, F., Gamliel, A., Skowronska-Krawczyk, D., Garcia-Bassets, I., Rosenfeld, M.G., 2013. "Seq-ing" insights into the epigenetics of neuronal gene regulation. Neuron 77, 606–23. doi:10.1016/j.neuron.2013.01.034

Thatcher, E.J., Patton, J.G., 2010. Small RNAs have a big impact on regeneration. RNA Biol. 7, 333–338. doi:10.4161/rna.7.3.12085

Thatcher, E.J., Paydar, I., Anderson, K.K., Patton, J.G., 2008. Regulation of zebrafish fin regeneration by microRNAs. Proc. Natl. Acad. Sci. U. S. A. 105, 18384–9. doi:10.1073/pnas.0803713105

Thisse, C., Thisse, B., 2008. High-resolution in situ hybridization to whole-mount zebrafish embryos. Nat. Protoc. 3, 59–69. doi:10.1038/nprot.2007.514

Thoreson, W.B., Mangel, S.C., 2012. Lateral interactions in the outer retina. Prog. Retin. Eye Res. 31, 407–41. doi:10.1016/j.preteyeres.2012.04.003

Thummel, R., Enright, J.M., Kassen, S.C., Montgomery, J.E., Bailey, T.J., Hyde, D.R., 2010a. Pax6a and Pax6b are required at different points in neuronal progenitor cell proliferation during zebrafish photoreceptor regeneration. Exp. Eye Res. 90, 572–82. doi:10.1016/j.exer.2010.02.001

Thummel, R., Enright, J.M., Kassen, S.C., Montgomery, J.E., Bailey, T.J., Hyde, D.R., 2010b. Pax6a and Pax6b are required at different points in neuronal progenitor cell proliferation during zebrafish photoreceptor regeneration. Exp. Eye Res. 90, 572–582. doi:10.1016/j.exer.2010.02.001

Thummel, R., Kassen, S.C., Enright, J.M., Nelson, C.M., Montgomery, J.E., Hyde, D.R., 2008. Characterization of Müller glia and neuronal progenitors during adult zebrafish retinal regeneration. Exp. Eye Res. 87, 433–44. doi:10.1016/j.exer.2008.07.009

Ueki, Y., Wilken, M.S., Cox, K.E., Chipman, L., Jorstad, N., Sternhagen, K., Simic, M., Ullom, K., Nakafuku, M., Reh, T.A., 2015. Transgenic expression of the proneural transcription factor Ascl1 in Müller glia stimulates retinal regeneration in young mice. Proc. Natl. Acad. Sci. 112, 13717–13722. doi:10.1073/pnas.1510595112

Urbich, C., Kaluza, D., Frömel, T., Knau, A., Bennewitz, K., Boon, R. a, Bonauer, A., Doebele, C., Boeckel, J.-N., Hergenreider, E., Zeiher, A.M., Kroll, J., Fleming, I., Dimmeler, S., 2012. MicroRNA-27a/b controls endothelial cell repulsion and angiogenesis by targeting semaphorin 6A. Blood 119, 1607–16. doi:10.1182/blood-2011-08-373886

Van Leeuwen, F., Gafken, P.R., Gottschling, D.E., 2002. Dot1p modulates silencing in yeast by methylation of the nucleosome core. Cell 109, 745–756. doi:10.1016/S0092-8674(02)00759-6

Vastenhouw, N.L., Zhang, Y., Woods, I.G., Imam, F., Regev, A., Liu, X.S., Rinn, J., Schier, A.F., 2010. Chromatin signature of embryonic pluripotency is established during genome activation. Nature 464, 922–6. doi:10.1038/nature08866

Veldman, M.B., Bemben, M. a, Goldman, D., 2010. Tuba1a gene expression is regulated by KLF6/7 and is necessary for CNS development and regeneration in zebrafish. Mol. Cell. Neurosci. 43, 370–83. doi:10.1016/j.mcn.2010.01.004

Vermeulen, M., Mulder, K.W., Denissov, S., Pijnappel, W.W.M.P., van Schaik, F.M. a, Varier, R. a, Baltissen, M.P. a, Stunnenberg, H.G., Mann, M., Timmers, H.T.M., 2007. Selective anchoring of TFIID to nucleosomes by trimethylation of histone H3 lysine 4. Cell 131, 58–69. doi:10.1016/j.cell.2007.08.016

Vierbuchen, T., Ostermeier, A., Pang, Z.P., Kokubu, Y., Südhof, T.C., Wernig, M., 2010. Direct conversion of fibroblasts to functional neurons by defined factors. Nature 463, 1035–1041. doi:10.1038/nature08797

Vihtelic, T.S., Hyde, D.R., 2000. Light-Induced Rod and Cone Cell Death and Regeneration in the Adult albino Zebrafish (Danio rerio) Retina. J. Neurobiol. 44, 289–307.

Walker, C., 1999. Haploid screens and gamma-ray mutagenesis. Methods Cell Biol. 60, 43–70.

Wan, J., Goldman, D., 2016. Retina regeneration in zebrafish. Curr. Opin. Genet. Dev. 40, 41–47. doi:10.1016/j.gde.2016.05.009

Wan, J., Ramachandran, R., Goldman, D., 2012a. HB-EGF is necessary and sufficient for Müller glia dedifferentiation and retina regeneration. Dev. Cell 22, 334–47. doi:10.1016/j.devcel.2011.11.020

Wan, J., Ramachandran, R., Goldman, D., 2012b. HB-EGF Is Necessary and Sufficient for Müller Glia Dedifferentiation and Retina Regeneration. Dev. Cell 22, 334–347. doi:10.1016/j.devcel.2011.11.020

Wan, J., Zhao, X.F., Vojtek, A., Goldman, D., 2014. Retinal injury, growth factors, and cytokines converge on β-catenin and pStat3 signaling to stimulate retina regeneration. Cell Rep. 9, 285–297. doi:10.1016/j.celrep.2014.08.048

Wang, Y., Medvid, R., Melton, C., Jaenisch, R., Blelloch, R., 2007. DGCR8 is essential for microRNA biogenesis and silencing of embryonic stem cell self-renewal. Nat. Genet. 39, 380–5. doi:10.1038/ng1969

Wei, C., Salichos, L., Wittgrove, C.M., Rokas, A., Patton, J.G., 2012. Transcriptome-wide analysis of small RNA expression in early zebrafish development. RNA. doi:10.1261/rna.029090.111

Wei, C., Thatcher, E.J., Olena, A.F., Cha, D.J., Perdigoto, A.L., Marshall, A.F., Carter, B.D., Broadie, K., Patton, J.G., 2013. miR-153 Regulates SNAP-25, Synaptic Transmission, and Neuronal Development. PLoS One 8. doi:10.1371/journal.pone.0057080

Werblin, F.S., Dowling, J.E., 1969. Organization of the retina of the of the Mudpuppy, Necturus maculosus. J. Neurophysiol. 32, 339–355.

Wernig, M., Meissner, A., Foreman, R., Brambrink, T., Ku, M., Hochedlinger, K., Bernstein, B.E., Jaenisch, R., 2007. In vitro reprogramming of fibroblasts into a pluripotent ES-cell-like state. Nature 448, 318–24. doi:10.1038/nature05944

Wienholds, E., 2005. MicroRNA Expression in Zebrafish Embryonic Development. Science (80-.). 309, 310–311. doi:10.1126/science.1114519

Wienholds, E., Plasterk, R.H.A., 2005. MicroRNA function in animal development. FEBS Lett. 579, 5911–5922. doi:10.1016/j.febslet.2005.07.070

Wightman, B., Ha, I., Ruvkun, G., 1993. Posttranscriptional regulation of the heterochronic gene lin-14 by lin-4 mediates temporal pattern formation in C. elegans. Cell 75, 855–62.

Wilmut, I., Beaujean, N., de Sousa, P.A., Dinnyes, A., King, T.J., Paterson, L.A., Wells, D.N., Young, L.E., 2002. Somatic cell nuclear transfer. Nature 419, 583–587. doi:10.1038/nature01079

Wohl, S.G., Jorstad, N.L., Levine, E.M., Reh, T.A., 2017. Müller glial microRNAs are required for the maintenance of glial homeostasis and retinal architecture. Nat. Commun. 8, 1–15. doi:10.1038/s41467-017-01624-y

Wohl, S.G., Reh, T.A., 2016. The microRNA expression profile of mouse Müller glia in vivo and in vitro. Sci. Rep. 6, 1–13. doi:10.1038/srep35423

Wohl, S.G., Reh, T.A., 2016. miR-124-9-9* potentiates Ascl1-induced reprogramming of cultured Müller glia. Glia 64, 743–62. doi:10.1002/glia.22958

Woods, A., Beier, F., 2006. RhoA/ROCK signaling regulates chondrogenesis in a context-dependent manner. J. Biol. Chem. 281, 13134–13140. doi:10.1074/jbc.M509433200

Woods, A., Wang, G., Beier, F., 2007. Regulation of chondrocyte differentiation by the act in cytoskeleton and adhesive interactions. J. Cell. Physiol. doi:10.1002/jcp.21110

Woods, A., Wang, G., Beier, F., 2005. RhoA/ROCK signaling regulates Sox9 expression and actin organization during chondrogenesis. J. Biol. Chem. 280, 11626–11634. doi:10.1074/jbc.M409158200

Wu, B.-T., Wen, S.-H., Hwang, S.-P.L., Huang, C.-J., Kuan, Y.-S., 2015. Control of Wnt5b secretion by Wntless modulates chondrogenic cell proliferation through fine-tuning fgf3 expression. J. Cell Sci. 128, 2328–2339. doi:10.1242/jcs.167403

Wu, D.M., Schneiderman, T., Burgett, J., Gokhale, P., Barthel, L., Raymond, P. a, 2001. Cones regenerate from retinal stem cells sequestered in the inner nuclear layer of adult goldfish retina. Invest. Ophthalmol. Vis. Sci. 42, 2115–24.

Yan, Y.-L., Miller, C.T., Nissen, R.M., Singer, A., Liu, D., Kirn, A., Draper, B., Willoughby, J., Morcos, P. a, Amsterdam, A., Chung, B.-C., Westerfield, M., Haffter, P., Hopkins, N.,

Kimmel, C., Postlethwait, J.H., 2002. A zebrafish sox9 gene required for cartilage morphogenesis. Development 129, 5065–5079.

Yan, Y.L., Hatta, K., Riggleman, B., Postlethwait, J.H., 1995. Expression of a type II collagen gene in the zebrafish embryonic axis. Dev. Dyn. 203, 363–376. doi:10.1002/aja.1002030308

Yao, K., Qiu, S., Tian, L., Snider, W.D., Flannery, J.G., Schaffer, D. V., Chen, B., 2016. Wnt Regulates Proliferation and Neurogenic Potential of Müller Glial Cells via a Lin28/let-7 miRNA-Dependent Pathway in Adult Mammalian Retinas. Cell Rep. 17, 165–178. doi:10.1016/j.celrep.2016.08.078

Yelick, P.C., Schilling, T.F., 2002. Molecular Dissection of Craniofacial Development Using Zebrafish. Crit. Rev. Oral Biol. Med. 13, 308–322. doi:10.1177/154411130201300402

Yi, R., Qin, Y., Macara, I.G., Cullen, B.R., 2003. Exportin-5 mediates the nuclear export of pre-microRNAs and short hairpin RNAs. Genes Dev. 17, 3011–6. doi:10.1101/gad.1158803

Yim, E.K., Sheetz, M.P., 2012. Force-dependent cell signaling in stem cell differentiation. Stem Cell Res. Ther. 3, 41. doi:10.1186/scrt132

Yin, L., Jao, L.-E., Chen, W., 2015. Generation of Targeted Mutations in Zebrafish Using the CRISPR/Cas System. Methods Mol. Biol. 1332, 205–17. doi:10.1007/978-1-4939-2917-7_16

Yurco, P., Cameron, D. a, 2005. Responses of Müller glia to retinal injury in adult zebrafish. Vision Res. 45, 991–1002. doi:10.1016/j.visres.2004.10.022

Zehir, A., Hua, L.L., Maska, E.L., Morikawa, Y., Cserjesi, P., 2010. Dicer is required for survival of differentiating neural crest cells. Dev. Biol. 340, 459–467. doi:10.1016/j.ydbio.2010.01.039

Zentner, G.E., Henikoff, S., 2013. Regulation of nucleosome dynamics by histone modifications. Nat. Struct. Mol. Biol. 20, 259–66. doi:10.1038/nsmb.2470

Zhang, C., McCall, M., 2012. Receptor targets of amacrine cells. Vis. Neurosci. 29, 11–29.

Zhang, R., Han, P., Yang, H., Ouyang, K., Lee, D., Lin, Y.-F., Ocorr, K., Kang, G., Chen, J., Stainier, D.Y.R., Yelon, D., Chi, N.C., 2013. In vivo cardiac reprogramming contributes to zebrafish heart regeneration. Nature 498, 497–501. doi:10.1038/nature12322

Zhao, X.F., Wan, J., Powell, C., Ramachandran, R., Myers, M.G., Goldman, D., 2014. Leptin and IL-6 family cytokines synergize to stimulate Müller Glia reprogramming and retina regeneration. Cell Rep. 9, 272–284. doi:10.1016/j.celrep.2014.08.047

Zhao, Y., Srivastava, D., 2007. A developmental view of microRNA function. Trends Biochem. Sci. doi:10.1016/j.tibs.2007.02.006

Zhou, Q., Brown, J., Kanarek, A., Rajagopal, J., Melton, D. a, 2008. In vivo reprogramming of adult pancreatic exocrine cells to beta-cells. Nature 455, 627–32. doi:10.1038/nature07314

Zhou, Q., Gallagher, R., Ufret-Vincenty, R., Li, X., Olson, E.N., Wang, S., 2011. Regulation of angiogenesis and choroidal neovascularization by members of microRNA-23~27~24 clusters. Proc. Natl. Acad. Sci. U. S. A. 108, 8287–8292. doi:10.1073/pnas.1105254108